

Production of Algae for Biomaterials and Bioenergy: Closing the Nutrient Cycle and Enhancing the Light Utilisation Efficiency

Présentée le 11 août 2020

à la Faculté de l'environnement naturel, architectural et construit
Groupe Ludwig
Programme doctoral en génie civil et environnement

pour l'obtention du grade de Docteur ès Sciences

par

Eya NICODEME, née Damergi

Acceptée sur proposition du jury

Prof. J.-L. Scartezzini, président du jury
Prof. C. Ludwig, Dr L. F. De Alencastro, directeurs de thèse
Prof. F. Fischer, rapporteur
Dr D. Refardt, rapporteur
Prof. M. K. Nazeeruddin, rapporteur

"A pessimist sees the difficulty in every opportunity,
an optimist sees the opportunity in every difficulty."

Winston Churchill

Acknowledgements

Now that I am about to finish my PhD, I realised how time goes fast and how my life changed after I came to Switzerland. All started on October 2nd, 2012, in Tunisia, when I decided to send an email to Prof. Ludwig looking for a master project opportunity. That day, everything changed! I was accepted to continue my study in one of the best schools in Europe, EPFL. It was like a “dream came true” working in such a mind-blowing research environment in comparison to anything else I have ever experienced. For that, and throughout all these years, I would like to thank all the people who contributed on both a professional or private level to the successful completion of this research project and the finalisation my PhD thesis.

I would first like to express my sincere gratitude to my doctoral father, Prof. Dr Christian Ludwig. He consistently supported me since I came to Switzerland. It was under his tutelage that I developed a focus and became more efficient in my work. He provided me with direction, technical support and became more of a mentor and friend than a professor. It was through his, persistence, understanding and kindness that I completed my PhD thesis, I doubt that I will ever be able to convey my appreciation fully. Still, I owe him my eternal gratitude. Thank you Chrigu!!

I am very grateful to my thesis co-director Dr Felipe de Alencastro for his scientific guidance and his trust for developing my own ideas. I wish you a wonderful retirement (A life without the daily traffic jams and mounts of paperwork).

Thank to Marie Sudki with whom I have shared moments of deep anxiety but also big excitement! Thank you for your support during hard times; you are a member of my family.

A warm word for Michel Rossi, for the pleasant moments I had with you, for the scientific discussions and the funny conversations during coffee breaks at Arcadie.

Warmest thanks are reserved for all my friends from EPFL and PSI that have taken some time to discuss and enrich my life: Horst, Arnaud, Mohammed, Shivom, Julien, Gaël, Bhavish, Albert, Julia, Hossein, Shivom, Pierre, Dorian, Johanna, Jordan, Vincent, Oscar, Enio, Adrian, Lorenzo... Thank you!

My profound thanks go to all the stuff from the Flow Cytometry Platform. They always gave me a hand to deal with the practicalities of working in their research platform.

Special thanks to Dr Nikolaos Boukis for accepting me in his group during the gasification campaign at Karlsruhe Institute of Technology and allowing me to use the Elena gasification unit.

I want to acknowledge all the co-authors in our publications for all their support and expertise. My sincere condolences go to the family of Jean-Paul I Schwitzguébel who left us suddenly in 2018. Rest in peace.

I am very grateful to Prof. Jean-Louis Scartezzini, Dr Dominik Refardt, Prof. Fabian Fischer and Prof. Mohammad Khaja Nazeeruddin for agreeing to be members of my PhD examination committee, for their valuable time and feedback, and the precious corrections and suggestions.

Where would I be without my family? Words cannot express how grateful I am to my parents, for all the sacrifices that you’ve made on my behalf. Your prayer for me was what sustained me thus far. To my two brothers and my little sister, I missed you tremendously and felt sorry I could not always be there when you needed me. To my step-parents and Delphine, Thank you all for your encouragement, love and support.

But besides all the people I met, the people I made friends with, the people who helped me out in numerous situations during work I want to say thank you to a special and beloved person, my husband Thomas “Choupinou” for his support, encouragement, and unwavering love, his tolerance of my occasional vulgar moods is a testament in itself of his unyielding devotion and love. I am so happy and grateful to be with you! Thanks for everything.

This work was carried out thanks to the financial support from Swisselectric Research and Competence Center Energy and Mobility ‘CCEM’ in the frame of PAWaSto project and SCCER-Biosweet.

Lausanne, 26.02.2020

آية

Abstract

Microalgae are small organisms that live in water and use solar energy or artificial light to grow. They are emerging to be one of the most promising long-term, sustainable sources of biomass for fuel, food, feed, and other high valuable co-products. Like any other plant, algae, when grown using sunlight consume carbon dioxide (CO₂) and release oxygen (O₂), but with a 5 to 10 times faster growth rate than conventional food crops. Thus, algae-based CO₂ conversion is considered as a cost-effective option for CO₂ capture and the mitigation of greenhouse gas emissions (GHG). Since the last decade, there have been repeated attempts to bring microalgae bioenergy and biomaterial production to an industrial level. So far, despite the enthusiastic boost towards commercialisation, the production of microalgae has been demonstrated mainly at pilot scale levels, and only a few large-scale facilities exist and produce microalgae today.

There are several issues related to microalgae cultivation from either the energetic, environmental or economical point of view. Further developments are needed for algal biomass technologies to improve their cost-competitiveness and their environmental sustainability. The major bottlenecks are mainly linked to water and nutrient supply, the high energy consumption of algal processing, the high surface area requirements for cultures, and finally, the relatively low solar conversion efficiency of microalgae in highly sunny regions. Therefore, to design economically feasible algae production processes, it is necessary to close the nutrient cycle, to reach the energy balance, and to opt for a biorefinery concept where products can be valorised.

This doctoral thesis aims to explore a new concept, PAWaSto, which attempts to overcome the limitations of microalgae production processes by combining different technologies to increase the energy and nutrient recoveries within the system. An urban environment was considered in the PAWaSto vision. This work focuses on four different research approaches which can be summarised as follows: (1) As low-cost water and nutrient supply source is critical to the success of microalgae production, a unique on-site sanitation system for nutrient and water recoveries (household effluents) was studied in this thesis. (2) Energy and nutrient recycling: The integration of a hydrothermal process (HT) for a fast conversion of household effluents to concentrated nutrient-rich effluents, free of pathogens, suitable for algae production was proposed. Besides, the produced energy-rich gas obtained from the HT is considered for electricity generation through a solid oxide fuel cell (SOFC). (3) The implementation of semi-transparent dye sensitised solar systems (DSCs) on the illuminated surface of an algae photobioreactor, and their effect on the algal biomass productivity was studied for the first time in this thesis. (4) Finally, for the economic viability of algal biomass production, the extraction of high-value products from wet algal biomass using green solvent was proposed, and the residual biomass generated from the extraction step was further treated through a HT process.

For nutrient supply, a major concern was dedicated to an on-site sanitation system as it provides a more concentrated nutrient effluent source than those from wastewater treatment plants (more dilute). Therefore, in this thesis, nutrient rich-effluent (called Leachate) has been collected and analysed from on-site sanitation system equipped with a unique dry-toilet and composter chamber, then treated through HT non-catalytic gasification for nutrient and energy recoveries. Likewise, the nutrients needed for microalgae growth can be recycled, and biogas produced can be transformed into electricity via SOFC. The results obtained proved that the hydrothermal gasification of the leachate feedstock could be conducted continuously up to 40 h with high nitrogen and phosphorus recoveries. However, the gasification efficiency did not exceed 41% due to the high salt content in the feedstock. The utilisation of the aqueous phase side stream from the gasification as a culture medium for microalgae was successfully conducted with a specific growth rate $\mu = 0.64 \text{ day}^{-1}$. Furthermore, the syngases produced from the HT process was directly used to feed the SOFCs after adding enough steam to the fuel. Nevertheless, operation with such biosyngases in real SOFC systems has to be handled with special care due to potential carbon deposition. The SOFC system integrated with gas turbines gives high efficiency for syngas to electricity conversion.

This work also presents the results of a new concept of a positive energy culturing system for microalgae, where the light source is selectively shared between the algal biomass through photosynthesis, and the production of photovoltaic energy through dye sensitised solar cells (DSCs). The coloured DSC panels were applied at the top of the photobioreactor (PBR) for maximum light exposure. The results showed, at higher irradiance, a net improvement of growth rate and productivity (g/L) using both coloured DSC filters compared to control cultures. The highest growth rate and doubling time were obtained in the case of DSC-Red and DSC-Green culture with $\mu = 0.86 \pm 0.01 \text{ day}^{-1}$; $td=0.80 \text{ day}$ and with $\mu = 0.85 \pm 0.03 \text{ day}^{-1}$; $td=0.81 \text{ day}$ respectively compared to normal glass control $\mu = 0.51 \pm 0.03 \text{ day}^{-1}$; $td=1.35 \text{ day}$. These results suggested that coloured DSC acted as a protective filter for microalgae culture. In addition, even with a low conversion efficiency of sunlight of 3%, the impact of the construction and integration of the DSC panel on the overall greenhouse gas balance remains negligible compared to photobioreactor without DSC.

Finally, once the algal biomass was produced, a combined process for high value compounds extraction and efficient bioenergy recovery from the wet microalgae biomass was proposed. High added-value products carotenoids could thus be extracted before the hydrothermal gasification of the residual biomass into biosyngases. Two green solvents, ethanol and 2-methyl-tetrahydrofuran (2-MTHF), were used to achieve the maximum extractability of selected carotenoids. Pure 2-MTHF was tested for the first time as an alternative renewable solvent for carotenoid extraction from wet biomass, and promising results were obtained (30 min at 110 °C), with 45% of total carotenoids being extracted. The energy content of the residual biomass corresponds to a high heating value (HHV) of 18.1 MJ kg⁻¹. With a 1:1 mixture of both 2-MTHF and ethanol, more carotenoids were extracted from wet biomass (66%), and the remaining HHV of the residual biomass was 15.7 MJ kg⁻¹. The perspectives of combined carotenoid extraction and energy recovery for a better microalgae valorisation were discussed.

Overall this doctoral research project studied key aspects for the integration of a biorefinery concept in urban areas contributing to the big vision of closing the materials cycles on the level of districts. A focus was put on an integrated system for efficient microalgae production, power generation, and closing the nutrient cycle.

Keywords

Microalgae, bioenergy, nutrients, biomass, high-value compounds, recycling, photosynthesis, dye sensitised solar cells, carotenoids extraction, 2-methyl-tetrahydrofuran, green solvent, hydrothermal gasification, solid oxide fuel cells, optimisation, biorefinery.

Résumé

Les microalgues sont de petits microorganismes qui vivent dans l'eau et utilisent l'énergie solaire ou la lumière artificielle pour se développer. Ils sont en train de devenir l'une des sources de biomasse la plus prometteuse à long terme pour les carburants, les denrées alimentaires, les aliments pour animaux et d'autres produits à haute valeur ajoutés. Comme toute autre plante, les algues, lorsqu'elles sont cultivées en présence de la lumière, consomment du dioxyde de carbone (CO_2) et libèrent de l'oxygène (O_2) comme sous-produit. Ceci rend la production de microalgue une option très intéressante pour la séquestration du CO_2 et la réduction des émissions de gaz à effet de serre (GES).

Depuis la dernière décennie, il y a eu plusieurs tentatives pour amener la production de bioénergie à partir des microalgues à un niveau industriel. Jusqu'à présent, malgré la poussée enthousiaste vers la commercialisation enregistrée au début de cette décennie, la production de microalgues a été principalement démontrée à l'échelle pilote et seules quelques installations à grande échelle existent et produisent des microalgues aujourd'hui. En fait, il existe plusieurs problèmes liés à la culture des microalgues du point de vue énergétique, environnemental ou économique. Le développement des technologies de production de microalgues est nécessaire afin d'améliorer leur compétitivité au niveau des coûts et leur durabilité environnementale. Les principaux problèmes sont liés à l'apport de nutriments, à la forte consommation d'énergie lors de transformation des algues en produits finis, aux besoins élevés en surface des cultures, et enfin, à la faible efficacité de conversion solaire des microalgues dans les régions très ensoleillées. Afin de concevoir des processus de production d'algues économiquement réalisables, il est nécessaire donc de fermer le cycle des matériaux, d'atteindre un bilan énergétique positive et d'opter pour un concept de bioraffinerie où des produits de haute valeur ajoutée peuvent être valorisés.

Pour surmonter les limites actuelles des systèmes de production de microalgues, cette thèse de doctorat vise à explorer un nouveau concept, PAWaSto, qui rassemble différentes technologies afin d'augmenter la récupération d'énergie et de nutriments dans le système globale. Un environnement urbain a été pris en compte dans la vision PAWaSto. Ce travail se concentre donc sur quatre différents axes de recherche qui peuvent être résumés dans les points suivants : (1) étant donné que la source d'approvisionnement en eau et en nutriments à faible coût était essentielle au succès de la production de microalgues, un système d'assainissement sur site unique pour la récupération des nutriments et de l'eau (effluents des ménages) a été considéré dans cette thèse. (2) L'intégration d'un procédé hydrothermal (HT) pour une conversion rapide des effluents ménagers en effluents concentrés riches en nutriments, exempts de pathogènes, adaptés à la production d'algues a été proposée. De plus, le gaz riche en énergie produit à partir du HT a été converti en électricité par une pile à combustible à oxyde solide (SOFC) à des fins de production d'énergie. (3) L'installation de systèmes solaires semi-transparentes sensibilisés aux colorants (DSC) sur la surface éclairée d'un photobioréacteur d'algues a été étudiée pour la première fois dans ce travail de thèse. (4) Enfin, pour la viabilité économique de la production de biomasse algale, l'extraction de produits de haute valeur à partir de la biomasse algale produite à l'aide de solvant vert a été proposée et la biomasse résiduelle humide générée à partir de l'étape d'extraction a ensuite été traitée par le biais d'un processus HT.

Pour l'approvisionnement en éléments nutritifs, une préoccupation majeure a été consacrée au système d'assainissement sur site, car il fournit des sources d'effluents nutritifs plus concentrées que celles des stations de traitement des eaux usées (plus diluées). Par conséquent, dans cette thèse, des effluents riches en micro-nutriments (appelés lixiviats) ont été collectés et analysés dans 13 appartements équipés d'un système d'assainissement basé sur le principe des toilettes sèches, puis traités par gazéification hydrothermale non catalytique pour la récupération des nutriments et de l'énergie.

Ainsi, les nutriments nécessaires à la croissance des microalgues peuvent être recyclés et le biogaz produit peut-être transformer en électricité. Les résultats obtenus ont prouvé que la gazéification hydrothermale de lixiviat pouvait être effectuée en continu jusqu'à 40 h avec une récupération élevée d'azote et de phosphore. Cependant, l'efficacité de la gazéification n'a pas dépassé 41% en raison de la forte teneur en sel dans le lixiviat. L'utilisation de la phase aqueuse obtenue de la gazéification comme milieu de culture pour les microalgues a été menée avec succès avec un taux de croissance spécifique de $0,64 \text{ jour}^{-1}$. De côté énergétique et selon des calculs thermodynamiques, les gaz de synthèse produits peuvent être alimentés directement aux SOFC après l'ajout de la vapeur d'eau. Néanmoins, le fonctionnement avec de tels biosyngases dans de vrais systèmes SOFC doit être manipulé avec un soin particulier. Le système SOFC intégré aux turbines à gaz offre une grande efficacité pour la conversion du biogaz en électricité.

Les résultats du nouveau concept basé sur le partage d'une manière sélective de la source de lumière entre la biomasse algale et les cellules solaires à pigment photosensible (DSC) ont montré, à un rayonnement plus élevé, une nette amélioration du taux de croissance et de la productivité quand les panneaux DSC colorés étaient intégrés à la surface des photobioréacteurs. Le taux de croissance et le temps de doublement les plus élevés ont été obtenus dans le cas de la culture DSC-Rouge et DSC-Vert avec $\mu = 0,86 \pm 0,01 \text{ jour}^{-1}$; $t_d = 0,80 \text{ jour}$ et $\mu = 0,85 \pm 0,03 \text{ jour}^{-1}$; $t_d = 0,81$ respectivement par rapport au témoin en verre normal $\mu = 0,51 \pm 0,03 \text{ jour}^{-1}$; $t_d = 1,35 \text{ jour}$. Ces résultats suggèrent que la présence du panneau semi-transparent DSC à la surface ensoleillée du photobioréacteur (PBR) permet de protéger les cultures d'algues. De plus, même avec une faible efficacité de conversion de la lumière solaire de l'ordre de 3%, l'impact de l'intégration du panneau DSC sur le bilan global du CO_2 émit reste négligeable comparé à un photobioréacteur sans panneau DSC.

Enfin, une fois la biomasse algale produite, un processus combiné d'extraction de composés de haute valeur ajoutées et de récupération de bioénergie à partir de la biomasse de microalgues humides a été proposé. Des produits à haute valeur ajoutée tels que les caroténoïdes pourraient ainsi être extraits avant une gazéification hydrothermale de la biomasse résiduelle en biosyngases. Deux solvants verts, l'éthanol et le 2-méthyltétrahydrofurane (2-MTHF), ont été utilisés pour atteindre l'extractibilité maximale de caroténoïdes sélectionnés. Le 2-MTHF pur a été testé pour la première fois comme solvant renouvelable alternatif pour l'extraction des caroténoïdes à partir de la biomasse humide et des résultats prometteurs ont été obtenus (30 minutes à 110°C), avec 45% du total des caroténoïdes extraits. De plus, le contenu énergétique de la biomasse résiduelle correspond à un pouvoir calorifique élevé (HHV) de $18,1 \text{ MJ kg}^{-1}$. Avec un mélange 1:1 de 2-MTHF et d'éthanol, plus de caroténoïdes ont été extraits de la biomasse humide (66%) et le HHV restant de la biomasse résiduelle était de $15,7 \text{ MJ kg}^{-1}$. Les perspectives de l'extraction combinée des caroténoïdes et de la récupération d'énergie pour une meilleure valorisation des microalgues sont discutées.

Globalement, ce projet de recherche doctorale a étudié les aspects clés de l'intégration d'un concept de bioraffinerie en milieu urbain contribuant à la grande vision de fermeture des cycles des matériaux au niveau des quartiers. L'accent a été mis sur un système intégré pour la production efficace de microalgues, la production d'électricité et la fermeture du cycle des nutriments.

Mots-clés

Microalgues, bioénergie, nutriments, biomasse, composés de haute valeur ajoutées, recyclage, photosynthèse, cellules solaires photosensibles à base de colorants, extraction des caroténoïdes, 2-méthyltétrahydrofurane, solvant vert, gazéification hydrothermale, piles à combustible à oxyde solide, optimisation, bioraffinerie.

Glossary

ADP: Adenosine diphosphate

AP: Aqueous phase

ATP: Adenosine triphosphate

ASR: Area specific resistance

BIOSWEET: BIOmass for Swiss Energy future.

CHP: Combined Heat and Power plants

DHA: Docosahexaenoic acid

DSC-PBR: Dye sensitised solar cells- Photobioreactor

DSCs: Dye sensitised solar cells

DW: Dry weight

Eg: Band gas

EPA: Eicosapentaenoic acid

EPICA: European Project for Ice Coring in Antarctica

FSC: Forward scattered light

GC-MS: Gas chromatography coupled with mass spectrometry

GE: Efficiency of energy-rich gas product

GHG: Greenhouse-gas

HHV: High heating value

HPLC: High-performance liquid chromatography

HT: Hydrothermal treatment

HTG: Hydrothermal gasification

HTL: Hydrothermal liquefaction

ICP-OES: Inductively coupled plasma optical emission spectroscopy

IEA: International energy agency

IGO: Insulated glazed photobioreactor

IR: Infrared wavelength

LCA: Life cycle assessment

Leachate: Nutrient rich effluent from dry toilet

LSCs: Luminescent solar concentrators

2-MTHF: 2-methyl-tetrahydrofuran

NADPH: Nicotinamide adenine dinucleotide phosphate

NER: Net Energy Ratio

NOC's: Nitrogenous organic cyclic amide

Fm': Maximum fluorescence with light-adapted algae

FO: Minimum fluorescence with dark-adapted algae

FV/FM: Variable to maximum fluorescence

NO: Non-regulated non-photochemical energy losses

NPQ: Regulated non-photochemical energy losses

OCV: Open circuit voltage

OSS: On-site sanitation system

PA: Paris Agreement

PAM: Pulse amplitude modulation fluorometry

PAR: Photosynthetically active radiation

PBR: Photobioreactor

PE: Photosynthetic efficiency

PFD: Photon flux density

PLE: Pressurised liquid extraction

PSI: Photosystem 1

PSII: Photosystem 2

PVs: photovoltaic devices

RCP: A Representative Concentration Pathway

RCs: Reaction centre proteins

RF: Recovery factor

RLCs: Rapid light curves

SB: Salt brine

SCCER: Swiss competence centres for energy research

SET: Strategic energy technology

SSC: Side scattered light

TPES: Total primary energy supply

UV: Ultraviolet

WWTP: Wastewater treatment plant

Greek letters

Symbol	Meaning	Units
μ	Specific growth rate	Day ⁻¹
ϕ (PSII)	The quantum yield of photochemical energy conversion PS II	-
ϕ (NPQ)	The quantum yield of Regulated non-photochemical energy losses	-
ϕ (NO)	The quantum yield of non-regulated non-photochemical energy losses	-
η	Power conversion efficiency	%

Contents

Acknowledgements	ii
Abstract.....	iv
Keywords.....	v
Résumé	vi
Mots-clés.....	viii
Glossary.....	ix
Contents.....	xii
Chapter 1 Introduction.....	15
1.1 Bioenergy from biomass	18
1.1.1 Global prospect of bioenergy from biomass	18
1.1.2 Biomass in Switzerland.....	19
1.1.3 Biomass feedstocks	20
1.1.4 Biomass conversion routes	20
1.2 Microalgae biomass production	22
1.2.1 Microalgae metabolism.....	22
1.2.2 Microalgae growth requirements	24
1.2.3 Microalgae cultivation systems.....	26
1.2.4 Microalgae potential for bioproducts and bioenergy	28
1.3 Microalgae hybrid technologies: Splitting the solar spectrum for the coproduction of biomass and electricity	29
1.4 PAWaSto project.....	33
1.4.1 Goal and scope of the thesis	33
1.4.2 Project framework	34
1.4.3 Structure of the thesis.....	35
Chapter 2 Materials and methods.....	39
2.1 Nutrient recovery system: cooperative equilibre	40
2.1.1 Phyto-purification for greywater (GW)	40
2.1.2 Composter chamber: Leachate effluent.....	40
2.1.3 Leachate effluents analysis	41

2.1.4	Hydrothermal non-catalytic gasification of leachate effluent.....	42
2.1.5	Hydrothermal catalytic gasification of algal biomass.....	45
2.2	Microalgae growth experiments.....	46
2.2.1	Selected algae and growth medium.....	46
2.2.2	Microalgae growth kinetics.....	47
2.2.3	Microalgae growth using aqueous phase from HTG.....	49
2.2.4	Microalgae growth for high-value product extraction.....	49
2.2.5	Microalgae growth using DSC-PBR technology.....	52
Chapter 3 A combined hydrothermal gasification-solid oxide fuel cell system for sustainable production of algal biomass and energy		57
3.1	Leachate effluents	58
3.1.1	Chemical characterisation of leachate effluent.....	58
3.1.2	Non-catalytic hydrothermal supercritical gasification HTG.....	59
3.2	Microalgae growth tests: Cell size and autofluorescence of <i>C. vulgaris</i>	61
3.3	SOFC performance.....	63
3.3.1	Thermodynamics of solid carbon formation.....	63
3.3.2	Performance of Leachate-feed SOFC	64
3.4	Valorisation of bio syngas or H ₂ -rich gas.....	66
Chapter 4 Recalcitrant nitrogen containing organics from the hydrothermal conversion of algal biomass.....		69
4.1	Distribution of hydrothermal liquefaction products and carbon elemental mass balance	70
4.2	Organic composition of the salt brine effluent.....	70
4.3	Toxicity microalgal assay	72
4.4	Continuous Hydrothermal catalytic gasification of salt brine and model brine effluent.....	75
Chapter 5 Enhancing algae biomass production by using dye-sensitised solar cells as filters		77
5.1	DSC solar panels Characterisation	78
5.1.1	DSCs and microalgae absorption spectrum.....	78
5.2	DSC-PBR growth under constant light intensities: <i>C. vulgaris</i> case study.....	80
5.2.1	Growth kinetics.....	81
5.2.2	Photochemical, regulated and non-regulated quantum yield variations.....	83
5.2.3	Pigments and macromolecule compositions	85
5.3	DSC-PBR growth under constant light intensities: <i>H. pluvialis</i> case study.....	86

5.4	Algal biomass and energy production under DSC-bioreactor	88
Chapter 6 Biomass valorisation: Extraction of carotenoids from <i>Chlorella vulgaris</i> using green solvents and syngas production from residual biomass.....93		
6.1	Hansen solubility parameters	94
6.2	Elemental composition before and after the extraction	94
6.3	Carotenoids extraction yields	95
6.4	Effect of changes in extraction set-up on mean extraction yield and mean extracted carotenoids	98
Chapter 7 Final remarks102		
7.1	Sustainable production of algal biomass and energy: OSS-SOFC-HTG combined system	102
7.2	Nitrogen-containing organics from the hydrothermal conversion of algal biomass.	103
7.3	Dye sensitised solar cells for enhanced algae biomass production	104
7.4	Biomass valorisation: Extraction of carotenoids using green solvents and syngas production from residual biomass.....	105
7.5	Conclusion	105
References.....107		
List of Tables.....115		
List of Figures.....117		
List of Equations121		
Appendix A : Supplementary information123		
Appendix B: Additional contributions126		

Chapter 1 Introduction

Matching environmental goals with those of an efficient renewable energy system is one of the top research priorities for sustainability worldwide. This is mainly due to climate change that comes in parallel with a global resource scarcity, such as that of fertilisers [1]. In nowadays, society must deal with the depletion of natural resources and the climate change threat, which promises to have severe and irreversible consequences if reduction of greenhouse gas (GHG) emissions is not considered. An increase of energy consumption to almost 50% is expected by 2050 [2]. Fulfilling this demand with fossil fuel energy sources would further contribute to the increase of GHG worldwide. Therefore, to meet the energy demand without compromising future generations, it seems evident that society will have to find and adopt “clean” and sustainable solutions. To be sustainable in the long term, future energy sources will need to fulfil many criteria, including renewability, limited impact on the environment, affordability, scalability as well as limited use of freshwater and finite resources.

Despite clear evidence of the human-caused climate change, support for the Paris Agreement (PA) on climate change, and the prevalence of clean, economical and sustainable energy options, energy-related carbon dioxide (CO_2) emissions have increased 1.3% annually, over the last five years [3][4]. In fact, and since industrialisation began, CO_2 concentrations have increased by 45%, from 280 ppm in 1750 to 415 ppm in 2019 [5]. This increase has occurred despite the uptake of more than half of the emissions by various natural “sinks/ moderators of climate change” involved in the carbon cycle [6]. For instance, ocean acidification is one of the direct consequences of a CO_2 increased level, due to the absorption of 30% of the emitted anthropogenic CO_2 [7].

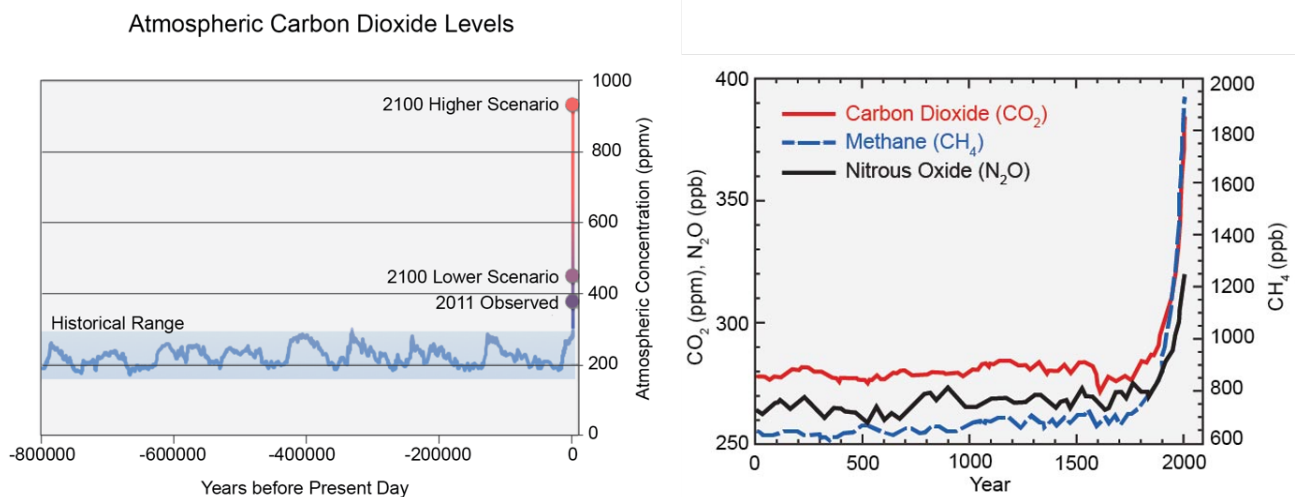


Figure 1: CO_2 levels in the past and the estimated increase scenarios of atmospheric CO_2 concentration at year 2100 (left). Present-day atmospheric levels of CO_2 , methane (CH_4), and nitrous oxide (N_2O) are notably higher than their pre-industrial averages (Right). The historical composite CO_2 record based on measurements from the EPICA (European Project for Ice Coring in Antarctica) Dome C and Dronning Maud Land sites and the Vostok station, adapted from [8].

By 2100, additional emissions from human activities are projected to increase CO_2 levels to 430 ppm under a very low optimistic scenario, (which would require immediate and sharp emissions reductions; Representative Concentration Pathway (RCP), more

details in **Appendix A**), and 935 ppm under a higher pessimistic scenario, which assumes continued increases of emissions; RCP, as illustrated in **Figure 1** [9].

Figure 1 also shows the present-day atmospheric levels of different GHG contributors; CO₂, CH₄ and N₂O, which are notably higher than their pre-industrial averages. One should mention that when CH₄ is anthropogenically emitted in the atmosphere, it can be oxidized and indirectly contribute to increase the CO₂ level in the atmosphere [10].

As stated in the Strategic Energy Technology (SET) roadmap of the European Commission: *“The decarbonisation of electricity production is the centrepiece of the Energy Roadmap 2050”* [11]. All scenarios studied in the Roadmap show that electricity with low carbon footprint will have to play a much greater role than now”. Although nuclear power has the advantage of being a low-carbon technology, it is becoming now highly controversial. Its two major drawbacks are related to the radioactive waste management and the irreversible consequences if a nuclear accident occurs [12].

Therefore, the supply of electric energy should be covered primarily by renewable energies such as hydraulic power, wind power, geothermal power, solar (organic and inorganic photovoltaic, concentrated solar power) and extended to the various biomass to bioenergy sectors (dry and wet biomass). Nonetheless, the transition to renewable energy will require a storage technology for smoothing out the electricity supply from these sources as they are intermittent with variable outputs. Present storing devices include pumped-storage hydroelectricity and batteries. In the future, compressed air and power to gas technologies coupled with fuel cells should also be used [13].

The urgent need to meet these objectives, and the complexity of these tasks, has boosted European countries to establish contingency plans to reduce their GHG emissions [14]. In this frame, the Swiss government signalled its long-term aim of reducing Switzerland's carbon emissions by 70-85% by 2050 [15]. With the commitment to gradually withdraw the nuclear energy supply, alternative low-carbon energy sources must be considered. Thereby, the Swiss Competence Centers for Energy Research (SCCERs) were created with the aim of developing the knowledge and technologies essential for the transition from the current nuclear and fossil fuel-based electric energy to a sustainable one. Among the objectives of this research centre, the SCCER BIOSWEET program (which stands for “BIOmass for SWiss Energy fuTure”) aims to increase the contribution of biomass to Switzerland's energy by deploying a high level of technological readiness [16].

Indeed, the energy from biomass is an exciting option for a resource-dependent country like Switzerland. Compared to photovoltaic or wind energy, biomass is an extremely versatile renewable energy source that can be extracted and stored independently of the variability of natural processes like the weather or seasonal changes. They refer to all organic matter existing in the biosphere, whether of plant or animal origin, as well as those materials obtained through their natural or artificial transformation [17].

Thus, the SCCER BIOSWEET postulates the vision of increasing the contribution of bioenergy from biomass to 100PJ [16]. This vision foresees one-third of this bioenergy to be covered by wood biomass, another third contributed by agricultural waste and the last third from so-called third generations biomass sources “algal biomass”. Understanding how algae can play an essential role in the future of Swiss energy is complex and requires a high degree of multidisciplinary approaches [16].

The potential to develop algal biomass to bioenergy is viewed as high thanks to the possibility they offer as the most productive photosynthetic organisms on earth with annual productivities of 10 to 150 tons of dry biomass per hectare and per year [16]. Moreover, microalgae production can utilise land and water resources unsuited from any other use which uncouple this bioenergy source from food production [18]. Indeed, contrary to bioenergy derived from agricultural biomass such as rapeseed, sunflower, soybean, peanut, rice bran, coconut, algal biomass doesn't affect the food security (arable land is not required) [19].

So far, the production of bioenergy from microalgae has been demonstrated at pilot scale levels. Despite the enthusiastic boost towards commercialisation registered at the beginning of this decade, there are few large-scale facilities operating to date. In fact, there are several issues related to microalgae cultivation from either the energetic, environmental or economical point of view [20,21]. Further developments are needed to improve algal biomass technologies in order to increase their cost-competitiveness and environmental performance. For instance, microalgae are known to be effective at consuming both nutrients and carbon from wastewater effluents [22–24]. The integration of wastewater treatment and algal biofuel production could provide cumulative benefits by offsetting a significant portion of algal production costs while delivering an efficient wastewater treatment service. This approach will limit the use of finite resources and freshwater and will increase the environmental sustainability of algae production.

Moreover, the reduction of electrical consumption of algal biomass production is essential also for the economic viability. In general, in outdoor microalgae cultivation systems, solar radiation is often too high relative to the photosynthetic solar photoconversion capacity of microalgae, this leads to photo-saturation, photoinhibition, overheating and eventually reduction of the productivity [25]. Shadowing microalgae with solar panels would, therefore, be a promising solution for both increasing productivity during hotter periods and producing local electricity for the process. Coupling algal biomass production with photovoltaic electricity generation represents an ideal opportunity to reduce the electrical demands for algae production systems. Although this solution is technologically appealing, its sustainability can be questionable as there is a clear trade-off between electricity and biomass production.

Microalgae is also known to be source of high-value compounds such as pigments, antioxidants and proteins, specific approaches suggested the use of microalgal biomass for bioenergy applications as well as for the extraction of biochemicals [26,27]. This approach could widen the market opportunities of microalgae products and open further possibilities of coupling production of algae biomass for biofuels and more valuable compounds. Thus, an innovative microalgae biorefinery structure implemented through the production of multiple products in the form of high-value products and biofuels may allow the economic feasibility and mitigate the overwhelming investments and operation cost of algae production plants [28].

All these emerging microalgae technologies are providing new horizons for bioenergy from algal biomass with a broader commercial opportunity. Thus, the splitting of algal biomass into bioenergy, chemicals, and biomaterials commodities to maximise the value of the raw materials and minimise the wastes, will enable the overall process to be economically viable.

In this thesis, the global vision of prospecting bioenergy from biomass in general, and from algae in particular, are discussed in the introduction of this thesis. The requirements of microalgae cultivation systems and the current approach for reducing the energetic and environmental impact as well as innovative integrated systems to promote sustainable processing of algal biomass are debated in this dissertation.

Material from this chapter has been partially published in:

(I) E. Damergi; J.-P. Schwitzguébel; D. Refardt; S. Sharma; C. Holliger, C. Ludwig.: Extraction of carotenoids from *Chlorella vulgaris* using green solvents and syngas production from residual biomass; Algal Research. 2017. DOI: 10.1016/j.algal.2017.05.003.

(II) M. Bagnoud-Velásquez; E. Damergi; G. Peng; F. Vogel; C. Ludwig: Fate and reuse of Nitrogen-containing organics from the hydrothermal conversion of algal biomass; Algal Research. 2018-04-21. DOI: 10.1016/j.algal.2018.04.005

(III) E. Damergi; H. Madi; S. Sharma; N. Boukis; F. Marechal; J. V. Herle; C. Ludwig: A combined hydrothermal gasification - solid oxide fuel cell system for sustainable production of algal biomass and energy; Algal Research. 2019. DOI: 10.1016/j.algal.2019.101552.

(IV) E. Damergi; P. Qin; S. Sharma; M. K. Nazeeruddin; C. Ludwig: Enhancing algae biomass production by using dye-sensitised solar cells as filters, (Ready for submission).

1.1 Bioenergy from biomass

1.1.1 Global prospect of bioenergy from biomass

The worldwide demand and consumption of primary energy increased consistently in the last 50 years [29]. This increase is a direct consequence of the demographic pattern where the world's population is estimated to grow by 0.9% per year on average, from 7.1 billion in 2013 to 9 billion in 2040. Today, the global energy system depends mainly on fossil fuels and this trend will continue if no radical political decisions are taken. As shown in **Figure 2**, coal, oil and natural gas constitute 81% of the total primary energy supply of the world. Renewables account for 14% with only a slight increase of 1% share since 2000.

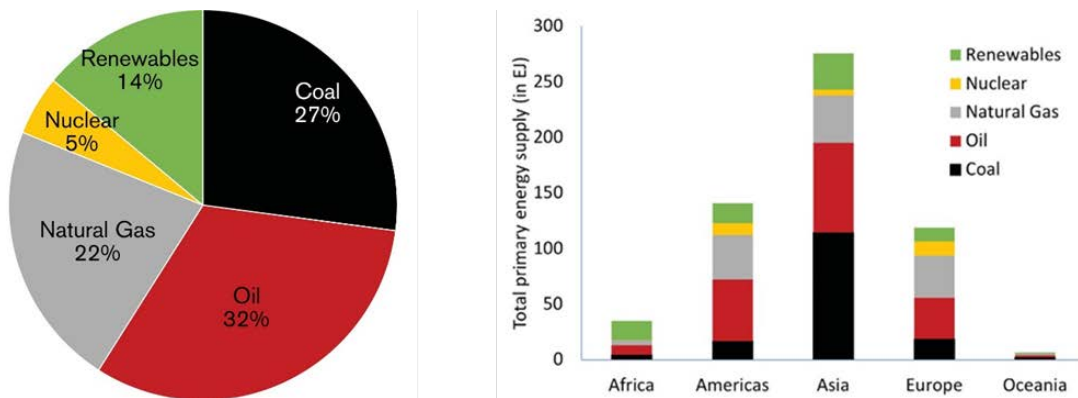


Figure 2: (Left) Total energy supply globally in 2016. (Right) Total Primary Energy Supply (TPES) or energy supply defined as production of energy sources including import and export of the source as well as storage in bunkers, adapted from [29].

Unfortunately, coal demand grows across much of Asia due to its affordability and availability as it is shown in **Figure 2**. This growth will continue until it reaches 36% of Southeast Asia's energy mix for power generation [30]. Or the combustion of coal adds a significant amount of CO₂ to the atmosphere per unit of heat energy more than does the burning of other fossil fuels. Interestingly, the African continent has the highest share of renewable in its energy supply.

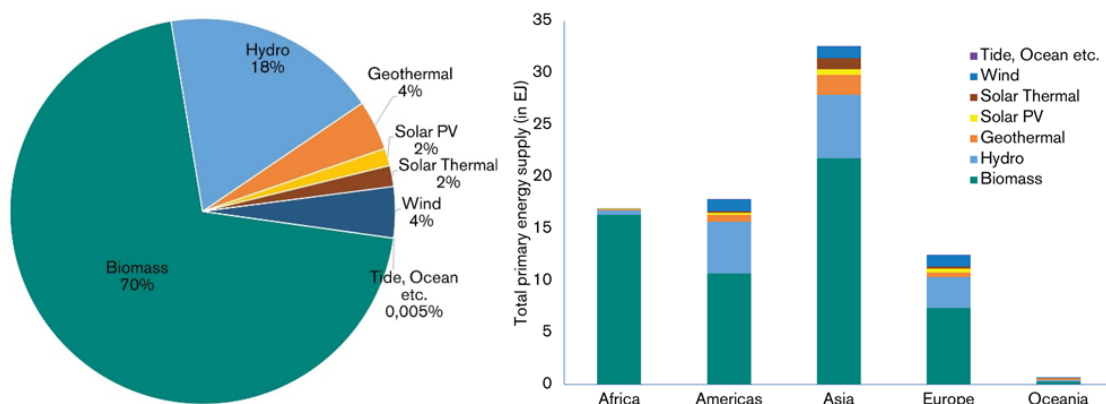


Figure 3: (Left) Total primary energy supply of all renewables in 2016. (Right) Total primary energy supply of all renewables per continent. Adapted from [29].

Almost 50% of the energy supply in Africa comes from renewables predominantly from biomass-based sources. In comparison, 10.5% of the energy supply in Europe is renewable [29]. The contributor sectors to the total primary energy supply of all renewable energies and what they represent per continent are illustrated above in **Figure 3**.

To give an overall view of the current framework, the total global primary energy supply of biomass resources was 56.5 EJ contributing to 70% of the share among all renewable energy sources. According to the International Energy Agency (IEA), the supply is expected to increase from 56 EJ to 160 EJ in 2050, with 100 EJ for the generation of heat and power [4]. In Africa, more than 90% of the total primary energy supply of renewable energy sources is from biomass. In every other continent, biomass is the largest renewable energy source in terms of supply and accounting from between 40% (Oceania) to almost 70% in Asia.

1.1.2 Biomass in Switzerland

The primary sources of energy in Switzerland are oil, hydropower and nuclear. Since 2005, Switzerland has seen a surge in the use of renewable energies such as biomass, wind, solar power and ambient heat. Currently, biomass is Switzerland's second most important source of domestic renewable energy (the first being hydropower with 638 hydroelectric power plants).

The Swiss biomass theoretical primary energy potential was estimated at 209 PJ per year, with the significant contributions from forest wood and animal manure as shown in **Figure 4**. Almost half of the theoretical potential can be sustainably used for bioenergy. According to B. Steubing et al.[31], there is currently no sustainable energy potential from agricultural biomass, such as energy crops, crop residues and grass. The main restrictions are competing material utilisations, environmental factors, supply costs, as well as scattered distribution and decentralised small-scale facilities. Depending on the location of the biomass, wood forest, for instance, can be procured at a high cost if it is located in an inaccessible region (mountain, road and railway embankments). Conservation areas also limit the amount of available wood [16]. Moreover, the Swiss policy on biofuels is not favourable now, and it excludes most biofuels from a tax exemption due to the environmental impacts that arise during the cultivation of energy crops. In 2010, only 3.6% of Switzerland's energy demand was covered by biomass resources. This value could be increased if the remaining energy potential was considered (this could provide an additional 3.3%) [31]. In order to overcome this bottleneck, and as a potential solution to the food-fuel dilemma, new fast-growing biomass should be considered.

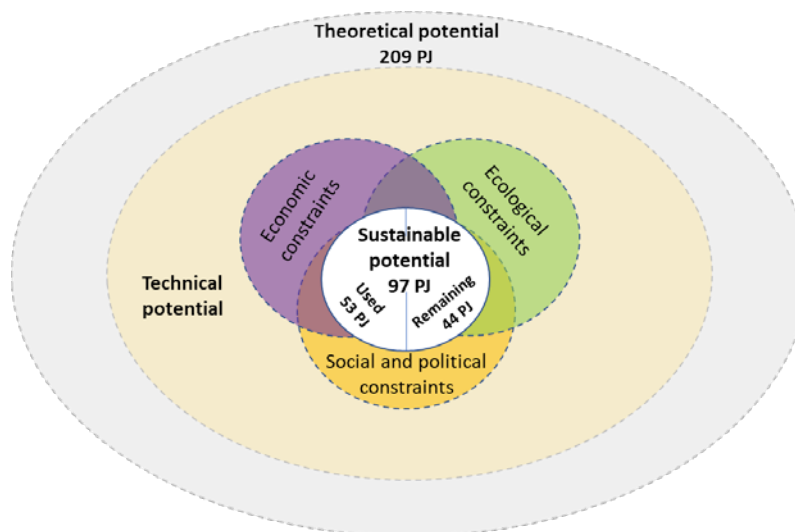


Figure 4: Schematic illustration of the Swiss technical biomass potential and constraints to the sustainable biomass potentials as well as the currently used and remaining biomass potentials modified from [31][32].

1.1.3 Biomass feedstocks

A typical composition of biomass contains in general, cellulose, hemicelluloses, lignin, lipids, proteins, carbohydrates, water, and inorganics (ash). This variability of biomass composition affects significantly its physical and chemical properties. As a result of different origins and variety of compositions, the classification of biomass resource assessment constitutes the foundation for integrated bioenergy planning to evaluate the sustainable feasibility and to estimate the additional bioenergy potential [33]. Biomass supply comes from a variety of feedstocks: wood fuel, forestry residues, charcoal, pellets, agriculture crops and residues, algae, municipal and industrial waste. Broadly, the supply can be classified into the following sectors:

- Dedicated energy crops (e.g., switchgrass, sunflower, soybean, peanut, coconut)
- Forestry residues (e.g., logging residues and forest thinning)
- Agricultural residues (e.g., corn stove)
- Algae (e.g., seaweed, microalgae)
- Waste streams and reusable carbon sources (e.g., sludge, waste food, and manure slurries).

Three different products can be obtained from the previously listed feedstocks, mainly electricity, heat and biofuels. In the case of biomass to biofuel, the type of biomass feedstock is divided into categories, or “generations”. First-generation biofuels are derived from food and oil crops, such as corn or sugar cane. They have reached a commercial level and are well established in many countries, but they are criticised for directly competing with food production and supply. The second-generation biofuels have been developed to overcome this relevant issue and are derived from non-food sources such as agricultural residues, switchgrass, etc., or in general lignocellulosic materials. In this case, the main problems are related to cellulose extraction and degradation, together with the spread and diversity of the feedstock material. Third-generation biofuels, like the previous ones, are derived from non-edible biomass sources but present much higher areal production yields compared to the former. Microalgae, belonging to this last category, have received wide attention as a promising feedstock to produce liquid biofuels due to their fast growth rate and their ability to grow on non-arable land and wastewater effluents [34]. Nevertheless, some drawbacks restrict the large-scale implementation of microalgae-based technologies and compromising its ability to become a real alternative to fossil fuels.

1.1.4 Biomass conversion routes

Bioenergy derived from biomass can be divided into two main categories: “modern” and “traditional”. Traditional category refers to the combustion of biomass for instance animal waste and wood. Modern categories refers to bioenergy technologies that allows to obtain liquid biofuels from bagasse and other plants, For example, biogas produced through anaerobic digestion of residues, wood pellet heating systems, and biorefinery fuel [35].

Figure 5 shows the currently known and investigated biomass conversion routes. It shows the three main groups of conversion technologies: chemical extraction, biochemical and thermochemical conversion. It also shows that many possible pathways mostly lead to the three following products: electricity, heat and fuels. The biochemical conversions include alcoholic fermentation (ethanol), anaerobic digestion (methane, hydrogen) and photobiological hydrogen production. Thermochemical processes include pyrolysis (bio-oil, syngas, charcoal), thermochemical liquefaction (bio-oil), gasification (syngas), transesterification (biodiesel) and direct combustion (electricity).

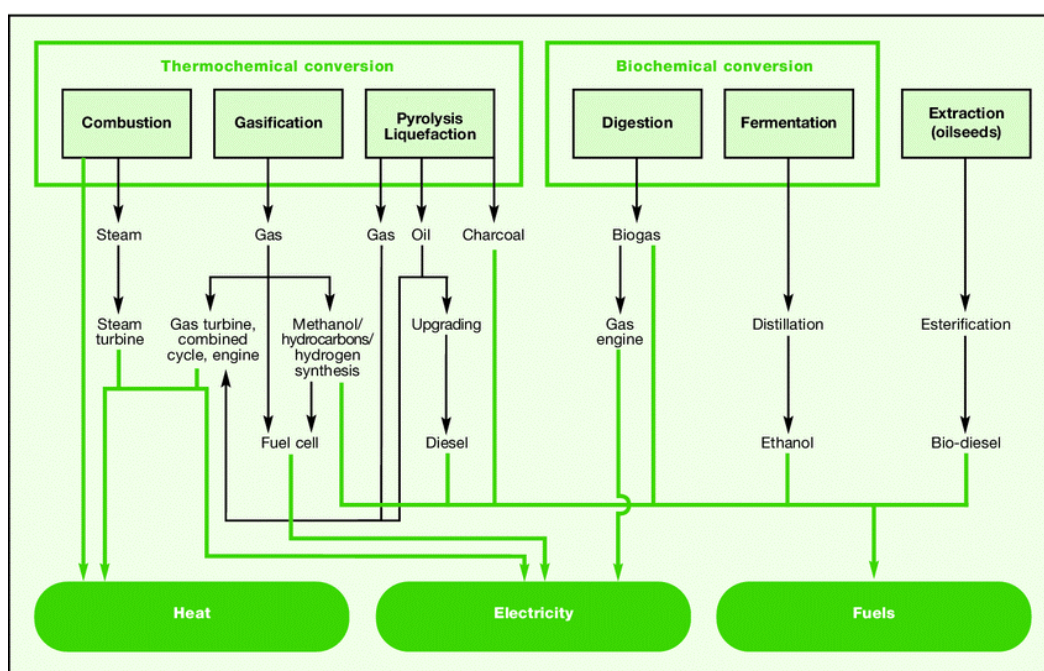


Figure 5: Main biomass conversion routes adapted from [35].

When considered as a primary energy carrier and depending on the conversion technique and the chemical composition of the feedstock, each category will have its specific benefits and problems. For instance, a high amount of ash in the biomass will lower the energy content of the fuel and may cause maintenance problems during and after the conversion process (presence of solid residues). In hydrothermal catalytic gasification, the ash content can lead to fouling and poisoning of the catalyst. Hence the salts must be separated from the process stream prior gasification, or a catalyst should not be used to avoid this issue [36]. Naturally present in raw biomass just like ash, moisture will lower the energy content of the fuel in almost all listed process in **Figure 5**. Therefore, the application of wet biomass in energy conversion systems is very challenging as in conventional systems, the biomass has to be dried. Or drying can be very energy-intensive, especially when the biomass has a moisture content above 50 wt% on a wet basis, e.g. sewage sludge, wastewater and algal biomass [37]. One exception where the presence of moisture is desired or even essential is with hydrothermal gasification conversion pathways. In fact, “Hydrothermal” designates an aqueous system operating at elevated pressures and temperatures and “gasification” refers to the gasification of carbon-containing compounds” [38]. This process operates under harsh environment especially, near the critical point of water (374°C, 22.1 MPa) or above it. Supercritical water is more like an organic solvent as it undergoes significant changes in its physical properties, e.g. drastic decrease in dielectric constant, density, ionic product, viscosity, and thermal conductivity. In one hand, supercritical water has a high ability to break down hydrocarbons and carbohydrates present in the biomass, resulting in the production of pressurised gases mainly rich in hydrogen (H_2), carbon monoxide (CO), CO_2 , and CH_4 [39]. In the other hand, salts are highly insoluble in supercritical water, and they precipitate out, which is a chance to recover nutrient from biomass to be reused as fertilizers in biomass production [40]. For energy optimisation, the efficiency of energy-rich gas production (GE) and the selectivity of the gas produced H_2 , CH_4 , syngas ($H_2 + CO$) can be steered by tuning the process conditions, increasing the temperature and/or using catalysts as illustrated in **Figure 6**.

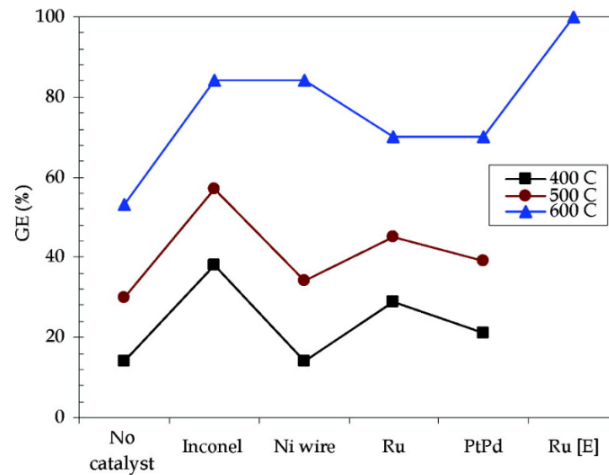


Figure 6: Influence of different catalysts on gas efficiency (GE) of hydrothermal gasification of microalgae biomass obtained at 400 °C, 500 °C and 600 °C. Different catalysts were tested in hydrothermal processes such as Inconel (austenitic nickel-chromium-based superalloys), Nickel (Ni), platinum/palladium (Pt/Pd) and Ruthenium based catalyst (Ru and Ru(E)). Figure taken from [39].

Basically, the hydrothermal gasification (with or without a catalyst) of biomass consists of three main reactions which are illustrated in **Table 1**. The first reaction includes the endothermic decomposition or reforming of biomass that is represented here by a generalised formula (CH_xO_y). From this step, a mixture of CO and H_2 (This mixture is also referred to as syngas or synthesis gas) is produced. Followed, the water-gas shift reaction takes place, where further H_2 production, as well as CO_2 , are formed. Part of the produced hydrogen, CO and CO_2 react to form methane, and this step is called Methanation [41].

Reaction	Formula	Enthalpy
1.Decomposition (syngas)	$\text{CH}_x\text{O}_y + (1-y) \text{H}_2\text{O} \rightarrow \text{CO} + (1-y + (x/2)) \text{H}_2$	$\Delta H^\circ_{\text{glucose}} = +608 \text{ KJ/mol}$
2.Water-gas shift reaction	$\text{CO} + \text{H}_2\text{O} \leftrightarrow \text{H}_2 + \text{CO}_2$	$\Delta H^\circ = -41 \text{ KJ/mol}$
3.Methanation of CO and CO_2	$\text{CO} + 3\text{H}_2 \leftrightarrow \text{CH}_4 + \text{H}_2\text{O}$	$\Delta H^\circ = -211 \text{ KJ/mol}$
	$\text{CO}_2 + 4 \text{H}_2 \leftrightarrow \text{CH}_4 + 2\text{H}_2\text{O}$	$\Delta H^\circ = -223 \text{ KJ/mol}$

Table 1: Basic reactions involved in the hydrothermal gasification of biomass. * (x): H/C molar ratio, (y): O/C molar ratio * ΔH° : Reaction enthalpy at reference temperature (25 °C). Adapted from [41].

1.2 Microalgae biomass production

Microalgae are microscopic aquatic unicellular organisms living in fresh or marine waters. They are mainly photosynthetic organisms with a similar mechanism as the one of land plants. These can be either eukaryotic microalgae (green algae, red algae and diatoms) or prokaryotic microalgae (cyanobacteria).

1.2.1 Microalgae metabolism

Microalgae are photosynthetic microorganisms capable of using light energy sources to fix atmospheric CO_2 and transform it into biological matter through a process called photosynthesis. This is the only significant solar energy storage process on Earth and is the primary source of biomass for human food and energy resources [42]. Microalgae use only a specific part of the solar radiation. Photosynthesis is restricted to wavelengths from 400 to 700 nm, the range of wavelengths which is termed photosynthetically active radiation (PAR). Photosynthesis involves two major types of reactions. The first type, the “light-dependent reactions”, comprises the capture of the light energy and its conversion to energy vector as nicotinamide adenine dinucleotide phosphate (NADPH) and adenosine triphosphate (ATP) as illustrated in **Figure 7** [43]. These reactions are the absorption and transfer of photon energy, the capture of this energy by photosynthetic pigments, and the generation of a chemical potential coupled with the release of oxygen. The latter

reaction generates NADPH due to the passage of the high energy excited electron along an electron transport system, whereas the second one generates ATP through a proton transfer across the thylakoid membrane [44]. Those compounds are formed from adenosine diphosphate (ADP) and NADP^+ thanks to chlorophyll which can transform light energy into a chemical one. ADP is transformed to ATP and NADP^+ is reduced to NADPH. The second type of reactions are the “light-independent reactions” of the Calvin-Benson cycle, in which this chemical potential is used to fix and reduce inorganic carbon in triose phosphates **Figure 8** [43].

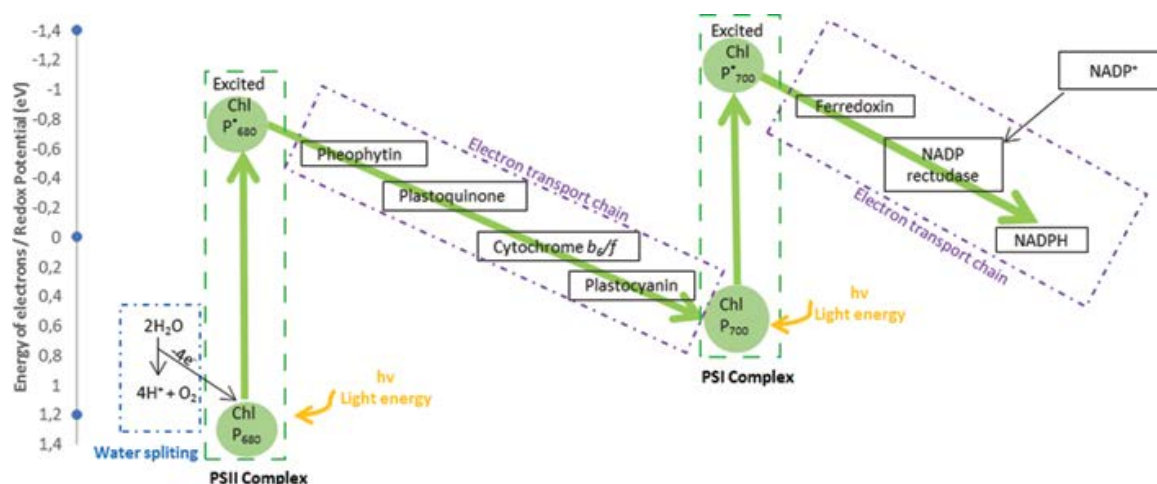


Figure 7: The Z-scheme of electron transfer processes involved in the light-dependent reactions of photosynthesis. Figure taken from [45].

To insert CO_2 in the Calvin cycle, microalgae can take the dissolved CO_2 or enzymatically convert HCO_3^- to CO_2 with the carbonic anhydrase enzyme [46]. The Calvin cycle forms hexose from CO_2 and H_2O , but in order to work, it needs energy and reducing power (electron source). These are respectively supplied by adenosine triphosphate (ATP) and nicotinamide adenine dinucleotide phosphate (NADPH). In order to capture more light, many microalgae can have antenna pigments of the family of the carotenoids, which absorb light energy and transfer it until it reaches a chlorophyll pigment [47]. As the light intensity increases, the photosynthesis accelerates. However, light-saturation of photosynthetic pigments occurs when the light intensity is 10 to 25 times lower than in the middle of the day on clear days [48].

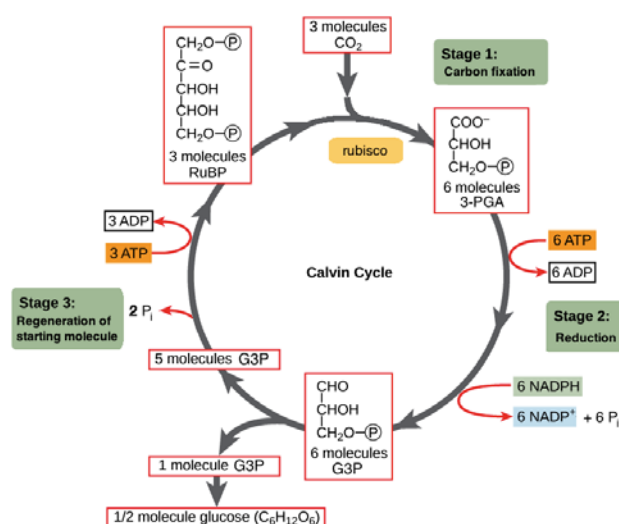


Figure 8: Inorganic carbon is fixed in the cells through the Calvin cycle. Figure taken from [49].

1.2.2 Microalgae growth requirements

1.2.2.1 Essential nutrients and their availability:

The average ratio of elements in microalgae in the literature is based on the Redfield ratio at 106 moles of carbon (C):16 moles of nitrogen (N):1 mole of phosphorus (P) [50]. However, the stoichiometry of elements within microalgae is variable between biogeographical provinces and as a function of interacting physical and biological factors. The role of these essential nutrients is discussed in the section below.

Carbon sources: Changes in carbon source affect the microalgal carbon pathways and intracellular organelle activity related to nitrogen assimilation. Autotrophic algae require only an inorganic carbon source in the form of HCO_3^- for photosynthesis while for heterotrophic growth they need an external source of organic carbon, e.g. acetate or glucose. Some microalgae are mixotrophic, they can perform both photosynthesis as well as using organic carbon sources [43].

Nitrogen Microalgae can easily assimilate different sources of nitrogen, and they can be classified in declining order: ammonium > nitrate > nitrite > urea. In the case of nitrate, algae cells transport it across the membrane and then reduce it to ammonia, in the process, consuming large amounts of energy, carbon, and protons. Other nitrogenous compounds like urea or urine are also assimilable by microalgae. Some microalgae can use urea as the sole source of nitrogen [23][51]. It is usually hydrolysed into ammonia and bicarbonate before its nitrogen is incorporated into cells. In microalgae, two enzymes can metabolise urea, urease and urea amidolysase.

Phosphorous is an essential compound of in microalgae metabolism, and it is considered as a fundamental nutrient for algal growth since it shares in intra-cell energy transfer, nucleic acid synthesis and specific reactions related to cell division. It phosphorous is, therefore, an important element for energy transport and genetic information inside the cells. The supply of Phosphorous salts is fundamental to the efficient growth of microalgae cells [52].

However, In the past 50 years, total nitrogen, phosphorus (NP) consumption in the world increased by a four-fold factor and reached already 170.7 million tonnes [53]. Phosphorus is mainly extracted from mines which makes it a non-renewable resource. A phosphorous peak is expected in 2033 with demand exceeding supply which could then endanger the world's food security [54].

1.2.2.2 Light and microalgae pigment absorption

Light availability and microalgae photoconversion efficiency of light are considered the main factors affecting microalgae biomass [55]. Light source in microalgae systems can be provided by solar light, artificial light or combinations of different light sources. On the one hand, cells grown under light-limited conditions have a lower capacity for accumulating CO_2 [56]. On the other hand, microalgae grown under high light intensity can be subject to photo-saturation and photoinhibition. Microalgae chlorophylls have two major absorption bands: a) blue or blue-green and b) red with different absorption peaks, e.g. chlorophyll a (430 and 670-690 nm), chlorophyll b (455 and 650-660 nm). Secondary pigments 'carotenoids' are another type of photosynthetic pigment weakly fluorescent with an absorption range between 400 and 550 nm, divided into two groups: carotenes and the xanthophylls. These accessory pigments are characterised by the C40 isoprenoid structure; they absorb mainly blue wavelength and transmit yellow and red [57]. Carotenoids play an important role in the protection against excess irradiance, chlorophyll triplets and reactive oxygen species [44]. They are overproduced in some algal species, e.g. *Haemotococcus pluvialis* when grown under unsuitable conditions. Variations in the light/dark regime and light intensities can lead to a photo-saturation of the photosystem. Or changes in the cell content of proteins, carbohydrates and lipids. For instance, In the case where algae are light-limited, they will respond by increasing their pigmentation. This process is called photo-acclimation [58].

A wide variety of artificial lamps employed for microalgae research exist and the spectral distribution of a number of lamps used in microalgae research is shown in **Figure 9**. Comparing the spectra of all these different lamps with those of the sun, it is evident that all are different from the sunlight. Thus, the choice of an artificial light source with a similar spectrum as sunlight is crucial for microalgae production as certain spectral effects cannot be excluded. Timing of cell division, for example, has been shown to depend on light colour [59]. One thing is certain: both the light spectrum (nature of light) and intensity of light are decisive factors in the growth behaviour of microalgae. In view of an efficient and inexpensive large-scale production of photosynthetic biomass, the only option is to rely on sunlight, improving the reactor performances to achieve better efficiency, however, to perform laboratory experiments, care must be taken when chosen the ideal lighting source as it will affect the growth of microalgae directly. **Figure 9** illustrates the most common ones.

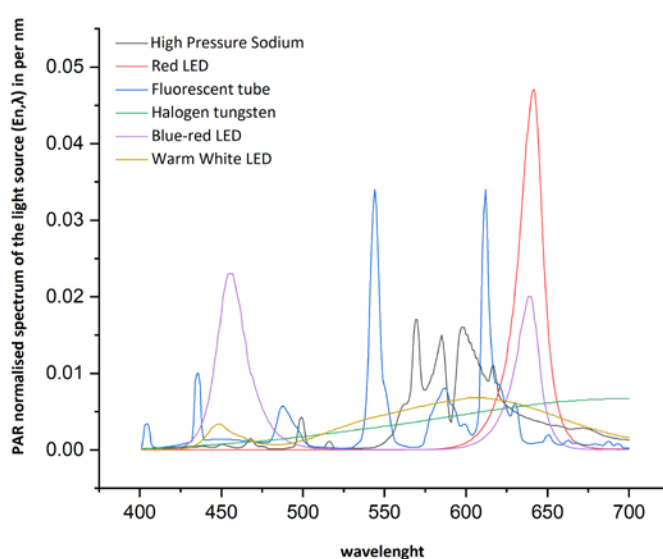


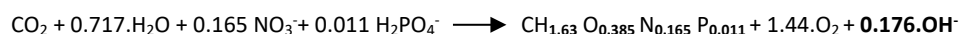
Figure 9: Spectral distribution of artificial lamps employed in microalgae research adapted from [60].

1.2.2.3 pH value

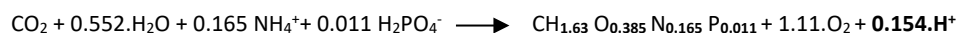
The consumption of nitrogen by microalgae can lead to a change in pH. The use of nitrate (NO_3^-) by microalgae cells leads to the release of hydroxide ion (OH^-) and an increase in pH. When combined with a CO_2 based pH control (air/ CO_2 mixture injected in the culture), the OH^- formed will react with CO_2 forming extra bicarbonate HCO_3^- . Consequently, more and more CO_2 gas needs to be supplemented to the gas stream in order to maintain the pH when the biomass density increases.

The use of ammonium (NH_4^+) by microalgae cells leads to the release of protons H^+ and a decrease in pH. When combined with a CO_2 based pH control, the H^+ formed will react with the bicarbonate HCO_3^- present in the liquid forming CO_2 and H_2O . The CO_2 is lost via the aeration. As soon as all bicarbonate HCO_3^- has reacted and disappeared, the pH will drop below the setpoint ($\text{pH}=7$), and the CO_2 addition will stop. Consequently, the microalgae will stop growing due to a lack of CO_2 .

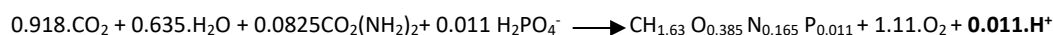
The use of urea ($\text{CO}(\text{NH}_2)_2$) by microalgae cells has a very small pH effect and will not interfere with a CO_2 based pH control. To illustrate this, the stoichiometry of the growth reaction at a neutral pH is shown based on the three different nitrogen sources:



Equation 1: Nitrate as nitrogen source for microalgae.



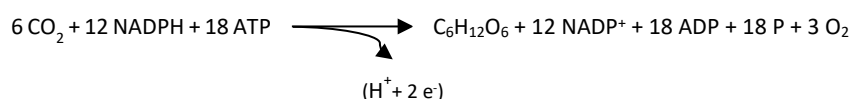
Equation 2: Ammonium as nitrogen source for microalgae.



Equation 3: Urea as nitrogen source for microalgae.

For the commercial production of microalgae biomass, it is preferable to use urea as a nitrogen source instead of nitrate and ammonium. As it is shown in the previous equations, urea affects slightly the pH when compared to ammonium and nitrate. A stable pH of 7 is generally favourable for a continuous growth of microalgae.

At pH values between 7 and 10, CO_2 is mainly in the form of HCO_3^- . This inorganic carbon is fixed in microalgae cells through the Calvin cycle whose overall stoichiometry is:



Equation 4: Chemical equation of the Calvin cycle.

It is crucial to maintain the pH value of the culture medium in the optimal range so that the cellular process is not arrested. An acceptable pH range can be accomplished by aerating the culture. In the case of high-density microalgae, the addition of carbon CO_2 acts as a pH buffer.

1.2.2.4 Temperature

Every microalgae species has an optimal temperature, which is generally between 15 °C and 35 °C. This value may vary with the composition of the culture medium and the strain [61]. For each 5 °C increase, photosynthesis, cell division and growth should expect to double until unfavourable temperatures are reached. For growth temperatures exceeding the optimal temperature, microalgae growth rates sharply decrease.

1.2.3 Microalgae cultivation systems

1.2.3.1 Culture mode

A culture can be defined as an artificial environment in which the algae grow. In theory, culture conditions should resemble the natural environment of the algae as far as possible. There are three types of microalgae culture systems in terms of the method, i.e. batch, continuous, and semi-continuous (fed-batch) cultures.

- Batch culture: it consists of a single inoculation of cells into a container of growth medium followed by a growing period of several days. The harvesting step occurs only when the microalgae cells reach their maximum or near-maximum density.

-Semi-continuous: This growth mode prolongs the use of large culture vessels by partial periodic harvesting, followed immediately by topping up to the original volume and supplying with nutrients to achieve the original level of enrichment.

- Continuous culture: In this case, fresh culture medium is continuously pumped to the homogeneously mixed culture close to the maximum growth rate, and the excess culture is washed out continuously or intermittently.

1.2.3.2 Culture technologies

There are two main cultivation systems for the current production of microalgae: open and closed systems. Each one of the systems has a series of advantages and disadvantages: The main differences between both systems are gathered in **Table 2**. Open systems such as raceway ponds are characterised by their lower investment and maintenance needs, their easy scaling. However, microalgae productivity within those systems is quite low and more exposed to contamination (direct contact with the environment). Moreover, the high evaporation of water and the losses of injected CO₂ make open ponds cultivation resources inefficient [62]. In the case of closed systems, also called closed photobioreactors, the reactors can maintain higher cell density values than the open systems, reaching higher productivity rates, achieving greater efficiency in the use and fixation of CO₂ injected. Moreover, the contamination issue encountered in the open system is drastically reduced, allowing better control of cultivation conditions. But, the construction, maintenance and operation costs of the closed systems are considerably higher. Moreover, cooling and heating systems are required to control the cultivation temperature. Photobioreactors commonly appear in three different configurations: vertical column reactors (bubble columns or airlift), tubular reactors, and flat-panel reactors.

Microalgae production systems were compared in **Figure 10** in terms of the net energy ratio (NER) of biomass production. By definition, NER is the sum of the energy used for cultivation, harvesting and drying, divided by the energy content of the dry biomass [63]. Profitable microalgae systems should have a NER value below 1. A positive energy balance is generally achievable for open systems. However, The NER of the PBR systems are more often greater than 1. Therefore, it is important to reduce the energy demand of PBR by integrating other sources of energy production within the system.

Factors	Open system (Raceway pond)	Closed systems (Photobioreactors)
Space required	High	Low
Area/volume ratio	Low (5 to 10 m ⁻¹)	High (20 to 200 m ⁻¹)
Evaporation	High	No evaporation
Water loss	Very high	Low
CO ₂ -loss	High	Low
Temperature	Highly variable	Require cooling
Weather dependence	High	Low
Process control	Difficult	Easy
Shear	Low	High
Cleaning	None	Required
Algal species	Restricted	Flexible
Biomass quality	Variable	Reproducible
Population density	Low	High
Harvesting efficiency	Low	High
Harvesting cost	High	Lower
Light utilisation efficiency	Poor	Good
Most costly parameters	Mixing	Oxygen removal and temperature control
Contamination control	Difficult	Easy
Capital investments	Low	High
Productivity	Low	3 to 5 times

Table 2: Comparison between microalgae production in open and closed bioreactors [62].

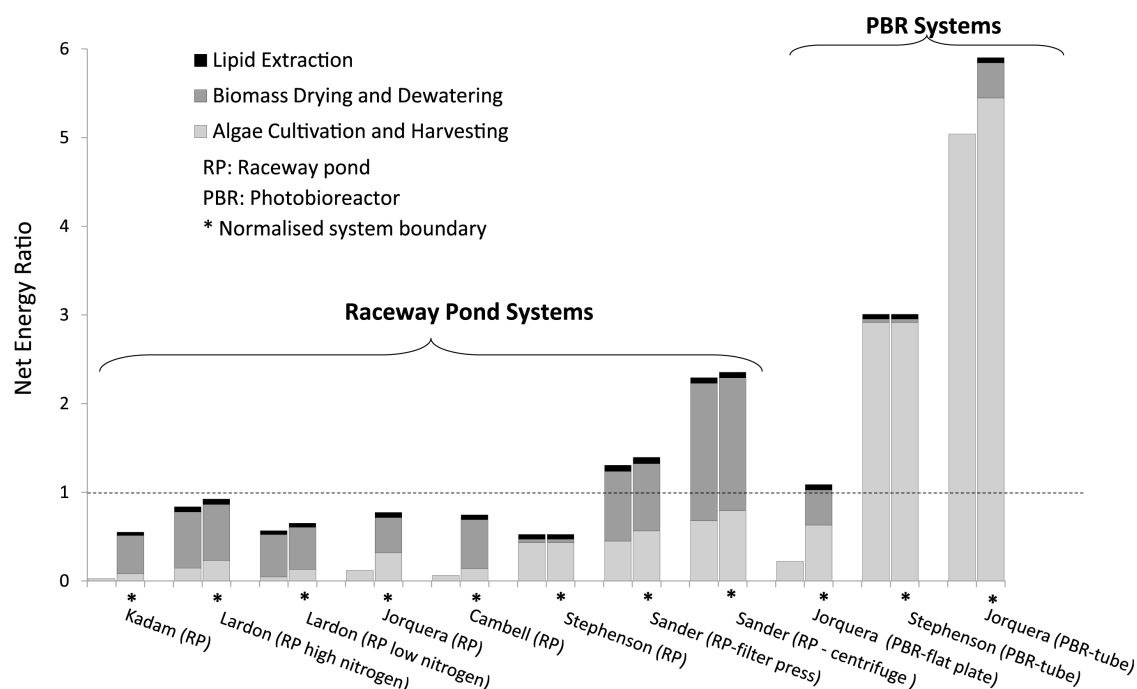


Figure 10: Net energy ratio (NER) for micro-algae biomass production: comparison of published values with normalised values. (The NER is defined as the sum of the energy used for cultivation, harvesting and drying, divided by the energy content of the dry biomass). All mentioned studies in the figure are listed in [63].

1.2.4 Microalgae potential for bioproducts and bioenergy

The conversion of algal biomass into several biochemical products, and bioenergy (section 1.1.4) with the aim of maximising the value of the raw materials and minimising the wastes is feasible employing a biorefinery concept. By definition, a biorefinery is an integrated facility, which combines various processes and equipment to co-produce bioenergy and high-value chemicals from biomass. Microalgae-based industrial exploitability ranges from basic biomass-based food and feeds nutraceuticals to high-value cosmeceuticals, pharmaceuticals, and biomedical applications. Cultivated under certain stress conditions such as nutrient starvation, high salinity, high temperature, etc., microalgae are able to accumulate considerable amounts of lipids or carbohydrates or proteins, as shown in **Table 3**. For instance, *Spirulina maxima* can reach high protein content, up to 71%, which make it an ideal candidate for alternative protein source. Microalgae are also capable of accumulating substantial amount of lipids such in the case of *Scenedesmus dimorphus*. Besides, other high value compounds such as essential fatty acids eicosapentaenoic acid (EPA), docosahexaenoic acid (DHA), omega 3, and γ -linolenic acid can be extracted from the lipid fraction. Depending on the growth condition, algae are capable of switching their metabolism, under stress condition, carbohydrates can be accumulated in *Scenedesmus dimorphus* up to 52%.

Strains	Protein (%)	Carbohydrates (%)	Lipids (%)
<i>Scenedesmus obliquus</i>	50–56	10–17	12–14
<i>Scenedesmus quadricauda</i>	47	–	1.9
<i>Scenedesmus dimorphus</i>	8–18	21–52	16–40
<i>Chlorella vulgaris</i>	51–58	12–17	14–22
<i>Chlorella pyrenoidosa</i>	57	26	2
<i>Dunaliella bioculata</i>	49	4	8
<i>Dunaliella salina</i>	57	32	6
<i>Spirulina platensis</i>	46–63	8–14	4–9
<i>Spirulina maxima</i>	60–71	13–16	6–7

Table 3: Chemical composition of algae expressed on a dry matter basis [64].

Other high-value compounds can be found in microalgae biomass such as vitamins and antioxidants and pigments. A vitamin that can be found in microalgae is riboflavin, which is essential for some maricultural animals [65]. Carotenoids are lipophilic secondary algal pigments used as a natural colourant in food or in cosmetics and offer an exciting perspective thanks to the extensive practical applicability and the relatively high market price of natural dyes, e.g. AlgalTechnologies (Israel) as well as Parry Pharmaceuticals (India) are two companies producing astaxanthin (carotenoids) from *Haemotococcus pluvialis* having a market value of 10,000 USD/kg [66]. However, such a product with a very high value typically have a low market size, and the production costs could be a major barrier. Therefore, establishing business models that look not only at the potential of algae for high-value products but which are also considering the possibility of producing energy from the same raw material is of great interest. Carotenoids extraction could thus contribute to make microalgal biofuel production economically feasible. However, conventional extraction techniques of these compounds are time-consuming and generally require using dry algal biomass.

1.3 Microalgae hybrid technologies: Splitting the solar spectrum for the coproduction of biomass and electricity

Photosynthesis may be defined as a light-driven redox reaction in which carbon dioxide CO_2 and H_2O are converted to energy-rich organic compounds $(\text{CH}_2\text{O})_n$ and oxygen [67]. Photosynthesis is the driving mechanism behind microalgae biomass production, which requires only a small fraction of the incident solar energy, primarily in the blue and red portions of the solar spectrum [68]. The primary role of the light photochemical reactions in photosynthesis is to provide the biochemical reductant (NADPH_2) and the chemical energy (ATP) for the assimilation of CO_2 [69]. In conventional outdoor cultivation system of microalgae, factors that influence microalgae growth are generally linked to solar irradiation intensity, quality, and physical orientation of culture systems. For instance, light atmospheric scattering leads to attenuation of direct beam and diffuse light of around 17%, an effect which increases with latitude by as much as an additional 30% as shown in **Figure 11**. In addition, adverse weather conditions added a further 65% loss based on the difference between the bright sky and measured irradiances at different locations [70]. Regarding culture orientation, indirect culture exposure or direct exposure towards the sun can reduce the irradiation intensity by another 50%. At the culture surface, 57% of typical sunlight is not useful for photosynthesis and is therefore considered to be lost relative to the sun. At peak sun intensity, saturation of photosynthesis occurs within the cells of microalgae and 80% of the absorbed sunlight may be wasted as heat. To that, additional losses related to energy transduction through the photosynthetic apparatus (73%) and biomass synthesis and metabolic regulations (10%–90%) may be added. Thus, a net photosynthetic efficiency, calculated from incident light on a surface culture to its storage as a simple carbohydrate, can range between 0.1% and 10% [70]. Thus, photosynthesis for terrestrial or microalgal biomass production suffers from the limited power conversion efficiency (PCE), approximately one order of magnitude lower than photovoltaic devices (PVs) [71].

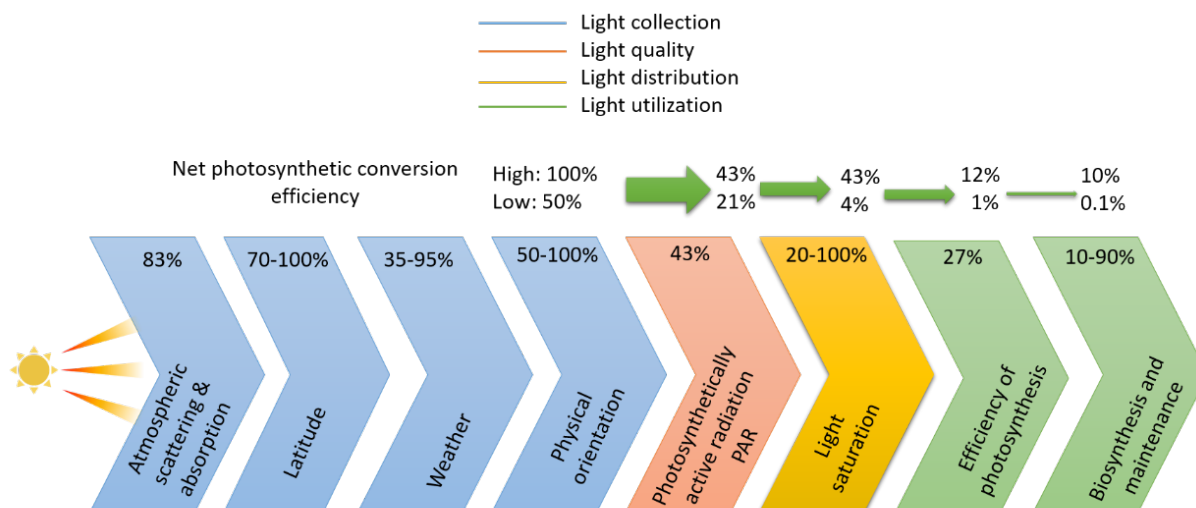


Figure 11: From sunlight-to-algal biomass: Solar conversion efficiency and strategies adapted from [70].

In microalgae, chlorophyll may be considered as a semiconductor with a band-gap (E_g) of 1.78 eV. Being below chlorophyll band-gap, infrared (IR) radiation is not absorbed (53%). Moreover, absorption of the blue photons (2.5–3.1 eV) could be inefficient during photosynthesis due to the excessive energy loss as heat in photosystem (PS) I or II. According to the literature, the absorption of those high-energy photons by the antenna complex may cause photoinhibition [72].

Besides the relatively low light conversion efficiency of microalgae, other limitations towards the development of a microalgae-based industry are attributed to the high economic costs of algal production platforms [73]. Considering the interest in industrial scaling, there has been a remarkable advance in the development of efficient microalgae production systems. New cultivation techniques based on sharing the solar energy between photovoltaics and microalgae culturing methods are gaining ground, and two different approaches have been already reported. The first approach consists of partially covering a microalgae bioreactor with non-transparent photovoltaic (PV) cells, allowing part of the light to reach the algae culture. The most widely used PV are silicon-based photovoltaic panels (Si-PV) because of their high solar light conversion efficiency. Several research reports demonstrated the feasibility of this concept. For instance, Tredici et al., 2015, [74] have shown that covering up to 20% of *Tetraselmis suecica* culture with a standard silicon photovoltaic strip does not increase productivity but can improve the NER by a factor of 1.7. This experiment was conducted in outdoor closed photobioreactors. The background theory was that the intermittent shading would increase dark-light cycles, resulting in an improved overall sunlight energy conversion of the algae. Another study has shown that with a covering of one-third of the photobioreactor, the growth rate increased by 49% in 1000 $\mu\text{mol photons/m}^2\text{s}$ for *Scenedesmus obliquus* [75]. However, under lower irradiation, the changes were not significant. In non-sunny regions, the use of non-transparent standard PV can reduce the PAR radiation and result in decreased productivity due to the reduction of irradiance required for photosynthesis [76].

Figure 12 illustrates how the solar spectrum can be divided between the growth of microalgae and the production of electricity by a photovoltaic device (solar cell). In comparison, highly efficient crystalline silicon solar cells can absorb light strongly across the solar spectrum as shown by the spectral response of solar cell in **Figure 12**. This indicates that these consumers of solar energy (microalgae and solar cells) appear to compete for the same resource. If the irradiance could be split between the two, the full utilisation of the solar spectrum would be possible, and this could revolutionise the microalgae industries. Or it is clear from the absorption spectra of microalgae that some parts of the spectrum are absorbed more strongly than others and could also be absorbed by the solar cell when a combined and overlapped system is considered.

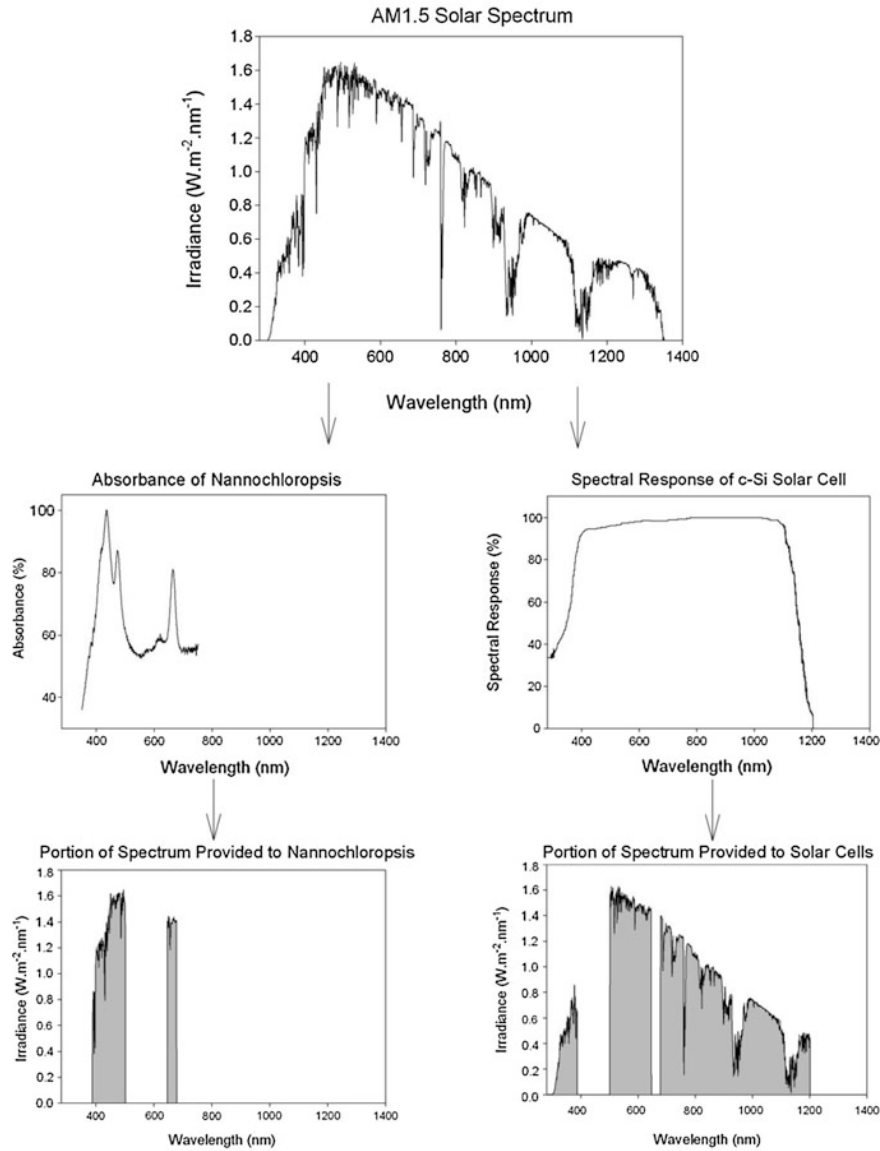


Figure 12: Splitting the solar spectrum for the coproduction of biomass and electricity. The shaded regions illustrate the portions of the solar spectrum that can be delivered to electrical generation and microalgae cultivation without reducing the productivity of the microalgae. The figure was taken from [77].

Therefore, new concepts of semi-transparent PV were suggested as a replacement of the standard non-transparent ones in the PV assistant microalgae production system. New photovoltaic technologies using either organic or inorganic materials, such as semi-transparent luminescent solar concentrators (LSC), dye-sensitised solar cells (DSCs), could be a promising alternative due to their transparency (space effective) and good solar conversion efficiency. For instance, Detweiler et al., 2015, have used transparent LSC to absorb unused photons in the green region and then re-emitted them as red photons. The red photons generated by fluorescence are either transmitted to boost algal growth or captured by a waveguide and directed to front-facing photovoltaic cells to be converted into electricity [78]. However, for electricity generation purposes, the LSC filters have to be combined with a PV unit which is not an adequate space solution. In a similar manner, Nwoba et al., 2020, showed the successful outdoor cultivation of *Nannochloropsis* sp under spectrally selective insulated glazed photobioreactor (IGP). The IGP design enabled transmission of more than 75 % of visible light while blocking 90% of ultraviolet and infrared radiation. No significant difference in biomass productivity of IGP and standard plate PBR's were observed, and significantly lower productivity was found in comparison to the raceway pond culture. One

should mention that 40% of the surface in the case of IGP-PBR was covered by an opaque cadmium telluride PV which can significantly affect the amount of light reaching the culture in the low irradiance region [79].

Another study relying on the same principle of using spectrally selective photovoltaic cells demonstrated the possibility of producing 20.3 g m²/day of algal biomass and 220 Wh m²/day of electricity by utilising multiple bandgaps in a single system under an illumination of 7.2 kWh m²/day [72]. Recently, the filtering effect of a semi-transparent hydrogenated amorphous silicon-based solar cell was also proposed [80]. Optical modifications of thin solar cell layer thicknesses and reactive ion etching of the glass substrate allowed to maintain a high PV efficiency while maintaining the growth rate of microalgae growing test of *Phaeodactylum tricornutum*. The growth and performance of photosynthetic microalgae are highly sensitive to the quality and quantity of available light, which generally induces a change in microalgae composition. The effect of these optical filters on macromolecules composition of algal biomass was not investigated.

Among other optical, semi-transparent dye-sensitised solar cells (DSCs) are a promising alternative due to the inexpensive fabrication costs and good performance **Figure 13**. In nature, light absorption by microalgae antenna complexes is followed by efficient charge separation across a membrane via photosynthetic reaction centre proteins (RCs).

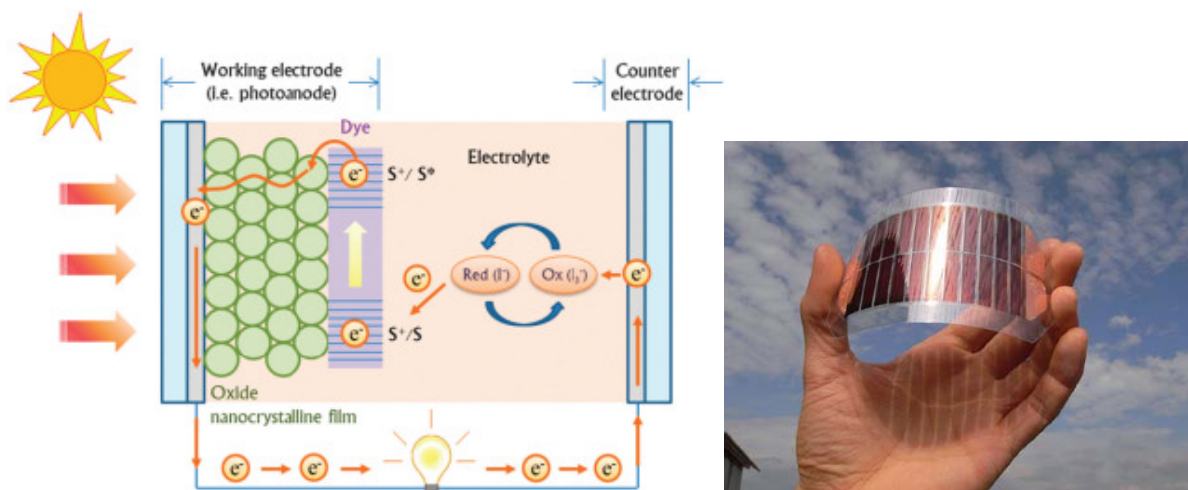


Figure 13: Schematic representation of a dye-sensitised solar cell constructed with a photo anode consisting of a dye-sensitised semiconducting oxide film, a counter electrode made of Pt coated glass substrate, and an electrolyte filled between the dye adsorbed photo anode and counter electrode [81].

Dye sensitised solar cells (DSCs) utilise an analogous mechanism to harvest sunlight and convert solar energy to electricity. In DSCs, the process begins with the photoexcitation of the dye, which is followed by electron injection into the conduction band of the oxide (TiO₂ in this case) until it reaches the counter electrode as illustrated in **Figure 13**. The oxidised dye recovers its original state thanks to the redox system (electrolyte) which is itself regenerated at the cathode [82]. To the best of our knowledge, these devices have never been used as a surface cover for microalgae production. Therefore, in this thesis, this new option was tested as in a combined culturing system for microalgae, where the light source is selectively shared between the algal biomass through photosynthesis, and the production of photovoltaic energy through dye sensitised solar cells (DSCs).

1.4 PAWaSto project

1.4.1 Goal and scope of the thesis

End of pipe systems: The key for sustainable nutrient supply of algal biomass?

Urban resources have the potential to fulfil microalgae basic need for nutrient and water supply. Thus, wastewater effluents should be of primordial importance for nutrient recovery as it contains valuable fertiliser which can be used for microalgae production if recovered properly (e.g. fertiliser) [83]. Urine contains less than 1% of the total volume of household wastewater and up to 80% of the nitrogen (N) and 40–50% of the phosphorus (P) [84]. Some studies have successfully used microalgae for the removal of nutrients such as phosphorus and nitrogen from concentrated human urine [88][89]. However, the urine content is highly diluted in wastewater effluents, which lowers the nutrient recovery potential. Since end-of-pipe systems dilute the nutrients, and therefore, their recuperation is made harder. A new approach in applied research that considers source separation of household effluent for nutrient recovery purposes was studied [85–87]. This separation enables the recovery of nutrients at the source level. Hereby, in this thesis, an on-site sanitation system (OSS) based on a dry-toilet principal was considered as it provides a more concentrated nutrient effluent than those from conventional wastewater treatment plants.

Besides the nutrients uptake that can be achieved during microalgae growth, the produced microalgal biomass could be further used as feedstock for bioenergy and biomaterial production. Nevertheless, microalgae production using domestic effluents faces several drawbacks for industrialisation. One of the main issues is related to the chemical and biological variability of these effluents (presence of viruses, bacteria, antibiotics, etc.) which affects the algae growth negatively. Furthermore, the produced algal biomass can only be used as feedstock for energy production and non-food application due to social acceptance issues.

To overcome these issues, hydrothermal gasification process (HTG) was proposed as a potential solution for nutrient and energy recovery from domestic wastewater effluent (principal details in section 1.1.4). Operating at high temperature and pressure, the HTG allows sterilisation of household effluent (elimination of bacteria and viruses). Moreover, it allows the recovery of nutrients as HTG by-product through precipitation due to the drastic decrease of water density with a viscosity close to its gas-like value at the critical point of water. Finally, an energy rich gas is generally produced during HTG process due to the decomposition of organic matter present in the effluent. This energy rich gas can be converted to electricity using a solid oxide fuel cell (SOFC).

From this perspective, the following points were investigated in this thesis and addressed as research questions:

RQ1-1: *Can we use on-site sanitation effluent as a feedstock for HTG process to recover nutrients and produce energy-rich gas?*

RQ1-2: *What is the potential to use this energy-rich gas to generate electricity using a SOFC?*

RQ2: *Is it feasible to use the HTG effluent as a microalgae growth medium?*

Dye sensitised solar cells and microalgae cells: Compatibility or overlapping?

One of the main novelties of this project is the use of dye-sensitised solar cells (DSC, or Grätzel cells) on top of the photobioreactor. Contrary to standard photovoltaics or solar concentrator, these cells are translucent photovoltaic and so allow the passage of wavelengths that are not used, leaving the rest of the light available for the microalgae. This could then significantly improve the solar energy harvesting and eventually protect the microalgae from excessive radiation in some cases. To our knowledge, this technology has never been tested before. In this thesis, two different ruthenium-dye were integrated fully at the illuminated structure of photobioreactor. The variation of growth kinetics, (2) microalgae pigments (chlorophylls and carotenoids) and (3) macromolecules

content (carbohydrates, proteins, and lipids) were investigated and compared to control cultures under two different solar simulated light intensities. The contribution of this new technology in the PBR was environmentally evaluated using life cycle assessment (LCA) technique. The results were expressed in terms of CO₂ emission equivalents produced for 1kg of algae using standard and combined DSC-PBR.

The main research questions concerning this combined technology were listed below:

RQ3-1: *What is the effect of DSC filter on the growth kinetics and the final microalgae biomass composition?*

RQ3-2: *In term of CO₂ emissions, what is the impact of adding a DSC panel to the structure of microalgae photobioreactor?*

Algal biomass for high-value compound extraction: wet biomass vs dry biomass

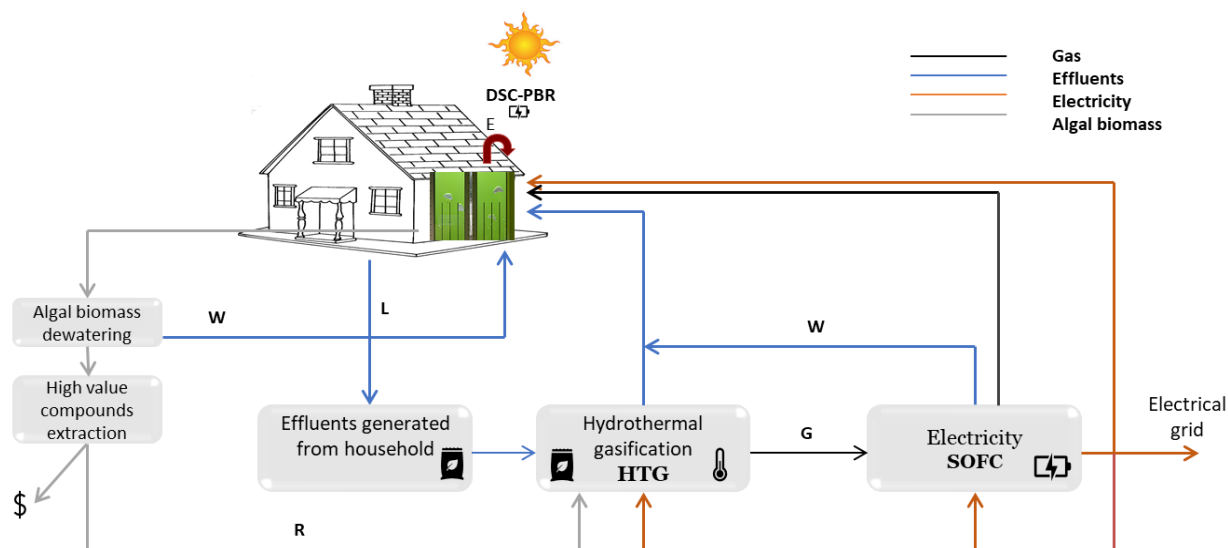
Process integration is an approach where separate industrial processes are combined to create an additional value. Recent studies have provided considerable evidence that microalgae-derived bioactive compounds could play a vital role in bioenergy sectors of the algal industry. Microalgae offer high biodiversity with an enormous potential to produce bioactive compounds which are difficult to produce via synthetic routes such as carotenoids. In this thesis, the aim of this study was to extract carotenoid prior the HTG of algal biomass as a strategy to create added value. However, carotenoids extraction generally requires dry algal biomass and the use of toxic organic solvents such as hexane. As drying algal feedstock was not an option prior the hydrothermal treatment, the high moisture content was challenging for carotenoids extraction. Therefore, to fulfil the requirements of a HTG process, the potential of extracting carotenoids from high moisture algal biomass was studied in this thesis. Moreover, the extraction was performed in a pressurised vessel to simulate the HTG preheating step. A green solvent, 2-Methyltetrahydrofuran was selected as an ideal solvent for carotenoids extraction based on its Hansen solubility parameters and its recyclability (with increasing temperature, 2-MTHF is inversely soluble in water). The following research question was addressed in this part of the thesis:

RQ4: *What is the efficiency of carotenoids extraction from wet algal biomass and the potential of energy recovery from residual biomass?*

1.4.2 Project framework

This work was performed thanks to the financial support of the former Commission of Technology and Innovation CTI (now Innosuisse), Swisselectric Research and Competence Center Energy and Mobility CCEM in the framework of the PAWaSto project. This thesis is part of the outcome of the research performed at EPFL, in the GR-LUD laboratory and at the Paul Scherrer Institute (PSI), in the research group of the Chemical Processes and Materials laboratory.

The PAWaSto project stands for **P**hotovoltaic **A**ssisted Algae Production and **W**astewater Treatment for Combined Heat and Power Generation and **S**torage (PAWaSto). It has officially started on January 2015 and was supported by the Competence Center Energy and Mobility (CCEM). The different steps of the process, which is suggested as an integrated part of a district (indicated by the house) are summarised in **Figure 14**. The idea is to cultivate photosynthetic biomass (microalgae) in a combined photovoltaic-PBR system in order to increase the photo-conversion efficiency of solar energy. The integration of hydrothermal non-catalytic gasification for combined heat and power generation was to fulfil the nutrient and energy demands of the algae system. Likewise, the nutrients and CO₂ needed for growth can be recycled, and biogas produced can be transformed into electricity via solid oxide fuel cells. The integration of such a concept in a building or district is envisioned in the frame of another future project.



GW: Grey Water; **BW:** Black Water; **U:** Urine; **NS:** Nutrient Solution; **DSC-PBR:** Combined dye sensitised solar cells and photobioreactor; **R:** Residues; **E:** electricity generated from the DSC--PBR, **W:** water; **G:** Energy rich gas, **L:** Leachate effluent (mixture of urine and faeces).

Figure 14: Simplified scheme of the Photovoltaic assisted Algae production, and Wastewater treatment combined heat and power generation and Storage project, so-called (PAWaSto).

Behind the complexity and interdisciplinary of this project, a lot of scientific experience was gained within a previous project carried out in our research group, “The SunChem project”. The global vision in that project was to produce bio-methane via hydrothermal catalytic gasification and to capture CO₂ using an algae-based process. Envisioned as a closed-loop system, the SunChem process also allowed the recycling of nutrients, water, and CO₂ and their reintegration in the algae growth cycle.

Nevertheless, limitations linked to the sulphur poisoning of the Ruthenium catalyst used in the gasifier unit were encountered in the SunChem process and this due to the high ash content of the used microalgae [88,89]. This issue affected one of the decisions taken during the elaboration of the PAWaSto project. In the case of high sulphur content biomass, hydrothermal gasification without the catalyst was seen as the appropriate solution to avoid poisoning of the catalyst. This decision also affected the operation condition of the gasifier, as higher temperature was necessary to reach an interesting yield of gas production.

1.4.3 Structure of the thesis

The topics addressed by this thesis are organised and subdivided in chapters as follows.

Chapter 1: Introduction

The global vision of prospecting bioenergy from biomass in general, and from algae in particular, are discussed in the introduction of this thesis. The requirements of microalgae cultivation systems and the current approach for reducing the energetic and environmental impact as well as innovative integrated systems to promote sustainable processing of algal biomass debated in chapter 1 of this dissertation.

Chapter 2: Materials and methods

Describes the methodologies, which are the underlying basis of this thesis and the experimental techniques that form the framework for the scientific results presented in the following chapters. This includes the nutrients recovery cycle, the photovoltaic-photobioreactor (DSC-PBR), the hydrothermal systems, and all the analytical instruments and methods applied in this thesis.

Chapter 3: A combined hydrothermal gasification- solid oxide fuel cell system for sustainable production of algal biomass and energy

In this chapter, a new composter sanitary system operating without external connection to sewer pipes was used to test the suitability of its effluent as a feedstock for the HTG process. Mainly, H₂ rich gas was obtained from the HTG process at 600 °C, 28 MPa. For an efficient power-generation system with low emissions, experimental tests combining solid oxide fuel cells (SOFC) with the obtained gas from the HTG were performed.

Chapter 4: Recalcitrant nitrogen-containing organics from the hydrothermal conversion of algal biomass

This chapter evaluated the possibility to treat the hydrothermal (HT) effluent by growing microalgae while producing renewable algal biomass. Upon continuous and multiple recycling of this hydrothermal effluent, in principle suitable for algal growth, the concentrations of some recalcitrant nitrogen organic compounds (NOC's) are likely to increase and could potentially attain toxic thresholds. The formation of recalcitrant organic products is mainly the result of algal biomass decomposition through a complex set of chemical reactions that occur during the hydrothermal gasification process. Toxicity assay with some identified NOC's in the HT effluent were performed with three different algae strains.

Chapter 5: Enhancing algae biomass production by using dye-sensitised solar cells as filters

Chapter 5 presents the experimental work carried out integrating photovoltaic dye sensitised solar cells (DSC) on the photobioreactor surface, to increase the impinging light utilisation efficiency. Two different colours of dye sensitisers were tested, DSC-green and DSC-red were integrated to the illuminated surface of a PBR. Different constant light intensities were investigated to ascertain the effect of DSC on microalgal growth kinetics and macromolecules content (lipids, carbohydrates, proteins). The contribution of this new technology in the PBR was environmentally evaluated using life cycle assessment technique (LCA). The results were expressed in terms of CO₂ emission equivalents produced and electricity generated.

Chapter 6: Biomass valorisation: Extraction of carotenoids from *Chlorella vulgaris* using green solvents and syngas production from residual biomass

A combined process for carotenoids extraction and efficient bioenergy recovery from the wet microalgae biomass is proposed. High added-value products could thus be extracted prior the hydrothermal gasification step of the algal biomass into synthetic natural

gas. The economic sustainability of biofuel production from algal biomass as well as the large energy demands of microalgae cultivation and harvesting was addressed in this chapter.

Chapter 7: Final remarks

In this last chapter. The concluding observations and possible perspective are presented for all the different topics discussed in the previous chapters.

Chapter 2 Materials and methods

The following chapter describes the methodologies, which are the underlying basis of this thesis and the experimental techniques that form the framework for the scientific results presented in the following chapters. This includes the nutrients recovery cycle, the photovoltaic-photobioreactor (DSC-PBR), the hydrothermal systems, and all the analytical instruments applied in this thesis. The roman number reported as superscript notation indicates the original publications on which certain sections of this chapter were taken.

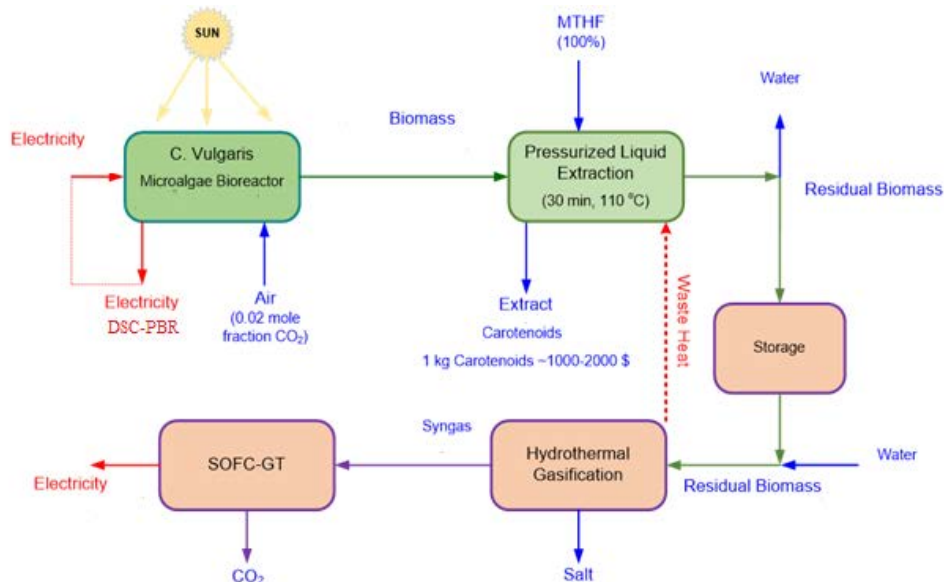


Figure 15: Production of *C. Vulgaris* and its valorisation within the scope of PAWasto project.

Material from this chapter has been partially published in:

- (I) E. Damergi; J.-P. Schwitzguébel; D. Refardt; S. Sharma; C. Holliger, C. Ludwig.: Extraction of carotenoids from *Chlorella vulgaris* using green solvents and syngas production from residual biomass; Algal Research. 2017. DOI: 10.1016/j.algal.2017.05.003.
- (II) M. Bagnoud-Velásquez; E. Damergi; G. Peng; F. Vogel; C. Ludwig: Fate and reuse of nitrogen-containing organics from the hydrothermal conversion of algal biomass; Algal Research. 2018-04-21. DOI: 10.1016/j.algal.2018.04.005
- (III) E. Damergi; H. Madi; S. Sharma; N. Boukis; F. Marechal; J. V. Herle; C. Ludwig: A combined hydrothermal gasification - solid oxide fuel cell system for sustainable production of algal biomass and energy; Algal Research. 2019. DOI: 10.1016/j.algal.2019.101552.
- (IV) E. Damergi; P. Qin; S. Sharma; M. K. Nazeeruddin; C. Ludwig: Enhancing algae biomass production by using dye-sensitised solar cells as filters, (ready for submission)

2.1 Nutrient recovery system: cooperative equilibre

Sensitive to environmental concerns such as sustainable water and nutrients management, the cooperative of habitations Equilibre in Geneva undergo constructions with on-site sanitation (OSS) systems in 2011. In collaboration with atba architects office, a 50-users building were constructed with an objective of treating 100% of effluents and valorise the dejections (black water and urine) via composting and phyto-purification for greywater. **Figure 16** illustrates the global structure of their concept.

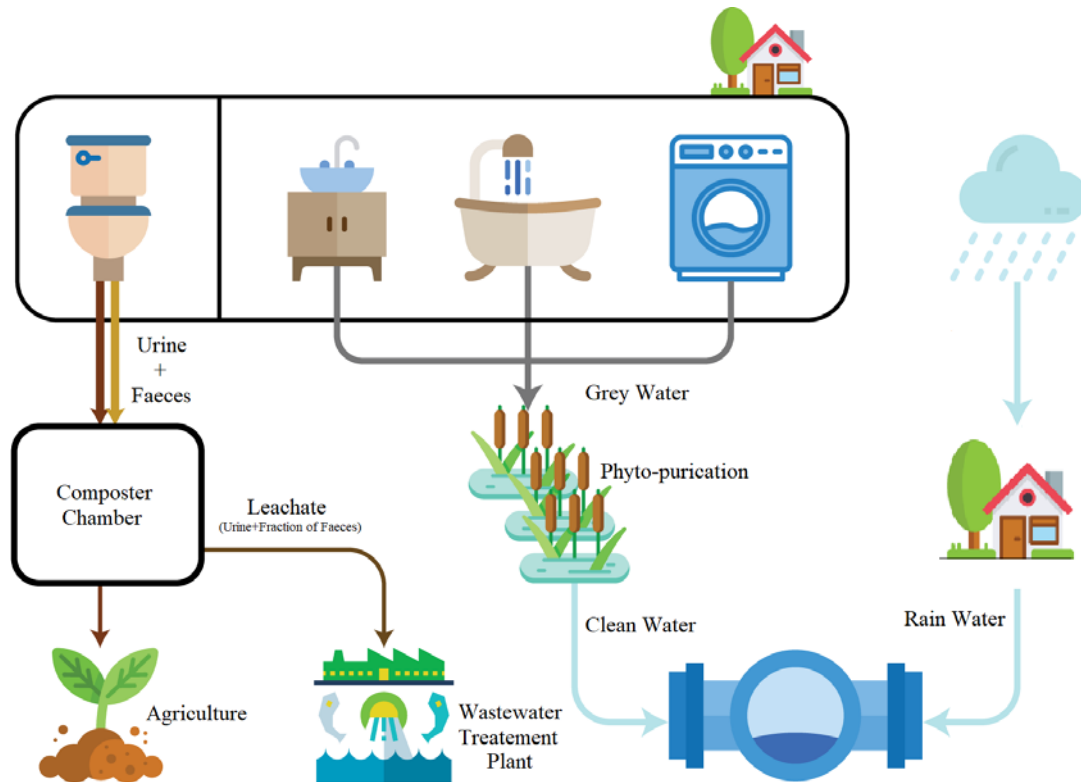


Figure 16: On-site sanitation (OSS) systems developed by atba architects office, cooperative equilibre, Geneva: a 50-users building were constructed with an objective of treating 100% of effluents and valorise the dejections (black water and urine) via composting and phyto-purification.

2.1.1 Phyto-purification for greywater (GW)

Greywater was treated separately through a system of phyto-purification. It is first decanted in a pit that collects most of the grease. Then it crosses a draining bed (with a waterproof bottom) composed of earth and gravel with *Phragmites australis* reeds planted on the top of it. The reeds have well-developed roots that provide enzymes and carbohydrates used by microorganisms to grow. They degrade organic matter and mineralise nitrogen and phosphorous, which will be available for plants. Reeds are well adapted to water-saturated soils and have a strong purification potential. After having crossed the system, the water is released clean in the rainwater sewer. The biggest constraint this system poses for the dwellers is to use biodegradable washing products to avoid harmful substances to the treating bacteria. An awareness of the habitants is necessary.

2.1.2 Composter chamber: Leachate effluent

Faeces and urine are collected through dry toilets installed on each at of the 3-floors building. Dejections are achieved in a tank in the basement by a vertical pipe. A fistful of wood chips is added to absorb urine and limit urease action, balance C/N ratio and improve compost quality. The toilet bowl of each apartment (13 apartments in total) is directly connected to the composting chamber/tank by a vertical pipe. The composting tank is divided into three compartments. The first one collects fresh matter where aerobic

bacteria start the composting process and decrease the dejection volume decrease by three to six-fold. In the second compartment, *Eisenia fetida* worms are maturing the compost by mixing, airing and maturing it. The compost produced is used in the gardens of the building. At the bottom of the composter, a brownish liquid consisting mainly of urine and organic fraction is the only fraction that is pumped into the conventional sewer system without any valorisation. In this thesis, the effluent was used as a feedstock for the hydrothermal treatment.

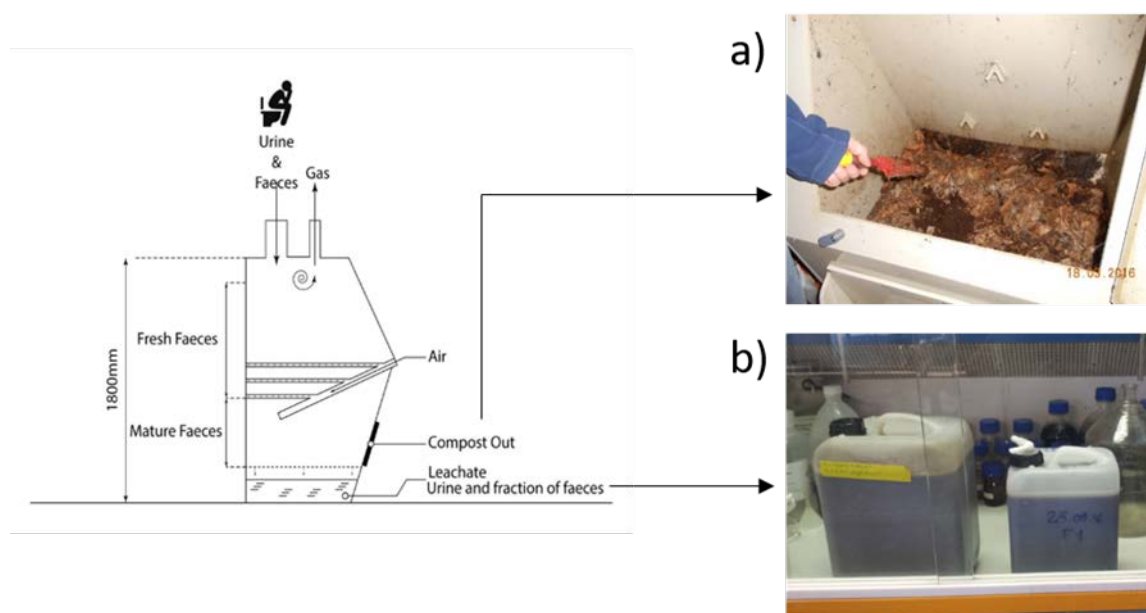


Figure 17: Composter chamber, a) fresh compost (2-month-old), b) Leachate effluent recovered at the bottom of the composter.

For the sampling, the automatic pumping of composters was switched off and done manually on the sampling day. This process allowed to accumulate leachate effluent produced between the performed samplings. The samples were transported in polyethylene high-density jerrycans (PE-HD) of 5 L. Daily sampling was performed in order to evaluate the fluctuation of the chemical composition. All samples were then stored in the fridge at 4°C prior to physical and chemical characterisations.

2.1.3 Leachate effluents analysis

2.1.3.1 Physical characterisation

The pH and conductivity were measured with a pH meter (In lab 735 ISM probe, Mettler Toledo). The salinity was measured with a salinity refractometer (Atago, master refractometer).

2.1.3.2 Chemical characterisation

Ion chromatography (Dionex ICS-3000): was performed to measure phosphates, nitrates, nitrites, ammonium, and other ions concentrations in the samples. Samples were diluted 200 times to fit the calibration range. The obtained results were used to calculate loads per person per day for inorganic nitrogen and phosphorus. Calculation is based only on the days when the total volume of effluent was collected.

Gas chromatography, coupled with mass spectrometry (GC-MS): Cyclic amide were quantified using gas chromatography coupled with mass spectrometry (Agilent Technologies 7802A) following a known method [90]. The separation was achieved with a Varian CP-sil 8 column (30 m×0.25 mm×0.25 µm) with helium at a flow rate of 1 mL/min. A 1µL injection of the extract was performed at 275°C.

Elemental analysis (CNS): The elemental analysis of Carbon, Nitrogen and Sulphur (CNS) was performed at the Chemical process and material lab at Paul Scherrer Institute (LECO TruSpec Micro instrument). Samples were previously freeze-dried, and thus, the results are presented on a dry matter basis.

Inductively coupled plasma optical emission spectroscopy (ICP-OES): ICP-OES was performed at the Chemical process and material lab at Paul Scherrer Institute to determine concentrations of several elements in the leachate samples. Aqueous samples were nebulised and sprayed into the argon plasma flame (temperature 6000-8000 °C) on a Varian Liberty 110 ICP-OES. The samples were acidified with a drop of concentrated HCl to assure that metals do not precipitate during sample storage. Leachate samples were digested for ICP-OES measurements with 6 mL HNO₃ and 2 mL HF according to the following method:

- Rotor 8SXF100 (MW3000 Microwave from Anton Paar), each vial (with TFM-Liner and high-pressure ceramic jacket) 200 mg algae sample, 3 mL HNO₃, 1 mL HF.
- Fan 1 (800 W - 5 min ramp - 40 min hold, 0 W - 0 min ramp - 20 min hold. - Fan 2, (cooling step), p-rate: 0.3 bar/s.
- Finally, a complexation step takes place with 12 mL H₃BO₃ (cold saturated): Fan1 (900 W - 0 min ramp - 30 min hold), cooling step.

2.1.4 Hydrothermal non-catalytic gasification of leachate effluent

Supercritical water gasification set-up was composed principally of a piston to feed the system at high pressure, an insulated and heated gasification tubular reactor, two filters, a gas-aqueous separator, a gas-meter and a bottle to recuperate the aqueous phase (AP). A tubular reactor (ID = 1.8 cm, L = 152 cm) of a total volume of 387 cm³ was used.

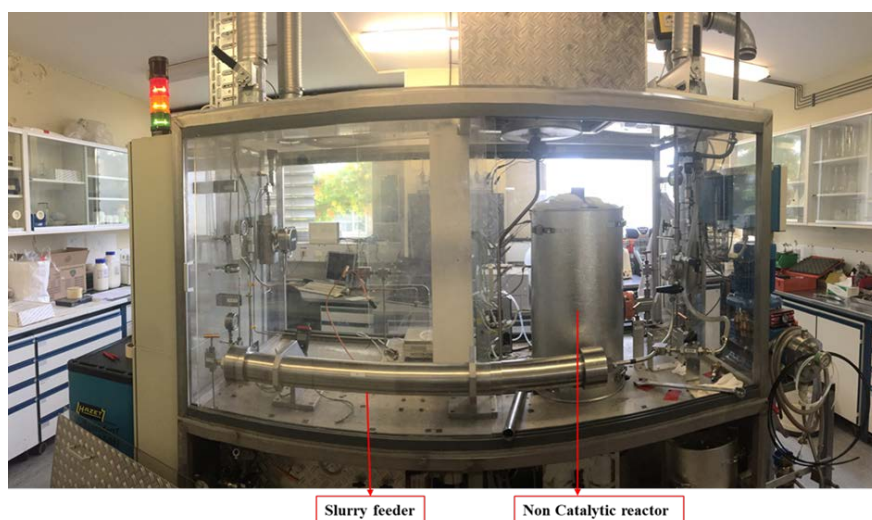
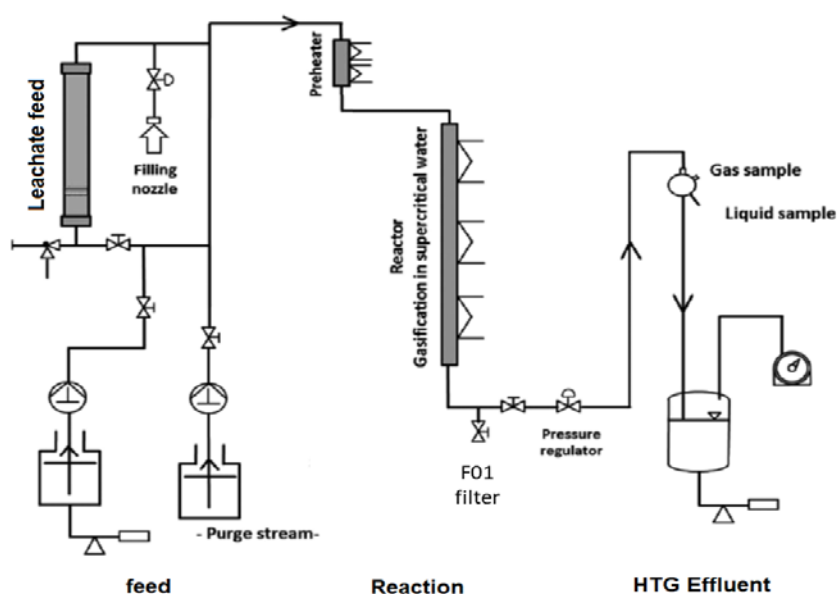


Figure 18: (top) Simplified schema of non catalytic hydrothermal gasification unit (Elena setup). (bottom) Photo of the Elena hydrothermal gasification unit, KIT Germany.

After leaving the reactor, the hot gaseous mixture was cooled down, its pressure relieved using a backpressure regulator (TESCOM), and the gas separated from aqueous phase AP (**Figure 19**), which was sampled, weighed and analysed. The volume of produced gas was measured using a gas meter (TG 3, Ritter Apparatebau GmbH) and analysed by a gas chromatograph (HP 5890, Hewlett Packard). Before experiments, several hours of cleaning by feeding pure water into the reactor were needed to remove any tar or residual biomass from previous tests.

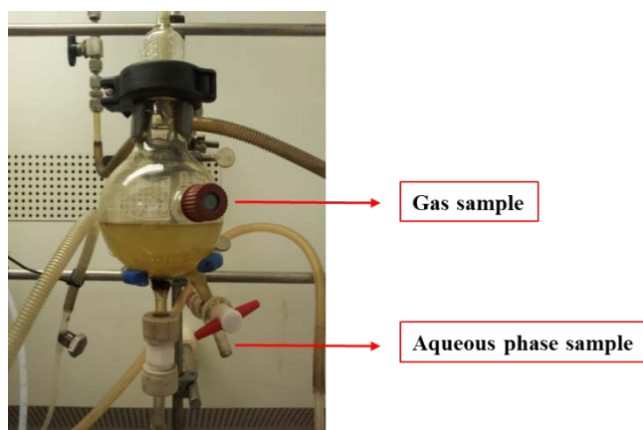


Figure 19: Gas separated from aqueous phase AP.

Experiment	Biomass conc [DW%]	Temperature [°C]	Pressure [bar]	Flow rate [g/h]	Duration [h]
M1	2.29	600	280	200	40.8
M2	2.29	600	280	350	5.1

Table 4: Parameters used during the non-catalytic hydrothermal gasification of Leachate effluent.

Experiment performed using continuous non-catalytic hydrothermal gasification and leachate as feedstock are described in **Table 4**. For all experiments, collected data represents steady-state operations as they were run for enough time before sampling and collecting data. Aqueous phases from both tests are referred to as AP1 and AP2. These effluents were recovered from being used later as a growth medium in the algae cultivation experiment.



Figure 20: F01 filter cleaning and recovery of precipitated salts.

The aqueous phase (AP1, AP2) were thoroughly characterised for its organic and inorganic contents. Total organic carbon, total inorganic carbon measurements were performed with a TOC, (Elementar) and ultimate analysis (elemental carbon, nitrogen and sulfur) was performed using a CNS analyser (LECO TruSpec Micro instrument). Conductivity, pH, and salinity were analysed.

HPLC-RI (1260 infinity, Agilent technologies) was used to determine the amount of organic acids, by means of a Biorad Aminex HPX-87H column at 60 °C coupled with a refractive index detector. The injection volume was 20 µL using 0.005M sulphuric acid as a mobile phase, and the flux rate was 0.6 mL/min.

(ICP-OES) was also performed to determine concentrations of several elements in the AP1 and AP2 samples. Cyclic amides were quantified using Ion chromatography (Dionex ICS-3000). The method was described previously in section 2.1.3.

Once an experiment was completed, the system was cleaned, and effluents from filter F01 and reactor were recovered for further analysis. The two primary effluents of the reactor are the produced gas that is diverted into a gas-meter (Ritter Apparatebau GmbH, TG 3) and the aqueous phase (AP) that is recuperated in a glass bottle which is weighted to monitor the production rate.

Carbon gasification efficiency and the mass balance of carbon, nitrogen phosphorus and sulfur were then calculated according to the formulas below:

- Total organic carbon conversion (X_c) from the feed to the reactor effluent was calculated according to the following equation:

$$x_{c(\%)} = \frac{m_{TOC\ Reactor}}{m_{TOC\ Feed}} \cdot 100\%$$

Equation 5: Total organic carbon conversion (X_c).

Where $m_{(TOC_{Reactor})}$ and $m_{(TOC_{Feed})}$ are the mass flow rates of carbon (TOC) in the reactor effluent and in the feed, respectively.

- Carbon gasification efficiency $GEc(\%)$ is the relation between the total amount of carbon in the gas phase the total amount of aqueous phase and the total amount of carbon in the feed, defined as:

$$GEc(\%) = \frac{mC_{Gas}}{mC_{Feed}} \times 100$$

Equation 6: Carbon gasification efficiency $GEc(\%)$.

Where mC_{Feed} is the mass flow rate of carbon in the feed and mC_{Gas} corresponds to the mass flow rate of carbon in the gas and the mass flow rate of carbon in the aqueous phase.

- The nitrogen, phosphorus and sulphur recoveries calculated during the experiments are expressed as:

$$N(\%) = \frac{mN_{AP}}{mN_{Feed}} \times 100$$

Equation 7: Nitrogen recovery $N(\%)$.

$$P(\%) = \frac{mP_{AP}}{mP_{Feed}} \times 100$$

Equation 8: Phosphorus recovery $P(\%)$.

$$S(\%) = \frac{mS_{AP}}{mS_{Feed}} \times 100$$

Equation 9: Sulphur recovery $S(\%)$.

2.1.5 Hydrothermal catalytic gasification of algal biomass

As the salt content in algal biomass is less critical than in the case of the leachate effluent, a hydrothermal gasification with the presence of a catalyst was preferred as it allows the conversion of organic carbon to methane at lower temperature and with a higher carbon conversion efficiency (avoid the deactivation of the catalyst in the presence of sulphur salts). The conversion plant consists of

six main sections: feeding section, salt separator, salt removal section, gasification reactor, pressure control, and release phase separator. The latter was described in detail elsewhere [89]. Briefly, microalgae biomass slurry was pumped at the desired flow rate to the salt separation unit (SITEC, stainless steel grade) using a hydraulic system. The salt separator has two outlets, one for delivering the liquefied feed to the gasification reactor (located at the top) and another for extracting the concentrated HT effluent (located at the bottom). The liquefied feed leaving the top of the salt separator was transferred to the catalytic reactor from the bottom (SITEC, stainless steel grade 1.4435; inner length, 1515 mm; inner diameter, 36 mm). The lower part of the reactor was filled with 713 g (on a wet basis, 5.2 wt. % H₂O) of a commercial ZnO adsorbent (Johnson Matthey Catalysts, KATALCO 32–5) containing 60–100 wt % of ZnO, and the upper part was filled with 493 g (on a dry basis) of a commercial 5% Ru/C catalyst (BASF).

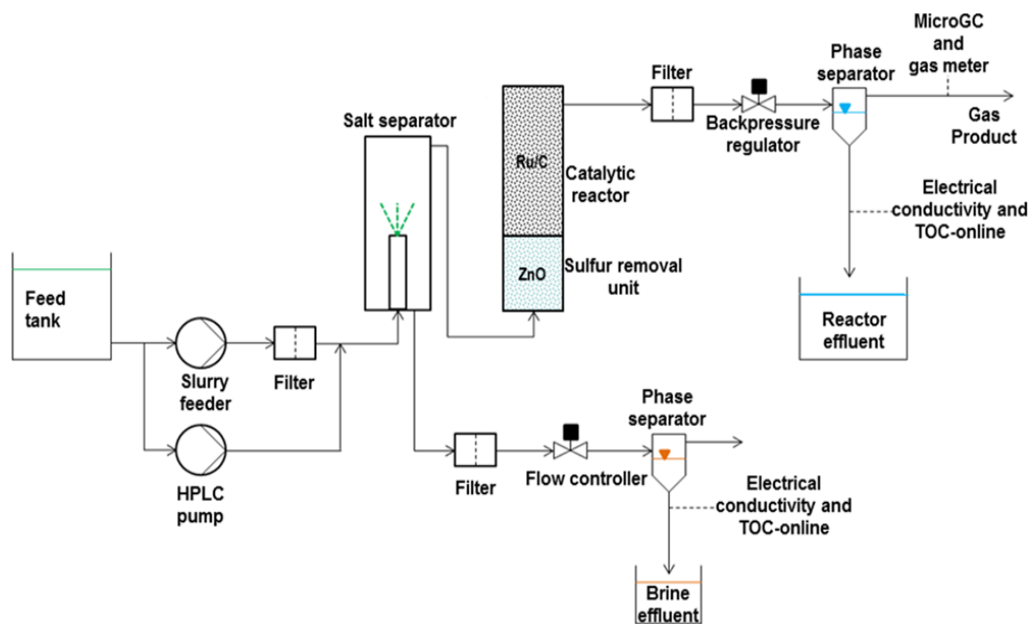


Figure 21: Detailed flow-scheme of the catalytic-hydrothermal unit at Paul scherrer institute, Switzerland [91].

Separation of different products at the end of the experiment was carefully performed starting with release of gases into gas bags while the liquid HT effluents, namely salt brine (SB, obtained from the salt separation unit, is a very rich effluent containing both inorganic and organic compounds) and reactor water (RW, collected from the gasification unit and providing a tiny fraction of inorganics) were vacuum filtered. A detailed flow-chart is displayed in **Figure 21**.

The elemental mass balance of HT effluent was calculated based on the element recovery in the aqueous phase. Once we determined the element distribution for the aqueous phase, the rest is considered to have entered the oil phase. The element recovery (% w/w) calculation is based on the ratio of the weight fraction of a particular element in the HT aqueous phase to the weight fraction of the same element in the original feedstock.

2.2 Microalgae growth experiments

2.2.1 Selected algae and growth medium

Two different growth mediums were used to growth *Chlorella vulgaris* (SAG 211-11B), *Chlorella sorokiniana* (SAG 211-32), *Haemotococcus pluvialis* (SAG 192.80), and *Scenedesmus vacuolatus* (SAG 211-8k), *Phaeodactylum tricornutum* (SAG 1090-1a). *Chlorella* species are known to be robust under stress conditions and used for the HT effluent growth tests. All microalgae strains were provided axenic from the culture collection of algae and protozoa ((SAG), Gottingen Germany).

Medium 1 'Doucha medium (DM)': DM was used for a maximum theoretical microalgae concentration of 2g/L. The nutrient requirements for the experiments were 0.3667 g CO(NH₂)₂, 0.0790g KH₂PO₄, 0.0680 g MgSO₄·7H₂O, 0.0133 g EDTA-FeNa, 0.0579 g CaCl₂·6H₂O, as well as trace elements: 0.277 mg/L H₃BO₃, 0.317 mg/L CuSO₄·5H₂O, 1.1 mg/L MnCl₂·4H₂O, 0.2 mg/L CoSO₄·7H₂O, 0.9 mg/L ZnSO₄·7H₂O, 0.057 mg/L (NH₄)₆Mo₇O₂₄·4H₂O, 0.005 mg/L (NH₄)VO₃. The pH was adjusted using NaOH at 7 (1M) [92].

For brackish water species such as *Phaeodactylum tricornutum* (SAG 1090-1a), an adapted f/2 medium was used. The pH was adjusted using NaOH at 7 (1M).

Medium 2 'Modified F2 medium': 75 mg/L NaNO₃, 5.65 mg/L NaH₂PO₄·2H₂O. Trace elements: 4.16 mg/L Na₂EDTA, 3.15 mg/L FeCl₃·6H₂O, 0.18 mg/L MnCl₂·4H₂O, 0.022 mg/L ZnSO₄·7H₂O, 0.01 mg/L CoCl₂·6H₂O, 0.006 mg/L Na₂MoO₄·2H₂O, 0.01 mg/L CuSO₄·5H₂O. Vitamins: 0.1 mg/L Thiaminhydrochloride (B1), 0.0005 mg/L Cyanocobalamin (B12) [93]. The solution is prepared in artificial saltwater (Instant Ocean, Aquarium Systems) with 20g/L of salts. Thus, all the above concentrations are given in mg per litre of artificial saltwater.

For culture system, microalgae growth tests were performed in batch mode using both open and close photobioreactor.

2.2.2 Microalgae growth kinetics

For measuring growth kinetics, cells daily counting was performed using an acoustic-assisted focusing flow cytometer (Attune NxT, Invitrogen), equipped with a 488 nm excitation laser. Forward-scattered light (FSC) and side-scattered light (SSC) are measured, and both give information on microalgae cells passing through the beam. FSC is positively correlated to the cell size, and SSC is positively correlated to internal cell complexity.

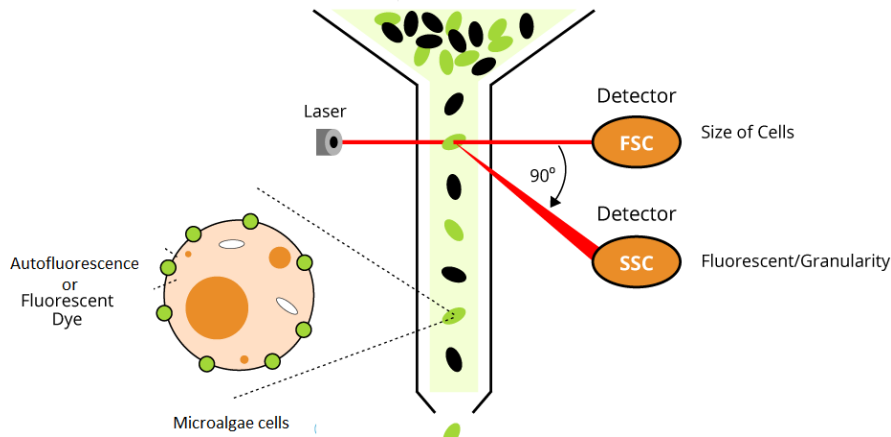


Figure 22: Flow Cytometry Fundamental Principle, adapted from [94].

Nonalgal particles were excluded from the analysis by setting an acquisition threshold on BL3 (emission of autofluorescence of chlorophyll-a at 670 nm) as a gate. Total cells present in a known volume of culture were counted, and cell density was subsequently calculated.

2.2.2.1 Specific growth rate

Specific growth rates (μ) expressed as day⁻¹ were calculated using the following formula:

$$\mu = \frac{\ln(N_t) - \ln(N_0)}{t - t_0}$$

Equation 10: Specific growth rates (μ).

For each cytometric parameter investigated, measurements were obtained on a logarithmic scale. Data were collected and analysed using the Attune software. All samples were carried out in triplicates.

2.2.2.2 Doubling time

The doubling time of a microalgae exhibiting exponential growth is the time required for this population to double. Cell doubling time can be calculated in the following way using specific growth rate:

$$T_d = \frac{0.693}{\mu}$$

Equation 11: Doubling time.

2.2.2.3 Dry weight (DW)

At the end of each experiment, biomass concentration was measured by filtering 10 mL of fresh sample on previously weighed and dried filters (0.22 µm cellulose acetate filter, Whatmann). Filters were dried at 85 °C for 3h. For each experiment, an average of 3 measurements was performed for the dry weight (DW) determination.

2.2.2.4 Pulse amplitude modulation Fluorometry (PAM)

Non-invasive fluorescence measurements were obtained using a PAM 2500 Chlorophyll Fluorometer (Heinz Walz GmbH, Germany) equipped with MKS-2500 chamber containing a micromagnetic stirrer for homogeneous measurements. Dark-adapted samples were incubated for 15 min, at 25 °C. Aliquots of 1mL samples were dispensed into Rapid light curves (RLCs) which were generated by applying a sequence of increasing actinic irradiance in 15 preset discrete increments ranging from 10 µmol photons m⁻² s⁻¹ to 1000 µmol photons m⁻² s⁻¹. Each actinic light incubation lasted for 10 s prior to a saturation pulse of blue light (0.6 s at 8 000 µmol photons m⁻² s⁻¹). The quantum yield of photochemical energy conversion $\phi(PSII)$, quantum yield of non-regulated non-photochemical energy loss $\phi(NO)$ and quantum yield of regulated non-photochemical energy loss in PS II $\phi(NPQ)$ were all measured every 24 h [95][96].

For dark acclimated autotrophic organisms, the reaction centres are open, and photosynthesis is at a maximum. Consequently, it corresponds to the minimum chlorophyll fluorescence, called F_0 . If a strong light pulse is applied, it closes the reaction centres, and photosynthesis is at its lowest value while the chlorophyll fluorescence is at its highest and the maximum of fluorescence is called **Fm**. For light-adapted samples, the maximum fluorescence is defined as **F'm**. All the listed below parameters were calculated automatically using PamWin-3 software.

The maximum quantum efficiency related to PS II described as F_v/F_m (variable to maximum fluorescence), gives information about the global health status of PS II. Low values are inherent to stress. It is determined as follows:

$$(F_v/F_m) = \frac{(F_m - F_0)}{F_m}$$

Equation 12: The maximum quantum efficiency related to PS II.

The quantum yield of photochemical energy conversion in PS II indicates the fraction of light energy converted in photochemical work. It is described as:

$$\phi(PSII) = \frac{(F'm - F)}{F'm}$$

Equation 13: $\phi(PSII)$, the quantum yield of photochemical energy conversion PS II.

where F is the fluorescence yield measured briefly before application of a saturation pulse.

The quantum yield of regulated non-photochemical energy loss in PS II $\phi(\text{NPQ})$ is calculated as:

$$\phi(\text{NPQ}) = \frac{F}{F'_m} - \frac{F}{F_m}$$

Equation 14: $\phi(\text{NPQ})$, quantum yield of regulated non-photochemical energy loss in PS II.

The quantum yield of the non-regulated non-photochemical energy loss in PS II $\phi(\text{NO})$ is given by the following equation:

$$\phi(\text{NO}) = \frac{F}{F_m}$$

Equation 15: $\phi(\text{NO})$, the quantum yield of non-regulated non-photochemical energy loss in PS II.

The sum of the three quantum yields is equal to 1:

$$\phi(\text{PSII}) + \phi(\text{NPQ}) + \phi(\text{NO}) = 1$$

Equation 16: The sum of the three quantum yields.

2.2.3 Microalgae growth using aqueous phase from HTG

C. vulgaris obtained from culture collection of microalgae (SAG, Gottingen), strain 211-11b was grown on Doucha medium with an inoculum containing an initial concentration of 10^5 cells/mL. The culture was incubated in a temperature-controlled incubator (27 ± 1 °C) at a light intensity of $180 \mu\text{mol photons m}^{-2} \text{ s}^{-1}$ measured on the surface of the cultures and a dark/light cycle of (8h/16h). Experimental conditions were set up for the growth of *C. vulgaris* in the aqueous phase by adjusting the nitrogen concentration (the key nutrient for algae) to be equal to that established for the commercial growth medium with a dilution factor of five. The inoculum came from an adapted pre-culture with the same cultivation parameters are described above. For growth kinetics, cells daily counting was performed using an acoustic-assisted focusing flow cytometer.

2.2.4 Microalgae growth for high-value product extraction

2.2.4.1 Microalgae cultivation and harvesting

C. vulgaris was cultivated in an open thin layer photobioreactor situated in a greenhouse on the Grüental campus of the Zurich University of Applied Sciences in Wädenswil, Switzerland. The design of the reactor has been developed at the Institute of Microbiology, Academy of Sciences of the Czech Republic, at Trebon [97]. With *C. vulgaris*, cultivation reaches a photosynthetic efficiency of approximately 7% and cell concentrations of up to 50 g/L [97]. In this study concentrations as high as 30 g/L were reached.

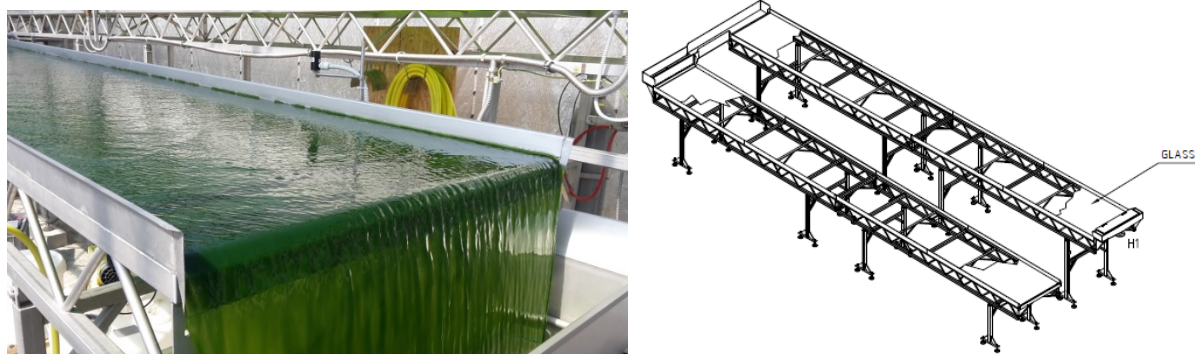


Figure 23: Open thin layer photobioreactor situated in a greenhouse on the Grüental campus of the Zurich University of Applied Sciences in Wädenswil.

The algal biomass was harvested using a conical plate centrifuge (Type SB7-47-076, Westfalia Separator AG), obtaining slurry with 20% dry weight content, and then stored at -20 °C. Before extraction, the microalgae biomass was then freeze-dried using a lyophiliser (CHRIST, LCG Iyo Chamber Guard) at -70°C and low pressure. As the experiment addressed extraction from both wet and dry biomass, the lyophilised biomass was either rehydrated to 50% moisture content or used directly without hydration (moisture content less than 5%).

2.2.4.2 Standard solution preparation and pigments quantification

Analytical and HPLC-grade solvents (acetonitrile, methanol, ethyl acetate and acetone) were obtained from Merck (Darmstadt, Germany). Trans carotenoids used as external and internal standards (astaxanthin, β -carotene, canthaxanthin β -apo-8'-carotenal, violaxanthin) were purchased from Sigma Aldrich, USA, whereas lycopene and lutein were purchased from AppliChem, Germany.

Before Accelerated Solvent Extraction (ASE), 0.2 g of lyophilised *C. vulgaris* was ground into powder with pestle and mortar. 5 mL of 80% acetone was added to the powder and followed by centrifugation at 2000 g for 6 min at 5 °C. The contents of chlorophyll a, chlorophyll b, total chlorophyll (a+b) and carotenoids in the supernatant were determined by measuring the absorbance (A) at 663, 646, and 450 nm, which are the major absorption peaks of these pigments. Concentrations were calculated, according to Jeffrey and Humphrey method [98]. The following calculations are relative to 80% of acetone extract and estimated as total extraction yield:

$$\text{Chlorophyll a } \mu\text{g/mL} = 12.25 (A_{663}) - 2.55 (A_{646})$$

Equation 17: Chlorophyll a content ($\mu\text{g/mL}$).

$$\text{Chlorophyll b } \mu\text{g/mL} = 20.13 (A_{646}) - 4.91 (A_{663})$$

Equation 18: Chlorophyll b content ($\mu\text{g/mL}$).

$$\text{Chlorophyll a + b } \mu\text{g/mL} = 17.76 (A_{646}) + 7.34 (A_{663})$$

Equation 19: Chlorophyll a+b content ($\mu\text{g/mL}$).

$$\text{Carotenoids } \mu\text{g/mL} = 4.69 (A_{440}) - 0.267(\text{Chl(a + b)})$$

Equation 20: Carotenoids content ($\mu\text{g/mL}$).

For the HPLC quantification, the standard stock solutions of β -carotene, violaxanthin, and lutein were prepared in 100% ethanol, while astaxanthin, lycopene and canthaxanthin were prepared in hexane. The internal standard solution was prepared by diluting β -

apo-8'-carotenal with acetone to a final concentration of 15 µg/mL. All the above solutions were stored at -20°C. Their concentrations were evaluated spectrophotometrically according to their specific absorption coefficients [99].

The concentrations of carotenoids (µg/g) were calculated using recovery factors relative to the internal standard (**Equation 21**). The recovery factor (RF) equalled the peak area of the internal standard in standard solution divided by the peak area of the internal standard after sample extraction.

$$W = RF \times \frac{\text{Amount of carotenoids in sample } [\mu\text{g}] * 100}{\text{sample weight } [\text{g}]}$$

Equation 21: Carotenoids content in (µg/g) of dry biomass.

Where W is the carotenoids content in µg/g dry biomass and RF is the recovery factor.

2.2.4.3 HPLC for carotenoid identification and quantification

Once the extraction was done and the solvents were evaporated under continuous nitrogen gas stream, the residues were resuspended in 5 mL acetone: hexane (2:3, v/v) and filtered with 0.2 µm hydrophobic PTFE filter prior to injection into the High-Performance Liquid Chromatography (HPLC) system. The composition of the carotenoid extract was analysed by HPLC coupled with a photodiode array detector, carried out in a Pelliguard LC18 guard column connected to a Vydac 201TP54 (250x4.6 mm) reverse phase C18 column. The injection volume of standards and samples was 15 µL. According to Strati et al. [99], the most appropriate solvent system was found to be composed of acetonitrile, 1-butanol and methylene chloride and applying a specific gradient elution as described in [99]. The UV-visible spectra were obtained between 450 and 570 nm. The flow rate was maintained at 1.5 mL/min and the column temperature at 25 °C.

2.2.4.4 Accelerated Solvent Extraction (ASE)

The homogenised samples in duplicates (respectively 1 g for dry and 2 g for 50% DW sample) were weighed on a precision balance with acceptance criteria of 0.0002 g.

Extractions were performed with two different solvents, namely 100% MTHF and a 1:1 mixture of MTHF and ethanol. An accelerated solvent extraction system ASE200 from Dionex Corporation (Sunnyvale, CA, USA) was used that was equipped with 11 cm³ stainless steel extraction cells, 40 cm³ collection vials, and a solvent controller unit **Figure 24**.

Extractions were performed at two temperatures (40 and 110 °C) for fixed times (15 and 30 min) and constant pressure (1500 psi, 103 bars). An extraction cell heat-up was carried out for a time, which changed depending on extraction temperature; 2 min heat-up was used when extraction temperature was set at 40 °C, and 6 min at 110 °C. After the extraction, the solvent was purged from the cell with N₂ gas and depressurisation did occur. Between extractions, a rinse of the complete system was made to avoid any extract carry-over.

The liquid extracts obtained were protected from light and stored at -20 °C until solvent evaporation with a continuous stream of gaseous nitrogen. Extraction yield was calculated as the ratio of the dry weight of extract to the dry weight of microalgae biomass used for the extraction.

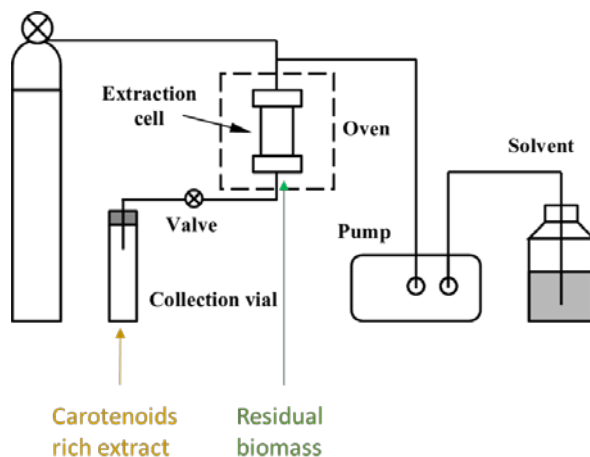


Figure 24: Detailed flow-scheme of the accelerated solvent extractor (ASE).

2.2.4.5 Elemental composition and High Heating Value (HHV)

Elemental quantification of carbon, hydrogen and nitrogen contents were done with a LECO TruSpec Micro instruments, and oxygen was quantified with LECO RO-478 device and sulphur was quantified with LECO CHNS-932 device. For the estimation of the High Heating Value (HHV), computation from Sokhansanj was used [100]:

$$HHV(dry) = 0.35 \times X_C + 1.18 \times X_H + 0.1 \times X_S - 0.02X_N - 0.1 \times X_O - 0.02 \times X_{ash}$$

Equation 22: High Heating Value (HHV) calculation.

Where X_i is the mass fraction (% mass dry basis) of compound i . In order to have a rough estimation of the ash mass fraction, the mass fraction of the elements was taken.

$$X_{ash} = 100 - [\sum X_i X_i]$$

Equation 23: Ash mass fraction calculation.

2.2.5 Microalgae growth using DSC-PBR technology

2.2.5.1 Dye sensitised solar cell module DSCs

The prototype of the designed DSCs panels used in the structure of the bioreactors were provided by SOLARONIX, Switzerland (Serial numbers, DSC-R:120216SX02; DSC-G: 160216SX01). Each DSC panel was made of two 100×100 mm glass substrates spaced by 4 mm for electrical contacts. The active part contained in a 65.1 cm² zone with 11 cells connected in series (each separated by 2 mm). The mesoporous TiO₂ film and iodide/iodine (I⁻/I₃⁻) redox couple were used as the semiconductor and the electrolyte, respectively. Among several dyes, two ruthenium complexes (N719-red panel and N749-green panel) were chosen as the light harvester to ensure high transparency in the wavelength range absorbed by microalgae culture. Additionally, a normal glass (T1) and a DSC panel without the dye (T1') were used as the reference in order to check the effect of the different material on the transmitted spectrum. In order to evaluate the contribution of the different materials in the absorbance of DSC panel, the UV–Vis Absorption Spectra were measured between 300–700 nm for DSC-R, DSC-G and DSC-T1 and T1'.

2.2.5.2 Power conversion efficiency (η) of DSCs

Solar cell efficiency refers to the portion of energy in the form of sunlight that can be converted via photovoltaics into electricity by the solar cell [101]. The open-circuit voltage, V_{oc} , is the maximum voltage available from a solar cell, and this occurs at zero current.

The short-circuit current is the current through the solar cell when the voltage across the solar cell is zero. The maximum power output (P_{max}) where the solar cell delivers most of its electrical power is determined by the maximisation of $V \cdot I$. The fill factor (FF) is defined as P_{max} divided by the product of I_{sc} and V_{oc} , which reflects the quality of a solar cell [101]. The overall solar energy to electricity conversion efficiency (η) is calculated by the ratio of the maximum output power to the intensity of the incident light (P_{in}).

$$FF = \frac{P_{max}}{I_{sc} \times V_{oc}}$$

Equation 24: Fill factor of a solar cell.

$$\eta = \frac{I_{sc} \times V_{oc} \times FF}{P_{in}}$$

Equation 25: Efficiency of a solar cell.

The nominal power (Peak Power or P_{max}) of a photovoltaic module or solar panel is determined by measuring current and voltage while varying resistance under defined illumination. The specific testing conditions are specified in standards such as IEC 61215,

IEC 61646 and UL 1703; specifically, the insolation level is 1000 W/m^2 , with a spectrum similar to sunlight hitting the earth's surface at latitude 35°N in the summer. A standard airmass of 1.5 and temperature of the cells at 25°C is assumed.

$$E = H \times \eta \times A$$

Equation 26: Electrical energy generated in the output of a photovoltaic system (losses not included).

E in kWh is electrical energy generated, H the annual average solar radiation on tilted panels (shadings not included), η = solar panel efficiency (%) and A = Total solar panel Area (m^2). Another formula can be used to calculate the energy production of the DSC module. This formula includes the performance ratio, which is a very important value used to evaluate the quality of a photovoltaic installation as it gives the performance of the installation independently of the orientation, inclination of the panel. It also includes all losses such temperature losses (5% to 18%), shadings and losses owing to presence of dust, snow (2%).

$$E = H \times \eta \times A \times PR$$

Equation 27: Electric energy generated in the output of a photovoltaic system (losses are included).

Where PR = Performance ratio, coefficient for losses (range between 0.5 and 0.9, default value = 0.75).

2.2.5.3 Microalgae culture and growth kinetics measurements

Starting culture of *C. vulgaris* and *H. pluvialis* tests were conducted at a constant temperature $25^\circ \text{C} \pm 1$ with an initial cell density of $1 \cdot 10^5$ cell/mL. Starting cultures were subject to a first adaptation period under low simulated solar light intensity. The growth tests were performed during two weeks inside the designed PBR-T1 (standard glass, T1). As shown in **Figure 25**, each PBR is divided into two equal compartments of 120 mL capacity each. All compartments of the bioreactors were continuously bubbled with 2% CO_2 /air mixture v/v and operated under feed batch condition. The pH was stabilised near 7 with a NaOH 1M solution. A 200 mL nutrient-rich medium 'Doucha medium' was used for a maximum theoretical microalgae concentration of 2 g/L.

For measuring growth kinetics, cells daily counting was performed using the Attune acoustic-assisted focusing flow cytometer (Attune NxT, Invitrogen) and total cells present in a known volume of culture and doubling time were subsequently calculated according to the formulas given in section 2.2.1. For each cytometric parameter investigated, measurements were obtained on a logarithmic scale. Data were collected and analysed using the Attune software. All samples were carried out in triplicates.

In addition, the quantum yield of photochemical energy conversion $\phi(\text{PSII})$, Quantum yield of regulated non-photochemical energy loss $\phi(\text{NO})$ and Quantum yield of regulated non-photochemical energy loss in PS II $\phi(\text{NPQ})$ were all measured every 24 h.

2.2.5.4 Experimental set-up

Figure 25 gives a short description of the experimental setup. The simulated light provided exposure very close to solar radiation using a solar simulator (XLS+, ATLAS) equipped with a sun cooling unit for temperature control. Growth experiments were performed during eight days in a designed DSC mini photobioreactor DSC-PBR divided on two equal compartments of 120 mL capacity each. Experiments with the two different DSC-PBR colours (green, red), the DSC-T1 and DSC-T1' controls were performed at two different constant light intensities 200 and 600 W/m^2 equivalent to 540 and 1620 $\mu\text{mol photons/m}^2 \text{ s}^{-1}$ of PAR respectively. The Irradiance profile of a typical summer day in Valais, Switzerland was used as a reference for the solar simulator XLS+. A day/night cycle of 12/12 was applied, and the temperature was fixed at 25 °C using the Sun cool unit of XLS+. A fixed gas flow rate with a mixture of 2% CO_2 was provided using a mass flow controller MFCs (red series, Vögtlin). All the sides of the DSC-PBR were covered with an aluminium foil to allow only light penetration through the DSC modules. All results were compared to the T1 and T1' control cultures. All samples were carried out in duplicates (biological duplicate)

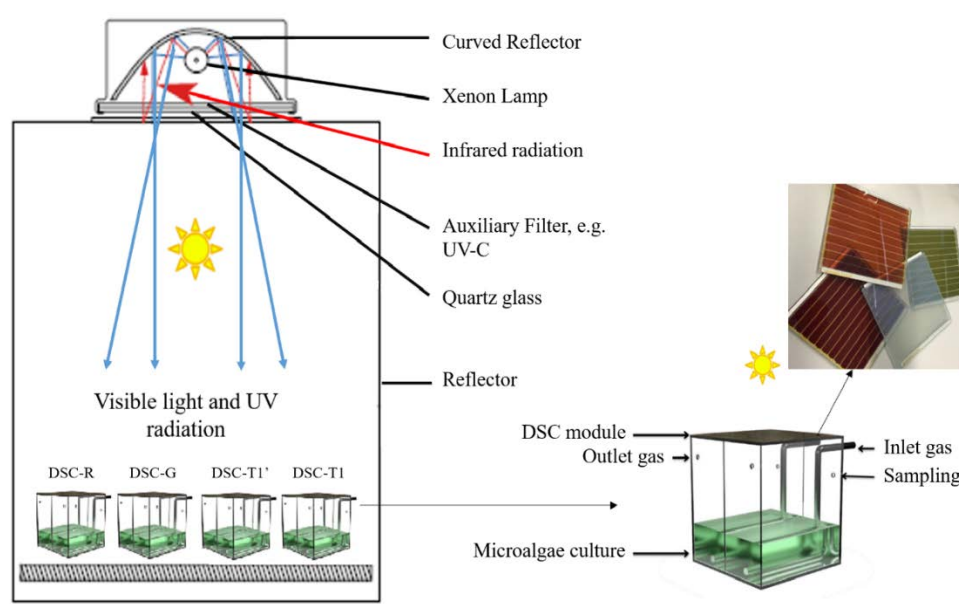


Figure 25: A schematic view of the experimental set-up inside the XLS+ solar simulator: DSC-G: Green DSC; DSC-R: Red DSC; DSC-T1': Blank DSC, DSC-T1: normal glass.

2.2.5.5 Lipids proteins and carbohydrate quantifications

For total protein determination, 5 mg lyophilised and freeze-fractured biomass (grinding in liquid nitrogen) was suspended in 2 mL 0.5 M NaOH and directly incubated for two h at 80 °C [102]. Total protein was determined using the Bio-Rad DC Protein assay.

Carbohydrate content was analysed using an adapted version of the phenol-sulphuric acid assay by Masuko et al., (2005) [103]. 2 mg of Lyophilised biomass samples were first resuspended in 280 μL aqueous solution and then a mixture containing 600 μL concentrated H_2SO_4 and 120 μL phenol was added. The sample was incubated for 5 min at 90 °C, cooled to room temperature, and the turbidity was measured at 490 nm.

The Bligh and Dyer method was used to extract total microalgae lipids [104]. Briefly, freeze-dried biomass (10 mg) was added to 1 mL solvent (chloroform and methanol in a 1:2 ratio) after thorough vortexing, the addition of 1 mL chloroform and water (1:1),

followed by centrifugation at 13,000 rpm for 15 min. The supernatants were collected and dried at 50 °C. The extraction process was repeated three times, and lipid content was measured gravimetrically; all the experiments were performed in triplicates.

2.2.5.6 Transmission electron in microscopy (TEM)

When the cells reached the stationary phase, 8 mL samples were taken from the cultures. They were given to the Bioelectron Microscopy Core Facility (EPFL) for fixation and embedding. Cultures were firstly centrifuged for 5 minutes at 1500 rpm and the supernatant was removed. A two-hour fixation with a solution of 2% paraformaldehyde (PAF) and 2,5% glutaraldehyde in cacodylate buffer (0.1M, 7.4 pH) was performed. Cells were washed three times with cacodylate buffer. Then, a mixture of 4% agarose low melting point in cacodylate (0.1M, 7.4 pH) was prepared, and the microalgae cells were subsequently suspended in this solution, centrifuged and put on ice for at least 15 minutes. Following this step, agarose gel was cut in small pieces and fixed as previously with a solution consisting of 2% PAF and 2,5% glutaraldehyde in cacodylate buffer for 30 minutes. The mixture was washed three times with cacodylate buffer. The cells were postfix with a solution of 1% osmium tetroxide and 1,5% potassium ferrocyanide in cacodylate buffer at room temperature for 40 minutes. Another post-fixation was performed with only 1% osmium tetroxide at room temperature for 40 minutes. The sections were washed twice with distilled water and stained in 1% uranyl acetate in water for 40 minutes. After a wash with distilled water, samples were then dehydrated using a graded ethanol series (50%, 70%, 2x96%, 2x100%) for 5 minutes each. Cells were firstly embedded in 1:1 Durcupan:100% ethanol for 1 hour with vials rotating continuously. The Durcupan was renewed and kept overnight. Finally, the resin was replaced again with fresh Durcupan for 4 hours. The resulting samples were embedded on coated glass slides and placed in an oven at 65°C overnight. The sections were thin-sectioned and ready for TEM observation. The instrument used was a Tecnai Spirit BioTWIN. It was equipped with a LaB6 gun, and observation was achieved at 100kV. The line resolution was 0,34 nm, and images were captured with a 4k x 4k FEI Eagle CCD camera with high sensitivity scintillator.

Chapter 3 A combined hydrothermal gasification-solid oxide fuel cell system for sustainable production of algal biomass and energy

Abstract:

Hydrothermal gasification treatment (HTG) is a process that allows the recovery of essential nutrients from wet biomass with simultaneous energy production. In this work, a new composter sanitary system operating without external connection to sewer pipes was used to test the suitability of its effluent as a feedstock for HTG process. Mainly, H₂ rich gas was obtained from the HTG process at 600 °C, 28 MPa. For an efficient power-generation system with low emissions, experimental results combining solid oxide fuel cells (SOFC) with the obtained gas from the HTG were performed. Thermodynamic calculations were performed on the gas compositions to evaluate the performance and the risk of solid carbon formation at a typical SOFC operation temperature 750 °C. Furthermore, for nutrient recycling purposes, the obtained nutrient-rich effluent from the gasification was used as a growth medium for microalgae *Chlorella vulgaris*. Finally, a complete valorisation chain based on both experimental study and model prediction that combine, energy conversion and microalgae valorisation was investigated.

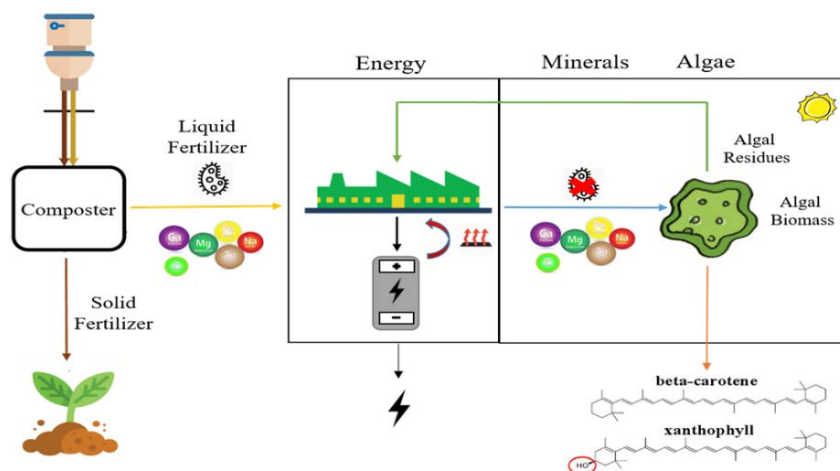


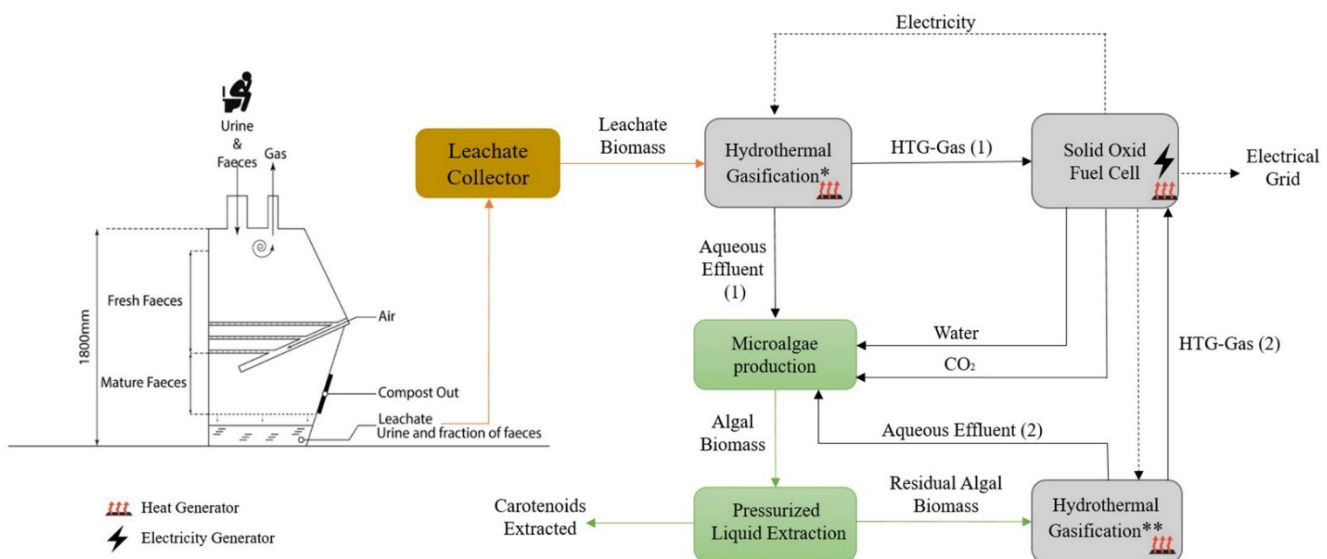
Figure 26: Simplified chart of the HTG-SOFC and microalgae production systems.

Material from this chapter has been published in:

(I) E. Damergi; H. Madi; S. Sharma; N. Boukis; F. Marechal et al.: A combined hydrothermal gasification - solid oxide fuel cell system for sustainable production of algal biomass and energy; Algal Research. 2019. DOI: 10.1016/j.algal.2019.101552.

The author performed the experiments with the hydrothermal gasification unit and the microalgae growth tests as well as the data treatment and characterisation of the leachate effluent. The author took the lead in compiling the first draft of the manuscript, resulting in the publication listed above.

The present work presents a complex concept based on combined hydrothermal gasification and SOFC processes with potential algal biomass production and biomass valorisation. Source separation of household waste streams was used to provide rich nutrient-feedstock for the HTG unit. Simulation results on the integration of SOFC and HTG are presented. Thermodynamic calculations were performed using the measured gas compositions to predict potential solid carbon formation at SOFC operating temperature of 750 °C. Finally, this work provides a description of possible sustainable production chains of biofuels and high-value chemicals using experimental and prediction data, as shown in **Figure 27**.



HTG: Hydrothermal gasification with or without a catalyst.

Figure 27: Simplified flow-scheme of the human faeces-composting chamber combined with HTG-SOFC and algae production unit. Biomass with low sulfur content was processed in the presence of a Ru/C catalyst, e.g. Residual algal biomass (**) (data reported from Damergi et al. (2017)). Biomass with high sulfur content was processed without the presence of a catalyst (this study), e.g. in the case of leachate (*).

3.1 Leachate effluents

3.1.1 Chemical characterisation of leachate effluent

The results of anion and cation analysis of the leachate effluent obtained from the composter 1 (family composed of 4 persons) are shown in **Figure 28**. A sinusoidal fluctuation trend was observed for almost all cations and anions. This behaviour could be due to the variation of composting chamber conditions (oxygenation and moisture content), the number of persons in reality present in the apartment and their diet. Moreover, ammonium and ammonia are in equilibrium and losses by volatilisation could occur. Nevertheless, ammonium and phosphate were found at high concentrations compared to conventional wastewater effluents. However, storage at low temperature was very important as nitrification or denitrification can change distribution between ammonium, nitrites and nitrates concentrations.

For stabilising the leachate sample composition, mixing the effluents from several families, as it would be the case in a decentralised district treatment system, could be a solution to homogenise the leachate by the higher effluent quantity of users.

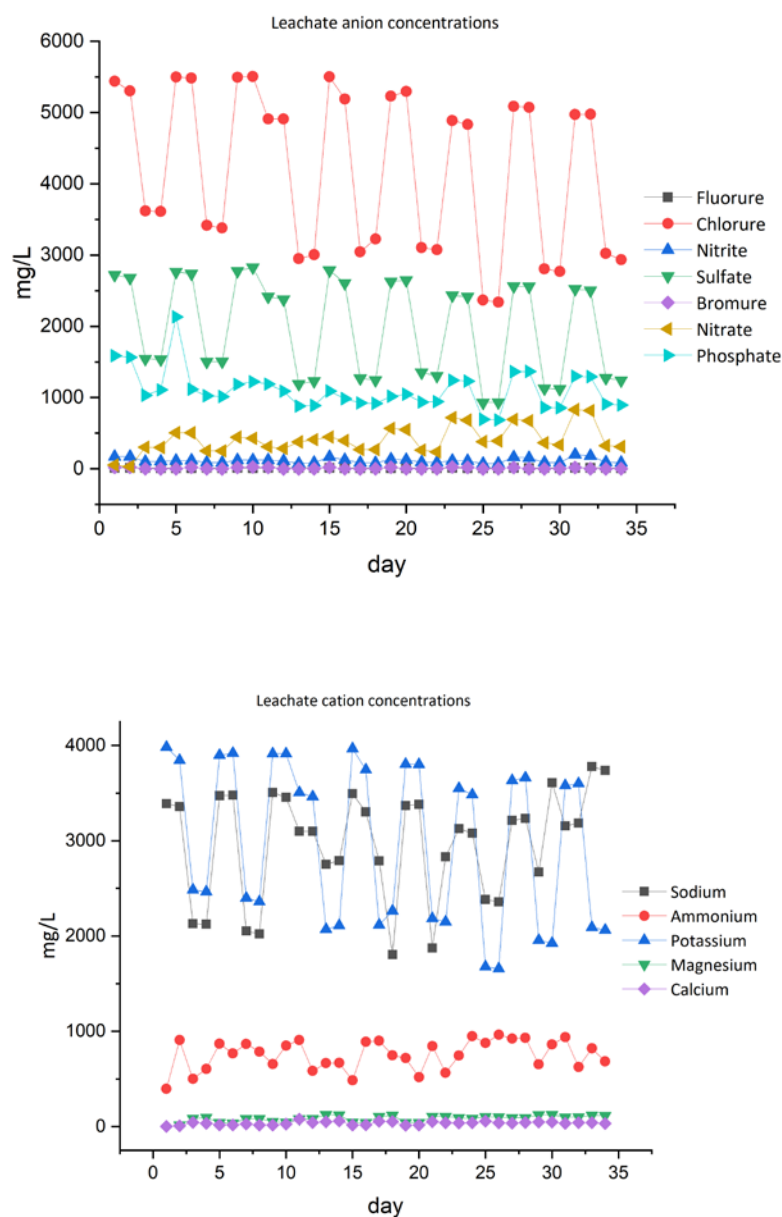


Figure 28: Leachate cation and anion concentration measured during 1-month period.

3.1.2 Non-catalytic hydrothermal supercritical gasification HTG

During M1 and M2 tests, H_2 -rich gas was produced as shown in **Table 5**. By contrast to the catalytic supercritical water gasification performed in the second part of this study at 400°C with the presence of Ruthenium catalyst, the main product gas was hydrogen H_2 instead of methane CH_4 . It is known that under supercritical hydrothermal gasification of biomass, Ru catalyst facilitates the C-O bond cleavage and therefore, the formation of CH_4 at relatively milder conditions [105]. However, with the absence of a catalyst, higher temperatures up to 600°C are required to achieve full biomass conversion. With a high S-containing compound present in the leachate biomass (up to 4 wt %), the use of catalyst was avoided. This is mainly due to the possible formation of a stable Ru-sulphate complex, which could deactivate the catalyst rapidly.

Gas composition (Vol%)	M1	M2	Gas composition* (Vol%)	M1*	M2*
H ₂	69.36 ±4.5	67.02 ±3.65	H ₂	57.2	52.2
CH ₄	10.6 ±2.8	14.10 ±4.10	CH ₄	8.7	11
CO ₂	17.5 ±4.7	16.88 ±3.5	CO ₂	14.4	13.3
C ₂ H ₄	0.44 ±0.13	0.29 ±0.01	H ₂ O	17.5	22
C ₂ H ₆	1.5 ±0.16	1.22 ±0.17			
C ₃ H ₆	0.32 ±0.18	0.23 ±0.08	C2 and above	2.2	1.5
C ₃ H ₈	0.43 ±0.03	0.25 ±0.01			

Table 5: Gas composition obtained after the hydrothermal gasification; the given results are mean values ± Standard deviation ($n = 10$), all the results were measured during the steady-state of the HTG experiment. * Gas composition used in the solid oxide fuel cell experiment; steam was added to avoid carbon deposition according to thermodynamic prediction.

A carbon conversion efficiency GE_c (%) of 41% and 43% were obtained for M2 and M1 tests, respectively. The low methane concentration shows that the methanation reaction is not favoured in the absence of the catalyst, as illustrated in **Table 5**. The losses on the carbon conversion efficiency were attributed to carbon deposition in the gasification reactor caused by the high inorganic content. Nevertheless, a long-term test of 40 h was achieved without any incident during the M1 test. This suggested that longer residence time favoured the carbon conversion into gas instead of carbon deposition inside the reaction as observed during the M2 test (only five of continuous gasification were achieved with clogging issues). **Table 6** illustrates the distribution of the salt within the different flows during M1 and M2 tests (feedstock and aqueous phase). Major anions and cations were recovered in the aqueous fraction and F01 filter, making possible their use as an algal growth media. The obtained aqueous phase showed high nitrogen recovery with 73%–74.4% for M2 and M1 tests, respectively. Most of the nitrogen was in the form of ammonium with the presence of other N-compounds, e.g., nitrogenous organics compounds (NOC's) and Maillard products, which explain the alkaline nature of the effluents. NOC's were absent in the leachate feedstock and present at low concentration in the AP, mainly: 2-pyrrolidinone, β -phenylethylamine as shown in **Table 6**. This suggested that NOC's were formed during the HTG processing of leachate as a degradation product of macromolecules. Similar results were obtained by Bagnoud et al. [40,90], where 87.5 (wt %) of nitrogen was recovered in the aqueous phase during HTG process, and NOC's detected in hydrothermal AP (More details about the NOC's are found in Chapter 4). Almost 92% and 71.3% of phosphorus recovered for M2 and M1 tests respectively. The slightly lower phosphorus recovery in M2 test compared to M1 was mainly due to the short residence time (350g/h vs 200g/h).

Achieving high phosphorus recovery was one of the objectives of this study. Besides being an essential nutrient for microalgae growth, phosphorus is a limited and vital resource. This makes phosphorus-recycling strategies one of the top priorities worldwide to slow down phosphorus consumption. Almost half of the sulfur content was recovered in the AP of M1 test. As sulfur gas compounds were not detected in the gas phase, sulfur deposition inside the reactor or/and the filter could explain the missing amount of sulfur. Others soluble organics such as carboxylic acids and phenols were detected in the AP. The analysis showed an initial concentration of phenols of 28.3 mg/L prior to the gasification, which increased up to 45.9 mg/L in the case of M2 AP and remained constant for M1 AP.

This is probably due to the short residence time during M2 experiment and incomplete degradation of macromolecules. As phenols are toxic for microalgae at relatively low concentrations [106], a dilution factor was considered for the algae growth experiment. Carboxylic acids compounds were also detected in the AP in both tests with a concentration of 33.46 mg/L. Lyophilised aqueous

phases samples obtained from M1 and M2 tests showed the presence of a high amount of salts recovered after the gasification, as illustrated in **Figure 29**.

Parameters	Unit	Leachate Feed (aq)		HTG AP (aq)	
		M1	M2	AP1 (M1)	AP2 (M2)
pH	-	7.16	7.20	9	9.2
Salinity	[g/l]	15 ±0.07	15.1 ±0.05	10 ±0.06	8 ±0.06
TDS		12.74 ±0.23	12.68 ±0.16	1.87 ±0.11	0.67 ±0.03
N		1.9 ±0.26		0.7 ±0.23	1.29 ±0.19
S	[Wt%]	4.2 ±0.31		2.3 ±0.18	3.73 ±0.04
C		7.3 ±0.13		2.3 ±0.09	2.65 ±0.1
Phenols	[mg/L]	28.3 ±0.36	28.7 ±0.32	29.4 ±0.24	45.9 ±0.39
Org. acids		21.2 ±0.27	19.4 ±0.14	33.46 ±0.47	25.4 ±0.5
TIC		710 ±1.26	689 ±0.94	490.1±0.80	307.4 ±0.57
P		815.89 ±0.66	776.74±1.35	740.2 ±0.55	535.3 ±1.3
Mg		53.96 ±0.65	83.55 ±0.94	0.8 ±0.11	<0,5
Ca		79.6 ±0.3	69.98 ±1.41	2.54 ±0.04	1.24 ±0.16
Na		3459,2 ±0.31	3196 ±3.87	1302.23 ±2.5	370.93 ±1.3
Cl		4110 ±3.56	3780 ±3.90	2135 ±3.21	351.2 ±1.85
K		4132 ±4.56	3830 ±4.6	2777.78 ±3.4	494.38 ±2.5
Ni		0.67 ±0.04	<0.5	1.09 ±0.22	<0,5
Fe		1.09 ±0.1	0.98 ±0.12	<0.5	<0.5
Nitrogen	2-pyrrolidinone	-	-	8.5 ±0.05	16,7 ±0.8
Aromatics					
compounds	β-phenylethylamine	-	-	2.2 ±0.02	3,05 ±0.1
NOC's					

Table 6: Elemental analysis of Leachate feedstock and the aqueous phase produced via hydrothermal gasification without a catalyst; AP(1) is the aqueous phase obtained from test M1 (200g/h feedstock) and AP(2) is the aqueous phase obtained from test M2 ((350 g/h feedstock). M1 and M2 feedstock were obtained both from the same homogenised leachate collector tank.); all values are given as value ± standard deviation (±SD) except wt%, were expressed as value ± relative standard deviation (%RSD). **TDS:** total dissolved solids, **TIC:** Total inorganic carbon.

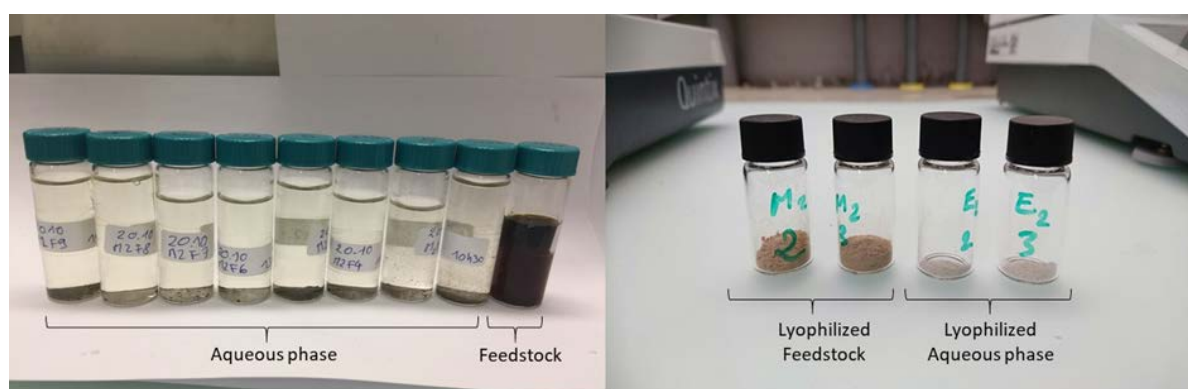


Figure 29: (Left) Visual aspect of the aqueous phase effluent samples taken during the gasification of leachate from M1 and M2 tests. (Right) Lyophilized feedstock and aqueous phase samples.

3.2 Microalgae growth tests: Cell size and autofluorescence of *C. vulgaris*

The analysis by means of flow cytometry of *C. vulgaris* cells showed a significant difference in autofluorescence and average cell size (t-test) among the control culture and aqueous medium experiments M1 and M2, as shown in **Figure 30**. This observation was

confirmed by the presence of a lag phase in both the cases; M1 and M2 medium compared to the control culture, **Figure 31**.

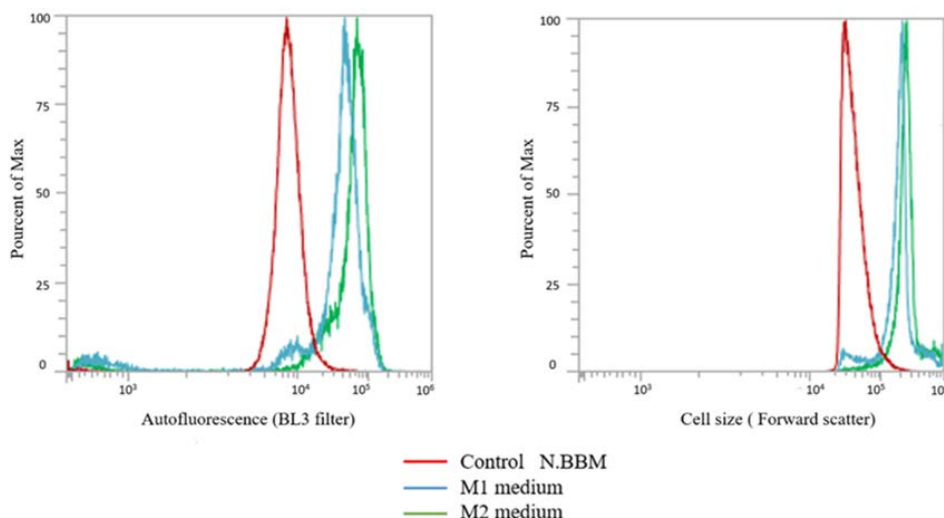


Figure 30: (Left) Autofluorescence intensity signal comparison between Control culture, M1 and M2 testes using BL3 filter. (Right): Average cell size comparison between Control culture, M1 and M2 testes using the forward scatter signal.

Residual organics detected in the AP effluent could modify the carbon uptake in microalgae, leading to a mixotrophic growth and in consequence, the observed slowdown could be associated with this shift in feeding metabolism [40]. Flow cytometry results for average cell size, given in **Figure 30** showed an increase of relative cell size for both M1 and M2 cells during the lag phase. The mean cell-size increased from 4.62 ± 0.98 to 7.53 ± 0.79 and 8.4 ± 0.78 μm , respectively, for control M1 and M2 cultures. The hypothesis for this increase in average cell size could be the inability of microalgae cells to undergo cell division. Nevertheless, cells were able to acclimate with the aqueous phase since in both cases M1 and M2, microalgae were capable of dividing after a period of adaptation with a specific growth rates of 1.12 day^{-1} for control and 0.64 day^{-1} and 0.54 day^{-1} respectively for M1 and M2. Total carotenoids content of both AP was slightly lower compared to the control $356.2 \mu\text{g/g DW}$, with $290 \mu\text{g/g DW}$ and $261 \mu\text{g/g DW}$ for M1 and M2 respectively.

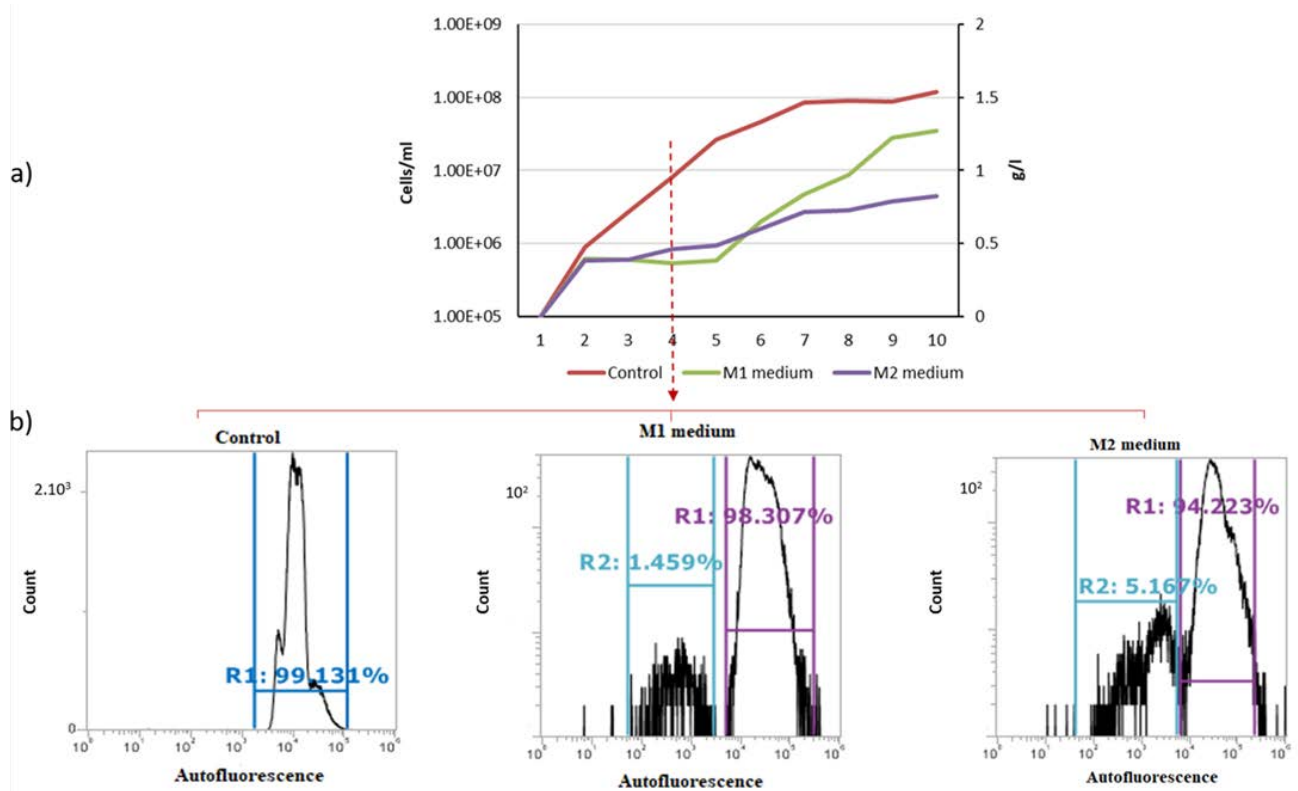


Figure 31: a) Growth rate curve of *C. vulgaris* using dilute aqueous phase from hydrothermal gasification of leachate. Control medium using standard control medium, M1 medium using aqueous medium obtained from test 1; M2 medium using aqueous medium obtained from test 2. b) Flow cytometry analysis of M1, M2 and control culture at day 4. The autofluorescence signal was acquired using BL3 filter (670 nm) where strong autofluorescence signal was detected in the control culture. This signal was used as a reference for M1 and M2 experiments. R1 and R2 gates were applied to differentiate respectively, normal microalgae cells from damaged ones.

3.3 SOFC performance

3.3.1 Thermodynamics of solid carbon formation

Thermodynamic calculations have been done to illustrate the chemical equilibrium behaviour of a C-H-O system under SOFC operating conditions. **Figure 32** shows the carbon disposition region at 750 °C for the two different fuel compositions that were used. Thermodynamic calculations show that the fuel compositions from M1 and M2 tests are within the carbon deposition region. One way to avoid carbon deposition is to add steam to the fuel gas. In this study, for the gas compositions, M1 and M2, and $\text{H}_2\text{O}/\text{CH}_4$ ratio of 2 (O/C ratio of 1.7) were considered [107] which shifts the gas composition to the carbon-free region as shown in **Figure 32**. In addition, when loading the fuel cells with current, steam is produced locally, which increases the oxygen content and helps the solid carbon to be removed. Based on these calculations, the gas compositions for the SOFC tests were chosen, as shown in **Table 5**.

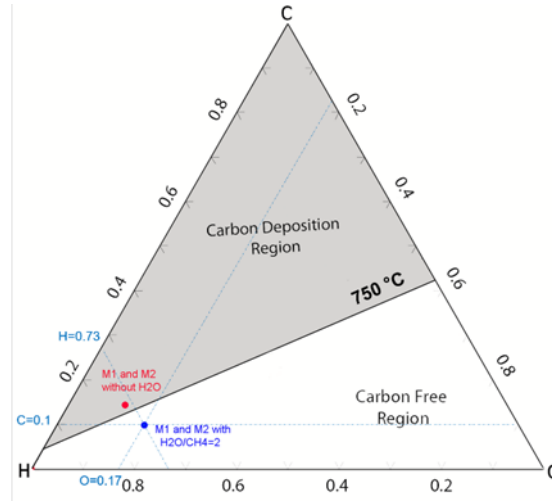


Figure 32: Carbon deposition region in a C–H–O phase diagram at 1 atm. It is calculated based on the anode feed balance.

3.3.2 Performance of Leachate-feed SOFC

3.3.2.1 Current-Voltage characterisation (I-V curve)

Current-voltage characterisation (I-V curves) was performed at the beginning of each experiment, and results are shown in **Figure 33**. The experimental open-circuit voltage (OCV) can be read from the I-V curves at zero current (maximum voltage). The theoretical OCVs are calculated using eq.28. Results are indicated in **Table 7**.

$$E_{OCV} = \frac{RT}{4F} \cdot \ln \left(\frac{P_{O_2,c}}{P_{O_2,a}} \right)$$

Equation 28: The theoretical open-circuit voltage (OCV).

where F is the Faraday constant 96,485 (C/mole), R the universal gas constant 8.314 (J/K.mole), T the temperature (K), $P_{O_2,c}$ the partial pressure of oxygen at the cathode side (0.21) and $P_{O_2,a}$ the partial pressure of oxygen at the anode side ($P_{O_2,a}$ is calculated using HSC Chemistry V7.1 software).

Gas composition	$P_{O_2,anode}$	Theoretical value	Experimental value	Error %
M1	$8.96E^{-22}$	1.033	1.02	-1.3
M2	$1.60E^{-21}$	1.021	1.00	-2

Table 7: Theoretical vs. experimental value of OCV for the gas compositions.

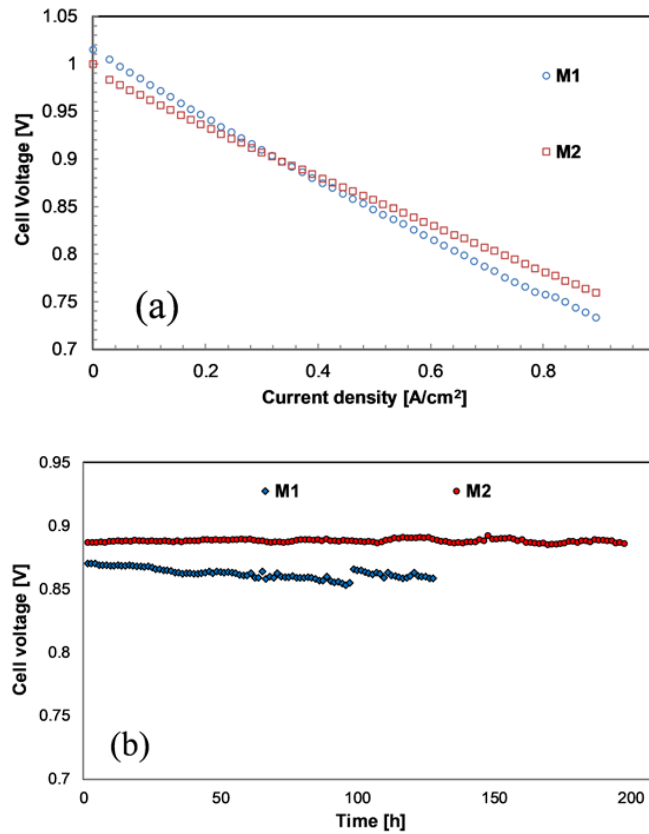


Figure 33: IV curves for the M1, M2 gas composition. **b)** Polarisation with time under a constant bias (0.3 A/cm²) for the different gas composition at 750 °C.

It is possible to read the total area-specific resistance (ASR) from the I-V curves, which indicates the total cell resistance and losses, i.e., activation, ohmic and concentration polarisations. The ASRs are calculated for the gas compositions M1, M2 to 0.32, and 0.26 $\Omega\cdot\text{cm}^2$, respectively. According to these results, the M2 gas composition has the lowest ASR and M1 higher ASR.

3.3.2.2 Polarisation with time

The fuel cells were polarized under a constant load (0.3 A/cm²), and the voltage was recorded with time. The pressure drop at the fuel inlet is also monitored over time. Decomposition of heavy hydrocarbons can lead to solid carbon formation at the fuel inlet tube. The increase in pressure drop indicates carbon formation. Solid carbon at the inlet blocks the fuel inlet over time, and consequently, a fuel shortage can occur. After dismounting these cells, some amount of solid carbon was detected at the fuel inlet, as shown in **Figure 34**.

For the case of M1, the degradation rate was >11%/kh. At time=100h, there was another jump in cell performance. At this time, it was decided to interrupt the experiment, to stop the higher hydrocarbons flow and inject more steam to remove the formed solid carbon at the inlet, as the pressure was increasing according to Figure 34. This interruption was only short (2–3h) to guarantee the continuation of the test.

Performance of the cell with the M2 gas composition was very stable. In this case, the degradation rate was only 0.23%/kh. M2 has the lowest amount of heavy hydrocarbons in the gas composition, which might explain the low degradation rate. The main reason for the higher degradation rates observed with M1 compared to M2 could be related to the difference in heavier hydrocarbons in the fuel flow, Table 5. They deposit on the active nickel catalyst area, block pores and reduce the TPBs, where the electrochemical reactions take place.

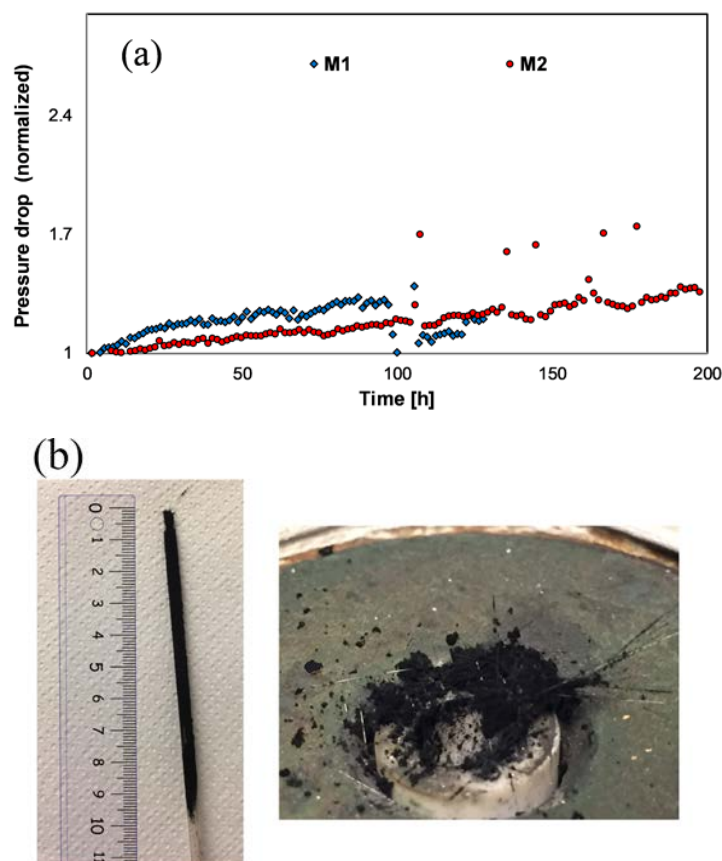


Figure 34: (a) Pressure increase with time for the three experiments, indicative of carbon deposits formation during SOFC operation. (b) Solid carbon formation at the fuel inlet (right) and on the evaporator tube which was inserted to the fuel inlet tube (left) – Test M1 – Test 1.

These experiments show that it is possible to operate SOFCs directly on gasified human leachate effluent. According to the results, a consistent and stable performance can be achieved if the amount of non-methane hydrocarbon is reduced. A gas cleaning section is required to reduce the amount of heavy hydrocarbons. Long-term stability tests are needed to specify the concentrations threshold level of these hydrocarbons.

3.4 Valorisation of bio syngas or H₂-rich gas

Initially, the leachate effluent has been collected and characterised as described previously and subject to hydrothermal gasification at 600 °C and 28 MPa. Mainly two outputs were valorised from the HTG, the produced biosyngas-1 and the aqueous phase. Based on the results obtained from the M1 experiment, 8 kg of feed/leachate produces 33.3 litres of biosyngas-1 and 7.761 kg of the aqueous phase. For nutrient recycling purposes, the aqueous phase was diluted five times and adapted as a growth medium for microalgae culture by adjusting the nitrogen concentration (the essential nutrient for algae) to be equal to that established for the commercial growth medium. With a total volume of 38.81 kg of growth medium and productivity of 1.3 g/L of algal biomass, a total of 50.4 g of microalgae biomass was produced.

After harvesting microalgae from the diluted residual water, the concentrated microalgae (sedimentation followed by centrifuge) are sent to the pressurised liquid extraction unit for extracting carotenoids. The pressurised liquid extraction results shown in **Figure 35** are based on the previous experimental study (Damergi et al., 2017) [100]. 1 kg (or 2 kg with 50% moisture) of *C. vulgaris* is used as basis for the valorisation chain of effluents from composted human excreta (M1 experiment). Hence, the feed/leachate,

Chapter 4 Recalcitrant nitrogen containing organics from the hydrothermal conversion of algal biomass

Abstract:

This Chapter evaluated the possibility to treat the Hydrothermal (HT) effluent by growing microalgae while producing renewable algal biomass. The HT aqueous product besides harbouring N, P and other essential nutrients, presents a small fraction of organic compounds rarely studied. Therefore, the extraction of heteroaromatic compounds in the HT effluent was the target of the present research which were profiled using GC-MS and LC-MS-MS. The results indicate the presence of cyclic amides, piperazinediones, amines and their derivatives. The most prominent N-containing organic compounds (NOC's) in the extracts were carefully examined by their effect on microalgae, namely 2-pyrrolidinone and β -phenylethylamine (β -PEA). These two substances have been prepared at three different concentrations (10, 50 and 150 ppm). This toxicity bioassay used three different microalgae strains: *Phaeodactylum tricornutum*, *Chlorella sp* and *Scenedesmus vacuolatus*. The confirmed IC50 was for all cases approximately 75 ppm. Experimental conditions were set up for the growth of microalgae in the aqueous phase by adjusting the nitrogen concentration (the key nutrient for algae) to fit the one established for a known commercial medium. The values of specific NOC's have been lowered to concentrations of 8.5 mg/L 2-pyrrolidinone; 1 mg/L δ -valerolactam and 0.5 mg/L β -PEA.

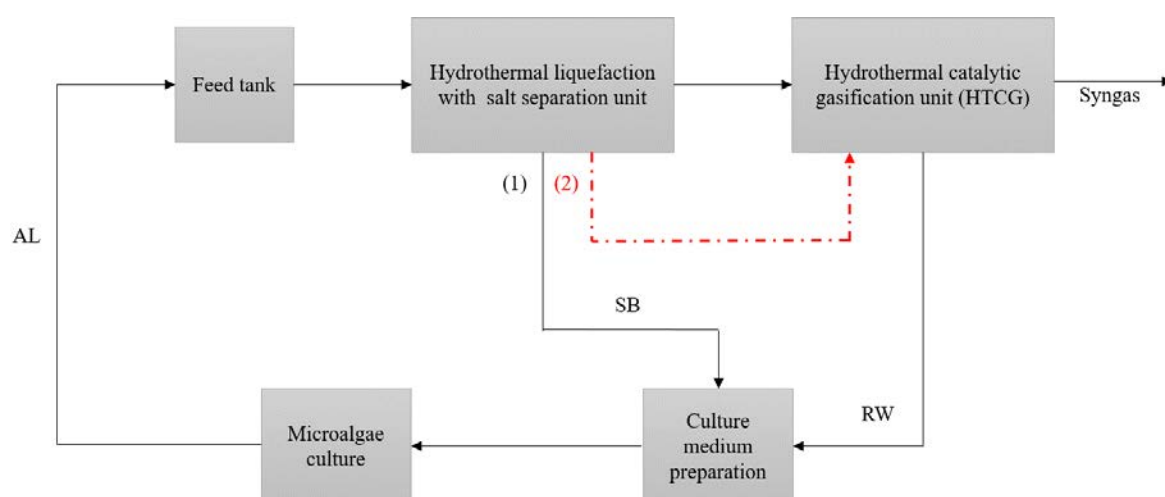


Figure 36: Simplified flow-scheme of the continuous-flow system, SB: Concentrated salt brine effluent (high salt and organic content), RW: Reactor water (low salt and organic content) used to dilute the SB, AL: algal biomass, (1): Direct use of SB in the preparation of algae culture medium, (2) Treatment of SB via hydrothermal catalytic gasification when NOC'S reaches toxic concentrations upon continuous recycling.

The growth using the diluted HT solution was kept constant, with no evidence of inhibition. An additional test was performed to address the possibility to implement an integrated water clean-up step making use of the existing hydrothermal catalytic facility. The conversion of NOC's to ammonium was successfully achieved.

Materials from this chapter has been published in:

(I) M. Bagnoud-Velásquez; E. Damergi; G. Peng; F. Vogel; C. Ludwig: Fate and reuse of nitrogen-containing organics from the hydrothermal conversion of algal biomass; Algal Research. 2018-04-21. DOI: 10.1016/j.algal.2018.04.00

The author performed all experiments as well as the data treatment. The author contributed to the compiling and the reviewing of the manuscript, resulting in the publication listed above.

4.1 Distribution of hydrothermal liquefaction products and carbon elemental mass balance

The microalgal slurry was successfully converted into oil with a yield of 31 %, while the SB aqueous phase represented 64 % of the same. The gas yield was not directly measured, but from the HT conditions applied, it was estimated to account for 5 % and consisted mainly of CO₂ with minor contributions of H₂S and NH₃ traces. Carbon recovery in the oil phase was as high as 80 %. This proportion was also confirmed with CNS analysis in the SB aqueous fraction with a measurement of 15 % carbon recovery. Carbon elemental mass balance additionally confirmed the assumption of 5 % CO₂ gas product.

Feed	Dry matter	Slurry feeder freq.	Time On stream	mZnO	mcat.	XC	Gas composition [vol %]			
	[wt%]	[kg/h]	[h]	[g]	[g]	[%]	CH ₄	H ₂	CO ₂	CO
<i>P. tricornutum</i>	3	1	7	529	444	75.1	36	57	7	0
<i>C. vulgaris</i>	3	1	7	529	444	74.5	39	53	8	0

Table 8: Process parameters of hydrothermal catalytic gasification of *P. Tricornutum* and *C. vulgaris*.

4.2 Organic composition of the salt brine effluent

The HPLC analysis showed a high diversity of organic acids such as oxalic 0.29 g/L, acetic 0.09 g/L, propionic 0.07 g/L and tartaric 0.02 g/L being the most important ones. The presence of these compounds is of interest, as they represent a potential carbon source for microalgae and could enhance the algae growth. According to literature, oxalic acid is formed by direct oxidation of monosaccharides from carbohydrates during the hydrothermal treatment [110]. Depending on the algae species, this organic acid may or may not be metabolised by the microalgae. However, acetic acid is a very interesting carbon source owing to its low molecular weight and is easily metabolised in the glyoxylate metabolic pathway of microalgae. Propionic acid is another observed organic acid that could promote algae growth. Nevertheless, its assimilation by microalgae depends on a series of more complex steps in the conversion pathway to acetyl Co-A [111]. Additionally, ethanol and glycerol were present in the SB aqueous phase. Those compounds are produced from the rapid hydrolysis of unstable fatty acids during hydrothermal treatment [112]. It is important to mention that the sample exposed to lower temperatures showed a higher amount of glycerol and a lower amount of ethanol. At temperatures higher than 370 °C, glycerol degrades into ethanol, acetaldehyde, methanol, and some other compounds [112,113]. This result is of interest when recycling the hydrothermal effluent as glycerol is known to stimulate the growth of some microalgal species, in particular, *P. Tricornutum* [114,115].

At the hydrothermal conditions applied, the formation of complex compounds with cyclic structures and N heteroatoms is expected. The organic nitrogen content was calculated as proteinaceous nitrogen and was equivalent to 375 mg/L. Therefore, a more detailed characterization of these compounds was mandatory in order to determine the complexity of the structure and the possible recalcitrant nature. These NOC's may be difficult to degrade due to their stability. By far, the most studied intermediates in toxicity assessments are the phenols. However, the phenol concentration of the HT effluent apparently depends on protein content and temperature and maybe strongly variable throughout the experiments. The study of N-containing organics such as amides, which, for instance, are more biologically recalcitrant than other forms of organic nitrogen is highly relevant [116]. The main organic compounds present in SB effluent studied besides carboxylic acids and alcohols were amines, alkylpyrrolidones, cyclic amides and traces of piperazinediones **Figure 37**. The presence of these soluble organics is the main source of potential inhibitors even if some of them may be used as a carbon nutrient for microalgal growth. Kruse et al. [117] suggested that the products of carbohydrate and protein degradation react with each other forming free radical scavengers such as cyclic NOC's via Maillard reactions, which are highly stable. All organic compounds identified in different SB aqueous phases are listed in **Table 9**.

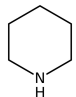
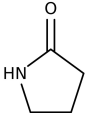
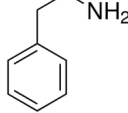
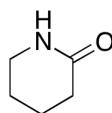
Compounds	Piperidine	2-Pyrrolidinone	β -Phenylethylamine	2-Piperidinone (δ -valerolactam)
Molecular structure				
Molar mass	85.14 g mol ⁻¹	85.11 g mol ⁻¹	121.1796 g mol ⁻¹	99.13 g mol ⁻¹
Density	0.8606 g·cm ⁻³	1.116 g cm ⁻³	0.965 g cm ⁻³	1.073 g cm ⁻³
Boiling point	106 °C	245 °C	200 °C	265 °C
Melting point	-7 °C	25 °C	-60 °C	38 to 40 °C
Solubility in water	Miscible	Miscible	Miscible	Miscible
Color	Colorless	Colorless	Colorless	Colorless
Volatility	High volatility	Low volatility	Low volatility	High volatility

Table 9: Main NOC's used in this study: chemical structure and physical properties.

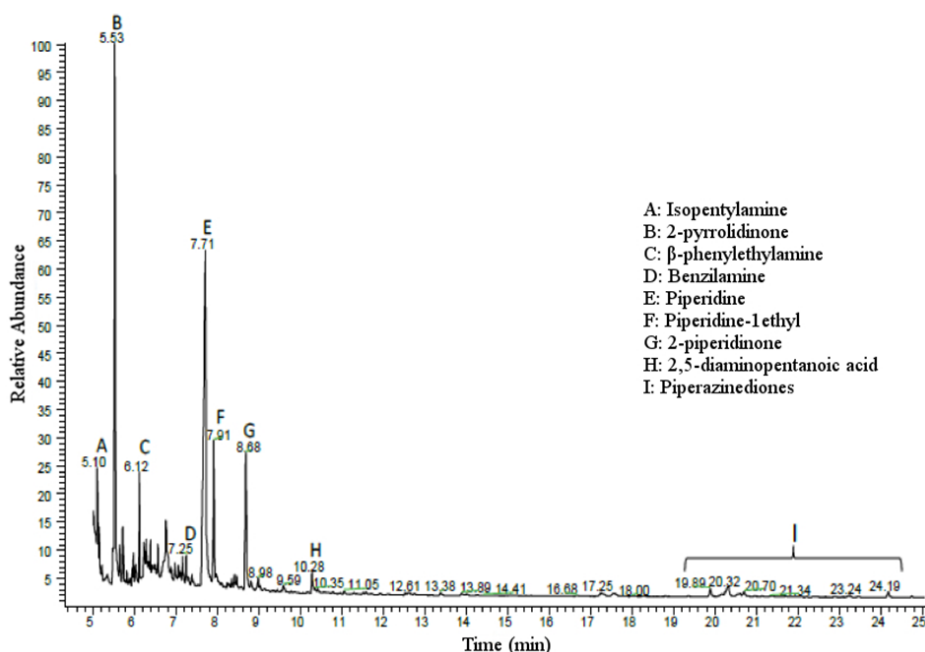


Figure 37: GC-MS chromatogram showing the different NOC's detected in the salt brine

The most prevalent compounds obtained in the SB effluent after application of the heteroaromatic extraction method were 2-pyrrolidinone (193 mg/L); β -phenylethylamine (16 mg/L) and 2-Piperidinone (42 mg/L). Even if pyrrolidones are frequently used to replace low volatile and toxic organic solvents, they are very stable compounds and of concern, as they are not degraded via hydrolytic pathways. The formation pathways of these compounds were studied. For instance, pyrroles and indoles are the major liquid phase heterocyclic NOC's resulting from the hydrothermal treatment of algae proteins [118]. Indole itself could form pyrroles during its conversion at high temperatures [119]. Pyrroles probably originate from proline [120]. β -phenylethylamine (PEA) was established via decarboxylation of phenylalanine during HT as phenylalanine is an amino acid present in algae proteins. However, the effect of these substances on the growth of microalgae was not thoroughly studied in the literature.

	Compounds	SB (step1)	SB (step 2)
Ultimate analysis (mg/L)	TN	1828 \pm 6.4	1627 \pm 2.1
	COD	14250 \pm 45.8	1267.3 \pm 1.5
	TOC	5392 \pm 2.33	85.9 \pm 0.5
	NH ₄ ⁺	889 \pm 5.14	950 \pm 2.41
	NO ₃ ⁻	24 \pm 1.23	28.5 \pm 1.4
Organic acids (g/L)	Oxalic acid	0.29 \pm 0.03	DL
	Tartaric acid	0.02 \pm 0.01	
	Glycerol	0.14 \pm 0.02	
	Acetic Acid	0.09 \pm 0.02	
	Propionic acid	0.07 \pm 0.015	
	Ethanol	0.19 \pm 0.012	
Phenols (mg/L)	Phenol	45.5 \pm 0.33	15.2 \pm 0.07
	Benzilamine	NQ	NQ
Nitrogen-containing organics NOC's (mg/L)	2-pyrrolidinone	193.04 \pm 0.5	33.4 \pm 0.15
	β -phenylethylamine	16 \pm 0.21	DL
	2-piperidinone	42.14 \pm 0.8	DL
	Isopentylamine	NQ	NQ
	Piperidine	148 \pm 1.58	DL
	Piperidine 1-ethyl	36.5 \pm 0.9	DL

Table 10: Organics compounds in the salt brine of *P.tricornutum* before the treatment (1) and salt brine after the treatment via hydrothermal catalytic gasification (2); NQ= not quantified, DL= below detection limit; mean values are given \pm SD (n=3).

4.3 Toxicity microalgal assay

The influence of increasing concentrations of 2-pyrrolidinone and β -phenylethylamine on microalgae cell densities during a timespan typical of an experiment (96 h) may be observed from growth curves displayed in **Figure 38**. The performed tests show that these individual NOC's are negatively affecting the microalgal growth rate when compared to controls. A complete growth inhibition of all microalgae strains was evident when treated with the two substances at 150 ppm. At 50 ppm, PEA also caused complete growth inhibition of *P. tricornutum* while the other two strains presented a decrease of about 30 % on the growth rate compared to the control. A concentration of 50 ppm 2-pyrrolidinone had the same effect on all strains, reducing their growth rate by approximately 30 %. Finally, with the 10 ppm treatments, the growth rate of all species tested diminished by 10 % compared to the control. The IC₅₀ for all cases is roughly 75 ppm. This value is similar to that obtained for 2-pyrrolidinone in a guideline study where an IC₅₀ of about 84 mg/L after 96-hours was found for an algal growth inhibition test. An IC₅₀ of 500 mg/L was also reported in another algal growth inhibition test but using 1-methyl-2-pyrrolidinone [121]. The results obtained represent the toxicity threshold for a single NOCs. This limit can be reached easily as these compounds are very recalcitrant.

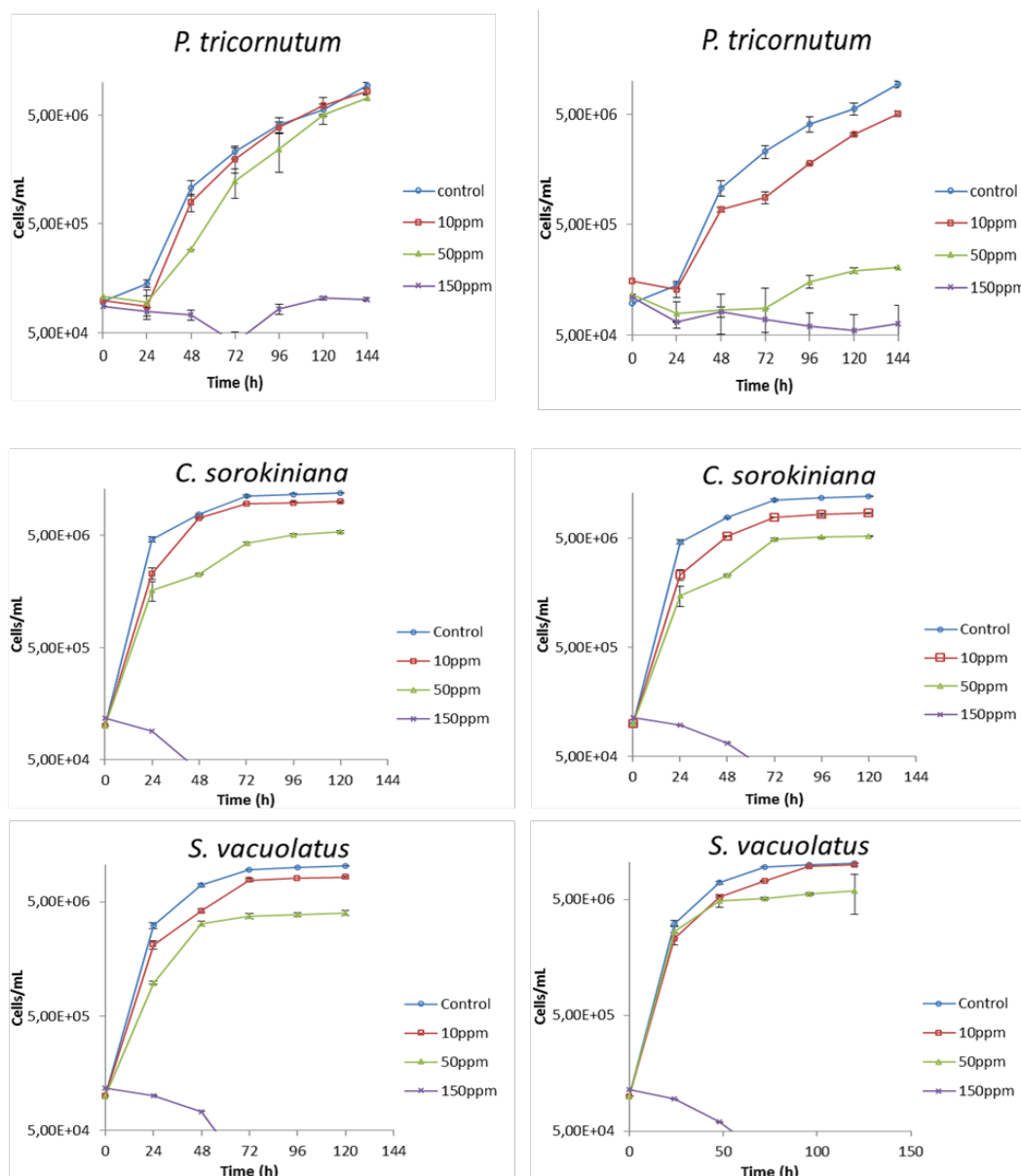


Figure 38: Microalgae toxicity assay with 2-pyrrolidinone (left) and β -phenylethylamine (right) with three microalgae species *P. tricornutum*, *C. sorokiniana* and *S. vacuolatus*. All experiments were performed in triplicate; mean values are given \pm SD (n=3).

The next test consisted of growing *P. tricornutum* in diluted SB effluent and to see whether or not a combined effect of these substances could enhance/suppress toxicity. Experimental conditions were set up for the growth of microalgae in the aqueous phase by adjusting the nitrogen concentration (the key nutrient for algae) to fit the one established for the commercial F2. A dilution of 20 was required to adjust the total N to an initial concentration of 233 mg/L. The concentration values of specific NOC's studied were lowered to 8.5 mg/L 2-pyrrolidinone; 1 mg/L δ -valerolactam and 0.5 mg/L PEA **Figure 39** shows the growth of *P. tricornutum* with the diluted SB aqueous phase.

The typical lag phase reported in previous work [120] was not evident here as the inoculum originated from an adapted pre-culture. *P. tricornutum* cultivated in the SB effluent first showed fast and more extensive growth until the third day when compared to the control. From the third day on the culture entered a stationary phase, whereas the control still exhibited an exponential growth.

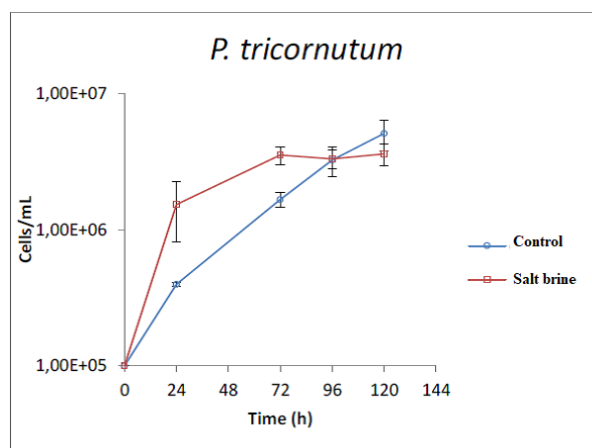


Figure 39: *P. tricornutum* toxicity assay using 20-fold diluted salt brine effluent. All experiments were performed in biological triplicate; mean values are given \pm SD (n=3), *P. tricornutum* control cultures were prepared with modified F2 medium.

The fast growth and subsequent shortening of the exponential growth phase in cultures using SB effluent as growth media was certainly related to the presence of organic compounds supporting mixotrophic growth. This has been confirmed from trends of the COD and TN curves displayed in **Figure 40**.

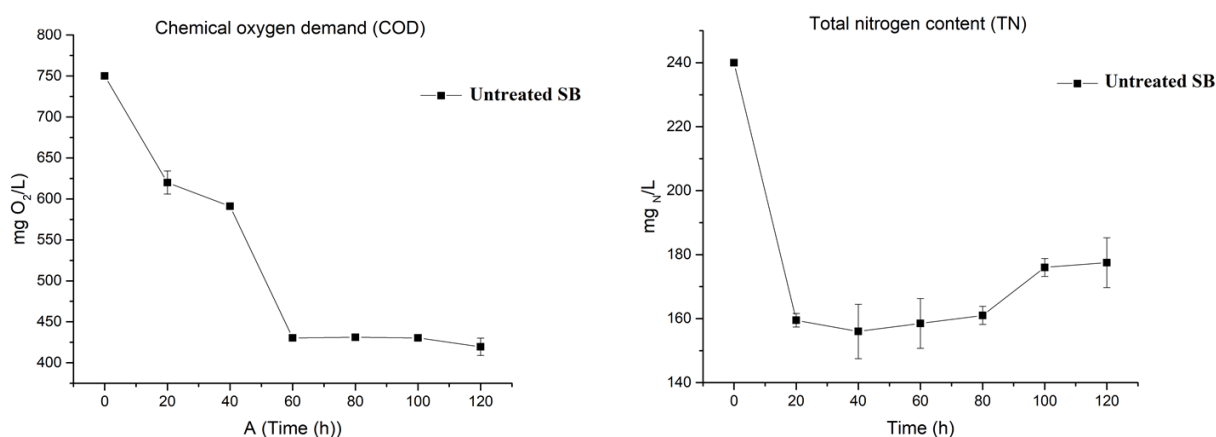


Figure 40: (left) Trend of chemical oxygen demand (right) and total nitrogen during the toxicity assay with *P. Tricornutum* using untreated salt brine effluent. All measurements were performed in biological triplicate (n=3)

The organic removal has been assessed by daily monitoring of COD and TN in algal cultures. Both curves showed that an important fraction remained in the culture and clearly indicated the presence of biologically recalcitrant organic compounds. The residual TN is interpreted as heteroatomic organic nitrogen. These results are not surprising when looking at calculated nitrogen contents accounting for almost half the quantity of TN on SB effluents.

The uptake of the specific studied compounds by algae was additionally tested by measuring their concentrations in the culture media at the beginning and the end of the cultivation period. Surprisingly, it was observed that algae were able to partially remove all three substances tested leaving a residual of 14 % for 2- pyrrolidinone, 53 % for δ -valerolactam and 41 % for PEA where the volatility of all tested substances was relatively low. The mixotrophic nutritional mode was partly validated when algae were exposed to a high organic nitrogen content when using directly the SB aqueous product. Even if volatility calculations from literature estimated relatively low rates, these compounds are of concern when present in the vapour phase as they are extremely alkaline. Neutralisation using physicochemical methods could be a way to turn them innocuous. Alternatively, their mitigation is also possible during catalytic supercritical water gasification as it would provide a way to recover N as ammonia for fertiliser purposes.

4.4 Continuous Hydrothermal catalytic gasification of salt brine and model brine effluent

As shown in **Table 11**, the model SB was efficiently gasified to CO₂ and CH₄. The catalyst was able to entirely convert the TOC contained in the feed, thereby showing its high catalytic activity for converting PEA, VAL, and PYR. The nitrogen recovery was close to 100 %. 652 mg/L nitrogen remaining in the liquid effluent was identified as ammonium. When the SB effluent was processed, the CH₄ concentration increased while the CO₂ concentration decreased. Such a shift of the gas composition may be explained by the change of the feed composition. In fact, a higher feed concentration, *i.e.*, a higher carbon concentration, increases the CH₄ yield [122].

Feed	Time on stream [h]	Recovery [%]	XC [%]	Gas composition [vol %]			
				CH ₄	H ₂	CO ₂	CO
SB Model	1.0	100	100	30	2	68	0
	3.0	99	100	32	3	65	0
SB effluent	4.6	89	100	46	2	52	0
	5.5	96	87	N.A.	N.A.	N.A.	N.A.

Table 11: Results for the hydrothermal catalytic gasification experiments of the salt brine and model brine effluents.

Interestingly, the TOC conversion was below 100 % at the end of the experiment. The presence of a sulphur-containing compound in the feed may be the main reason for the loss of catalytic activity. Indeed, sulphur is known to irreversibly poison Ru/C catalysts. The use of a zinc oxide adsorbent for sulphur, upstream of the catalyst bed, was successfully tested in a recent work [123]. The small fraction of nitrogen losses (as reflected on the nitrogen recovery being slightly below 100 %) is attributed to volatile ammonia.

Chapter 5 Enhancing algae biomass production by using dye-sensitised solar cells as filters

Abstract:

One of the most promising options for decreasing the costs of microalgae production is enhancing the production and reducing the energy demand of the culturing systems, and the high surface area requirements. Since microalgae growth requires only specific wavelengths of the solar spectrum, the remaining part of the solar spectrum may be simultaneously used by a translucent photovoltaic layer to produce electricity, which leads to a reduction of space and energy requirements.

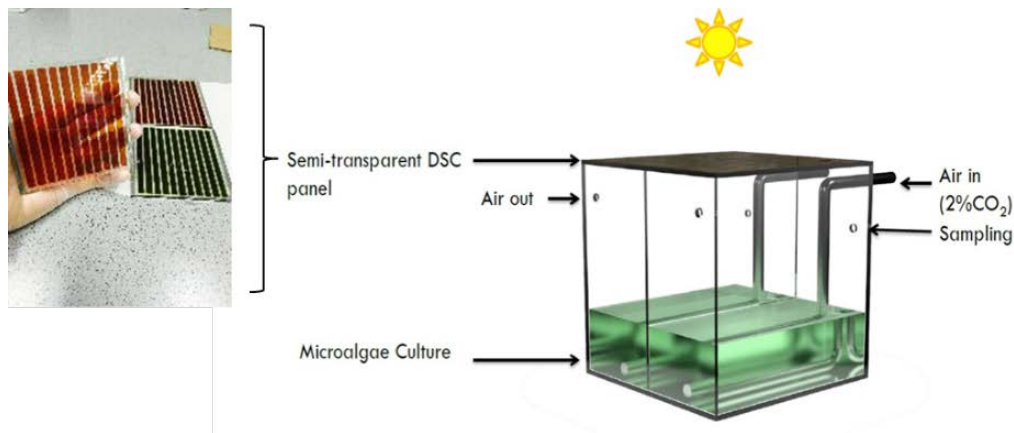


Figure 41: A schematic view of the DSC-Photobioreactor technology and the different colours used in the study.

This work presents the results of a new concept of a positive energy culturing system for microalgae, where the light source is selectively shared between the needs of the algal biomass through photosynthesis and the production of photovoltaic energy through dye-sensitized solar cells (DSCs). To ascertain the DSC (DSC-Red, DSC-Green) light-filtering effects on microalgal biomass: (1) the variation of growth kinetics, (2) microalgae pigments (chlorophylls and carotenoids) and (3) macromolecule content (carbohydrates, proteins, and lipids) were investigated and compared to control cultures under two different solar simulated light intensities (200 and 600 W/m²). The results showed, a net improvement of growth rate and dry weight (DW) at the higher irradiance using both coloured DSC filters compared to control cultures. The highest growth rates (μ) and doubling time (td) of *C. vulgaris* cells were obtained using the DSC-Red (DSC-R) and DSC-Green (DSC-G) solar cells as filters with $\mu = 0.86 \pm 0.01 \text{ day}^{-1}$; td=0.80 day and $\mu = 0.85 \pm 0.03 \text{ day}^{-1}$; td=0.81 day, respectively compared to normal glass control $\mu = 0.51 \pm 0.03 \text{ day}^{-1}$; td=1.35 day. A significant increase in Chlorophyll a content was obtained under low light intensity for both DSC-coloured compared to control culture, and no significant variation in macromolecule content measured under the tested light intensities. Finally, a life cycle assessment (LCA) based on a

functional unit of 1 kg of produced algal biomass using the DSC-photobioreactor (DSC-PBR) was performed and compared to a normal glass photobioreactor. The results were expressed in terms of CO₂ emission equivalents produced and electricity generated.

Material from this chapter has been taken from:

(I) E. Damergi; P. Qin; S. Sharma; M. K. Nazeeruddin; C. Ludwig: Enhancing algae biomass production by using dye-sensitised solar cells as filters; (Ready for submission)

The author performed all experiments related to microalgae as well as the data treatment and characterisation and a part of LCA calculation. The author took the lead in compiling the first draft of the manuscript, resulting in the publication listed above.

In this chapter, we propose for the first time a fully integrated and coloured DSC-PBR system (red and green) for microalgae production. With respect to the used DSCs, an understanding of the optical properties is essential for the interpretation of the results.

5.1 DSC solar panels Characterisation

5.1.1 DSCs and microalgae absorption spectrum

The transmitted irradiance in the photosynthetic active radiations (PAR) region that reach the algae culture was measured in all different photobioreactors and visualized in **Table 12**.

Experiments	Irradiance PAR ($\mu\text{mol photon / m}^2 \text{ s}^{-1}$)				
	Before	540.0	810.0	1350.0	1620.0
		Cycle 1	Cycle 2	Cycle 3	Cycle 4
DSC-T1	After	519.3	780.0	1326.0	1603.0
DSC-T1'		460.8	749.4	1279.0	1543.0
DSC-G		372.6	556.9	935.5	1150.8
DSC-R		325.5	509.8	841.7	1015.2

Table 12: Irradiance PAR ($\mu\text{mol photon m}^{-2} \text{ s}^{-1}$) at the reactor front surface and at the back measured in all photo-bioreactor. DSC-T1 (normal glass); DSC-T1' (DSC without the dye); DSC-G (DSC-Green); DSC-R (DSC-Red).

According to **Table 12**, the PAR irradiance reaching the algae culture was reduced by almost 40% and 32% in the case of DSC-R and DSC-G, respectively, compared to the initially applied light intensity. One should mention that in the case of DSC-T1' that contains all DSC compounds except the dye, a reduction of 15% was observed. This is mainly due to the absorption of other compounds used in the construction of the DSC cell such as titanium dioxide TiO₂ and the electrolyte. These results are consistent with the absorbance spectra obtained in **Figure 42**.

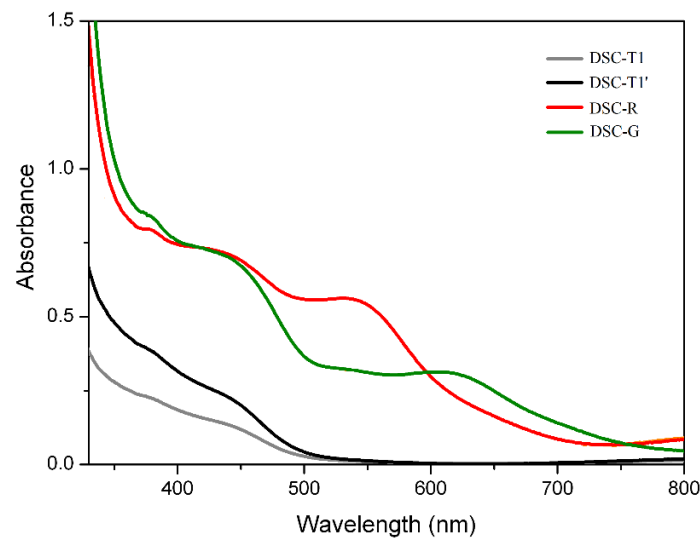


Figure 42: Absorbance spectra of DSC-T1 (normal glass); DSC-T1' (all DSC compounds except the dye); DSC-G (green solar panel); DSC-R (red solar panel).

Sensitiser	Absorption wavelength max (nm)
Red dye(N719)	313, 393, 522, 533
Green dye (N749)	315, 411, 536, 610

Table 13: Dye absorption wavelength max (nm).

The TiO_2 shows a strong peak in the ultraviolet region that decreases drastically within the PAR range. In fact, it is well known that the mesoporous TiO_2 film has the potential to block the UV light by absorbing and scattering the higher energy photons in the UV region. Knowing that microalgae growth can be negatively affected by the presence of UV radiation in outdoor cultivation, the presence of TiO_2 as a protective layer at the illuminated surface of the photobioreactor could be beneficial for the algae culture. Coloured DSCs contributed greatly to the absorption of the UV radiation, as shown in **Figure 42**. The principal UV/VIS absorption peaks ascribed for each dye are mentioned in **Table 13**.

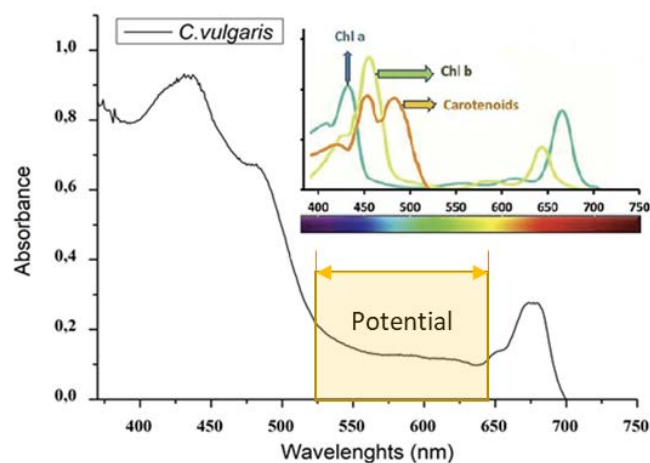


Figure 43: *C. vulgaris* absorbance spectrum and major pigment peaks (inset adapted from [124]).

The advantage of the red DSC panel over the green one is that the major absorption in the visible region occurs between 500-600 nm. The absorption of the green panel, however, is further extended to the red region. This is relevant when the DSC panels are integrated into the structure of the photobioreactors. As revealed in **Figure 43**, the majority of *C. vulgaris* pigments absorb strongly

within the red and blue region of the spectrum and weakly between 520-600nm (potential part of the spectrum to be shared with DSCs, see **Figure 43**). These preliminary results indicated the better compatibility of *C. vulgaris* culture with the DSC-R comparing with that of DSC-G due to the spectral overlap.

2.1.1. Power conversion efficiency of DSCs (η)

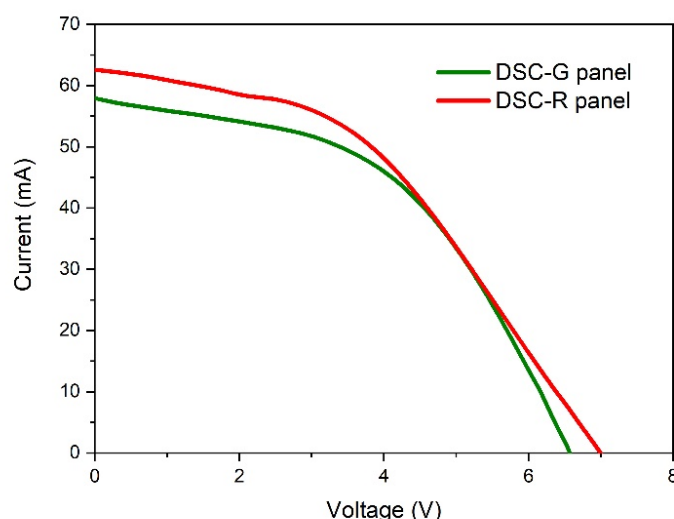


Figure 44: Current-voltage curves for DSC-R and DSC-G panels.

All parameters that were used to calculate the power conversion efficiency (η) of DSC panels are given in section 2.2.5. The DSC-G and DSC-R showed power conversion efficiency of 2.8% and 3.0%, respectively, leading to a maximum output power of 185.3 mW and 192.6 mW. The slightly lower power conversion efficiency was attributed to the large dimension of the DSC panels (100×100 mm). The corresponding solar cell parameters, i.e. I_{sc} , V_{oc} , FF, and η , were obtained from **Figure 44** summarised in **Table 14**.

	I_{sc} (mA)	V_{oc} (V)	P_{max} (mW)	ff	η (%)	Energy production per year (kWh)*	Energy production per year (kWh)**
DSC-G panel 8 μm TiO_2	57.9	6.58	185.33	0.49	2.8	0.36	0.27
DSC-R panel 8 μm TiO_2	62.6	6.99	192.55	0.44	3.0	0.39	0.29

Light intensity: 100 mW cm^{-2}

Table 14: Photovoltaic performance of the DSC panels: I_{sc} (short circuit current), V_{oc} (open circuit voltage), ff (fill factor), η efficiency, P (output power). The measurements were done at a light intensity of 100 mW/cm². * Energy production per year was calculated using the solar panel efficiency (%) without including the potential losses that can occur (**Equation 26**) **Energy production per year was calculated in this case using Performance Ratio (**Equation 27**).

5.2 DSC-PBR growth under constant light intensities: *C. vulgaris* case study

A first set of experiments with the two different DSC-PBR colours (green, red), the DSC-T1 and DSC-T1' controls were performed at two different constant light intensities: low light intensity at 540 $\mu\text{mol photons/m}^2 \text{ s}^{-1}$ and high light intensity at 1620 $\mu\text{mol photons/m}^2 \text{ s}^{-1}$. **Figure 45** shows the growth rate curves of *C. vulgaris* cultivated under coloured DSC-panels and control cultures at the two simulated solar light intensities. At low light intensity, no significant difference ($P > 0.05$) was observed in terms of cells and dry weight (DW) between *C. vulgaris* cultivated under DSC-G panel and both control cultures.

All three algae cultures reached almost 0.9 g/L at day 9. A long lag phase was observed in the case of DSC-T1 (normal glass) until day four suggesting that direct light and/or UV presence slightly slowed down the cell division (All other cultures were able to enter the exponential phase within day 2). A slight decrease in DW was obtained in the case of DSC-R compared to controls and DSC-G.

5.2.1 Growth kinetics

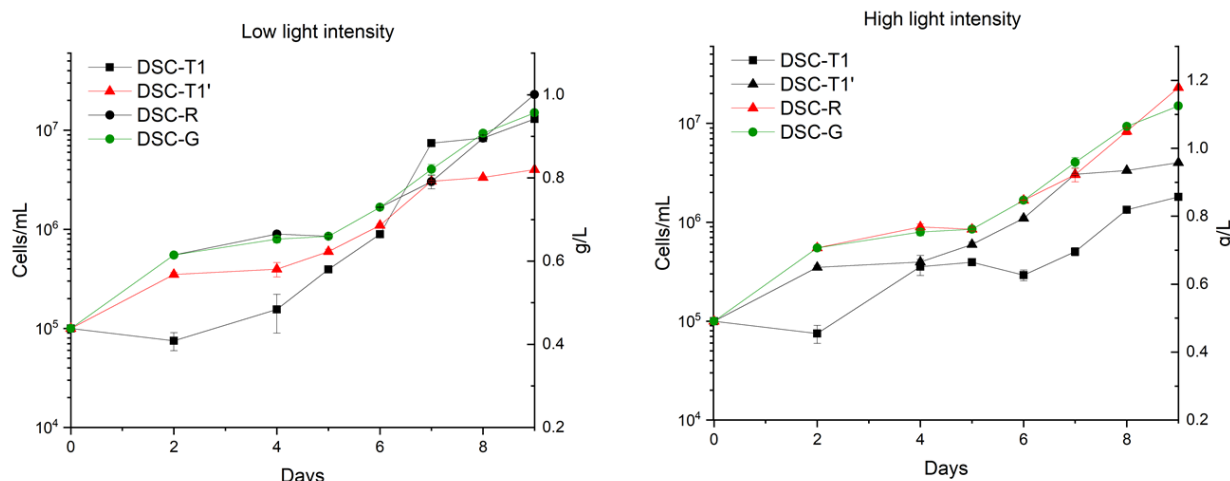


Figure 45: shows the logarithmic growth and stationary phases of *C. vulgaris*. Growth curves (Cells/mL) and biomass concentration (g/L): (left) growth under low light intensity (Right) and high light intensity using DSC-T1; DSC-T1'; DSC-G and DSC-R.

	<i>C. vulgaris</i>							
	Low light intensity				High light intensity			
	DSC-T1	DSC-T1'	DSC-R	DSC-G	DSC-T1	DSC-T1'	DSC-R	DSC-G
Specific growth rate (d^{-1})	0.62 \pm 0.02	0.75 \pm 0.01	0.58 \pm 0.01	0.69 \pm 0.05	0.51 \pm 0.03	0.63 \pm 0.02	0.86 \pm 0.01	0.85 \pm 0.03
Doubling time (d)	1.11	0.92	1.19	1.08	1.35	1.10	0.80	0.81
DW (g/L)	0.96 \pm 0.03	0.94 \pm 0.05	0.82 \pm 0.03	0.95 \pm 0.04	0.88 \pm 0.02	0.95 \pm 0.06	1.19 \pm 0.03	1.12 \pm 0.03

Table 15: Only data collected during the exponential growth phase were used for growth kinetic analyses. Growth rate (μ) was determined individually for each replicate using a linear regression of the log-transformed cell density over time. Doubling time (td) was determined by dividing log 2 over the growth rate.

One hypothesis to explain this decrease, even if statistically the difference was not significant ($P > 0.05$), is attributed to the reduction of red photons due to the reflection properties the presence of DSC-R. In algae culture, red and blue lights are the most efficient in deriving photosynthesis [125]. According to G. Anderson et al. (2012) [126], red light produced the highest number of microalgae cells with the highest weight.

At higher light intensity, a significant difference in growth was observed between coloured DSC's and controls, as shown in **Figure 45**. *C. vulgaris* cultivated under coloured DSC filters exhibited a high growth rate compared to both control cultures. The results showed that identical growth rate and doubling time were obtained in the case of DSC-R and DSC-G culture with $\mu = 0.86 \pm 0.01 d^{-1}$; $td=0.80 d$ and $\mu = 0.85 \pm 0.01 d^{-1}$; $td=0.81 d$ but higher compared to normal glass control $\mu = 0.51 \pm 0.03 d^{-1}$; $td=1.35 d$. By far, the control culture exposed to direct radiation showed the slowest growth and DW among all tests. Flow cytometry analysis was performed to investigate if the increase in DW and growth rate was accompanied with some deeper metabolic changes. **Figure 46**

illustrate the measured autofluorescence graphs (BL3-A, right side) as well as the cell population distributions (left side) at the end of the experiment. When both forward scatter FS and side scatter SS are measured, this allows for some degree to interpret the cellular differentiation within a heterogeneous population. Interestingly, a sharp autofluorescence peak was obtained as a signature for both coloured DSC-PBR with a very distinct cell population pattern in the dot-plots (FS vs SS). Contrary, both control cultures presented less intense autofluorescence compared to coloured DSC-PBR experiments. However, in the case of DSC-T1', a split in autofluorescence peak was observed as an indication of the presence of different cell types with variable chlorophyll intensity. DSC-T1' present less scattered cells compared to DSC-T1 but the split in autofluorescence peaks was expressed as almost two different cell groups in the dot-plots. The stationary phase observed at the end of DSC-T1' the experiment could be, in fact, subject to an adaptation period where cells are still preparing to undergo cell divisions (presence of mother and daughter cells). This observation suggested that under high light intensity and with a net reduction in UV radiation (presence of TiO₂ layer), *C. vulgaris* can favour survival pathways on cell division during a period of acclimation. However, the dot-plots of DSC-T1 showed scattered and non-homogeneous cell distributions with different degree of internal complexity (increasing SS) and size (increasing FS). The autofluorescence peak was very weak compared to all three experiments, suggesting that *C. vulgaris* are bleached and stressed under 600W/m² direct exposure (UV radiation presence).

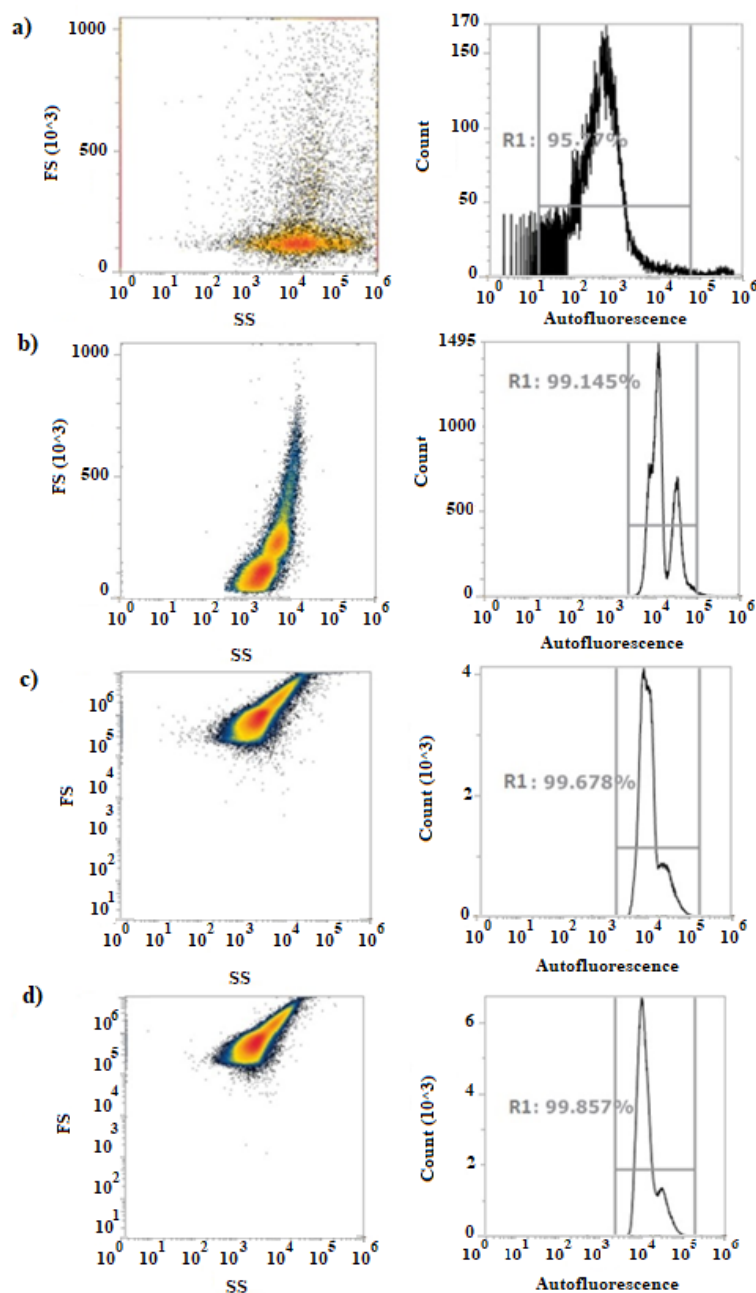


Figure 46: The analysis by means of flow cytometry of *C. vulgaris* cells at the end of the experiment under high light intensity using a) DSC-T1 (normal glass); a) DSC-T1' (all DSC compounds except the dye) DSC-G (green solar panel); d) DSC-R (red solar panel). R1 represents the gating for autofluorescent cells due to the presence of Chlorophyll a, SS: Side scatter, FS: Forward scatter.

5.2.2 Photochemical, regulated and non-regulated quantum yield variations

The effect of light intensity on time courses was studied by daily calculating the maximum photochemical yield with dark-adapted microalgae (dark cycle). F_v/F_m ratio is a precise measure of the potential maximal quantum yield of PS II fluorescence, and it represents an indicator of photoinhibition that may occur at high light exposure radiation. A decrease in this ratio is highly correlated to a reduction in PS II and a decrease in the algal biomass. The measured F_v/F_m ratio for *C. vulgaris* was compared to another algae, *Haematococcus pluvialis* cultivated under the same conditions. This strain is not a fast-growing microalga, but it has the advantage of reacting under high light intensity or UV radiation via the accumulation of secondary pigments. This could be helpful for the comparison with *C. vulgaris*.

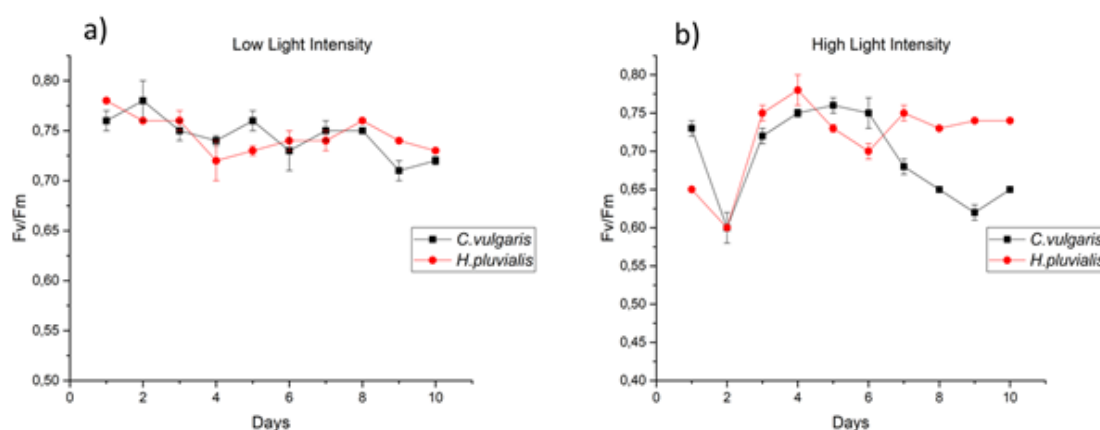


Figure 47) F_v/F_m fluorescence ratio of *C. vulgaris* and *H. pluvialis* at low and high light intensity; F_v is the difference between the maximum fluorescence F_m (all QA reduced) and minimum fluorescence F_0 (all QA oxidised)

Under low light intensity of $540 \mu\text{mol photon m}^{-2} \text{s}^{-1}$, the ratio remained stable over time with a slight decrease at the end of the experiment, suggesting that light at this intensity didn't trigger any stress factor such as photo-inhibition. Therefore, the photosynthetic apparatus can efficiently utilize the absorbed photons when the rate of light absorbed does not exceed the rate of photosynthesis. In contrast, *C. vulgaris* and *H. pluvialis* cell grown under high light intensity presented an F_v/F_m ratio that decreased drastically from 0.74 and 0.65 to almost 0.59 within one day of exposure at $1620 \mu\text{mol photon m}^{-2} \text{s}^{-1}$. At higher irradiance, the relation between absorbed light and photosynthesis rate is not linear. Consequently, F_v/F_m decreased. This decrease was followed by an increase and stabilisation during the four consecutive days. The variation of the ratio at the beginning of the experiment indicated that the cells were stressed at $1620 \mu\text{mol photon m}^{-2} \text{s}^{-1}$ resulting in a slightly impaired photosynthetic apparatus. The rate of photon absorption by the chlorophyll antenna exceeds the rate at which photosynthesis can utilize them, which generally results in dissipation and loss of excess photons as heat or fluorescence. Nevertheless, a progressive increase of F_v/F_m especially in the case of *H. pluvialis* was observed and may be explained by a metabolic adaptation to the environment and several protection strategies such as non-photochemical quenching via heat dissipation and repair mechanisms.

According to **Figure 48**, DSC-T1 control *C. vulgaris* grown under high light intensity presented a lower starting value of photosynthetic efficiency (also called photochemical conversion) ϕ (PSII) compared to DSC-T1' and coloured DSC. These results are in line with the previous results from **Table 15**, indicating a lower growth rate and DW in the case of direct exposure. The fact that DSC-T1' led to a higher ϕ (PSII) could be explained by the net reduction in UV radiation reaching the algae culture. Furthermore, DSC-T1 and DSC-T1' showed a different response reaction for high light intensity with an increase in the starting value of ϕ (NPQ) for DSC-T1' compared in the case of DSC-T1. This is a strong indication that a part of absorbed light is dissipated via Non-photochemical quenching (NPQ), which is a mechanism employed by algae to protect themselves from the adverse effects of high light intensity. Moreover, a significant difference was obtained for ϕ (NO) in the case DSC-T1 compared to all other cultures. The ϕ (NO) mechanisms predominate the ϕ (NPQ) pathway, which can be seen in **Figure 48**. When a molecule of chlorophyll absorbs light, it is promoted from its ground state to its first singlet excited state. The excited state then has three main fates. Either the energy is i) passed to another chlorophyll molecule by Förster resonance energy transfer (in this way excitation is gradually passed to the photochemical reaction centres of photosystem I and photosystem II) where energy is used in photosynthesis (called photochemical quenching), ii) the excited state can return to the ground state by emitting the energy as heat (called non-photochemical quenching, NPQ), and iii) the excited state can return to the ground state by emitting a photon (fluorescence).

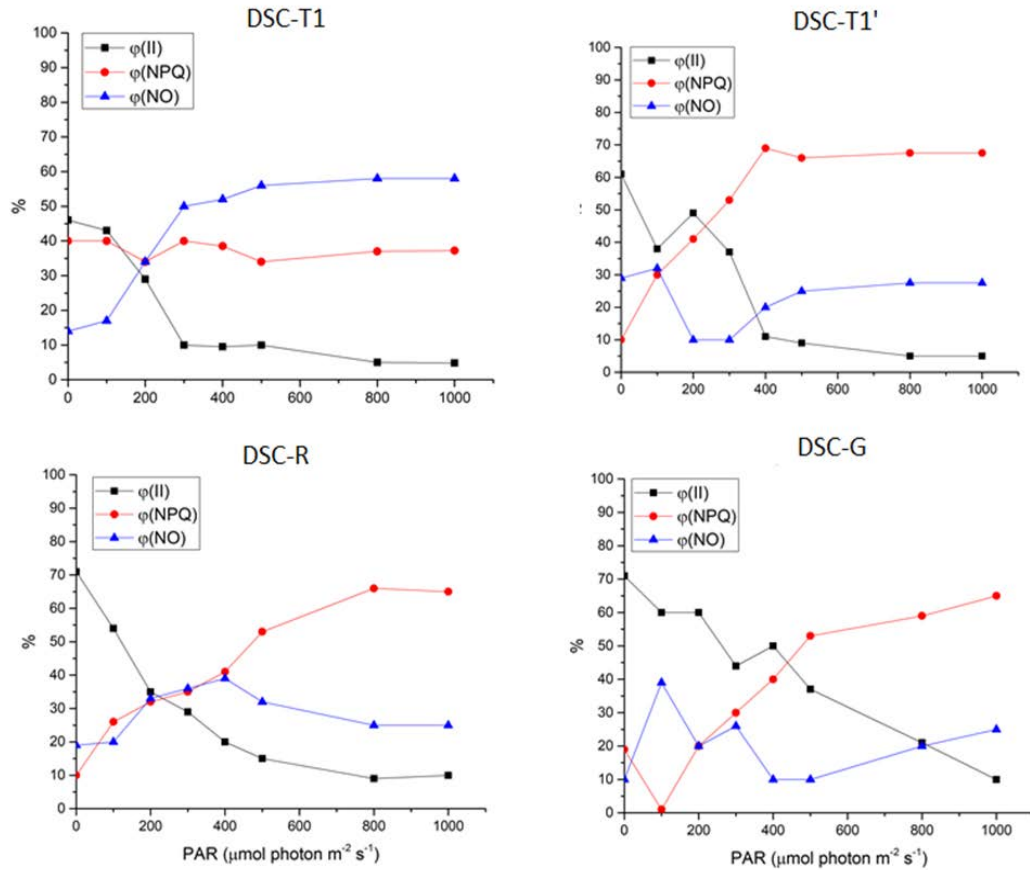


Figure 48: $\phi(II)$, photochemical conversion, $\phi(NPQ)$, regulated thermal energy dissipation related to NPQ, $\phi(NO)$, "primarily constitutive losses", corresponding to the sum of non-regulated heat dissipation and fluorescence emission.

5.2.3 Pigments and macromolecule compositions

	<i>C. vulgaris</i>							
	Low light intensity				High light intensity			
	DSC-T1	DSC-T1'	DSC-R	DSC-G	DSC-T1	DSC-T1'	DSC-R	DSC-G
Chl a ($\mu\text{g}/\text{mg}$)	8.50 \pm 0.50	9.55 \pm 0.32	11.25 \pm 0.18	11.68 \pm 0.38	5.98 \pm 0.23	8.85 \pm 0.11	9.57 \pm 0.32	10.03 \pm 0.57
Chl b ($\mu\text{g}/\text{mg}$)	1.11 \pm 0.02	1.60 \pm 0.04	1.52 \pm 0.05	1.45 \pm 0.07	0.75 \pm 0.02	1.80 \pm 0.01	1.62 \pm 0.04	1.57 \pm 0.04
Car ($\mu\text{g}/\text{mg}$)	0.49 \pm 0.01	0.59 \pm 0.04	0.52 \pm 0.05	0.58 \pm 0.03	0.30 \pm 0.01	0.8 \pm 0.02	1.11 \pm 0.03	0.92 \pm 0.01
Car/Chl (a+b)	0.05	0.045	0.040	0.04	0.04	0.07	0.09	0.07
Lipids ($\mu\text{g}/\text{mgDW}$)	142 \pm 11.22	112 \pm 5.41	127.3 \pm 4.13	133 \pm 6.47	130 \pm 19.05	185 \pm 5.40	188 \pm 6.82	179.20 \pm 5.14
Carbohydrates ($\mu\text{g}/\text{mgDW}$)	175.5 \pm 14.00	201 \pm 15.13	165 \pm 10.50	171 \pm 14.52	102 \pm 4.80	230 \pm 9.50	150.2 \pm 13.40	131 \pm 1.51
Proteins ($\mu\text{g}/\text{mgDW}$)	490.4 \pm 9.80	482 \pm 12.00	507.2 \pm 23.24	538 \pm 49.20	387.1 \pm 5.25	410 \pm 9.41	514 \pm 14.00	528 \pm 21.32

Table 16: Total Chlorophyll, carotenoids and macromolecule content.

Table 16 displays data of pigment contents obtained from the previous tests and it appeared that under low light intensity the chlorophyll a and b contents were higher for the coloured DSC than for the control cultures. This observation seems to be shared in the literature. A common trend when lower light intensity is provided to green algae culture is that chlorophyll a and other light pigments tend to increase. This increase in pigment content will decrease the optical cross-section $a^*(m^2mg^{-1} \text{ Chl a})$ and therefore, the gain in light-harvesting. A doubling of cellular chlorophyll does not bring a doubling in the rate of light absorption. These results could be relevant when indoor microalgae production with DSC-PBR technology under low intensity is considered.

At higher light intensity experiments, the total chlorophyll yield decreased, and a net increase on carotenoid content was observed for all cultures except for DSC-T1, indicating a more active xanthophyll cycle. The increase was about 26% for the control DSC-T1', 52.72% and 35.55%, respectively, for red and green DSC-PBR. These carotenoids are generally involved in energy capture and dissipation, and they are located at the peripheral of PSII antenna in the case of *C. vulgaris*. Under high light intensities, acidification of the chloroplast lumen activates *de-epoxidase* enzymes that convert violaxanthin into zeaxanthin. Violaxanthin transfers energy to Chl facilitating light harvesting at low light intensities while zeaxanthin dissipates excess Chl excited states at high light intensities as heat. This photo-acclimation allowed the cells to reach higher productivity via the regulation of light absorbance pathways.

The concentration of the major macromolecules of *C. vulgaris* were quantified for all four experiments and results are shown in **Table 16**. No significant difference between protein lipids and carbohydrate content was observed in all test cultures under low light intensity. Some variation in concentration occurred but was considered statistically not significant ($P>0.05$). Under high light intensity, a net decrease in the case of DSC-T1 was measured in all biomolecule content, confirming the stressed state of this culture. A slight increase of lipid content was generalised in DSC-T1', and coloured DSC compared to the results obtained at low light intensity. Nevertheless, protein and carbohydrate ratio remained constant, which implies that the shadowing and UV protection effects applied in the presence of DSC affected mainly the pigment content and very slightly the biochemical composition of *C. vulgaris*.

5.3 DSC-PBR growth under constant light intensities: *H. pluvialis* case study

A second set of experiments was performed using *H. pluvialis* with similar conditions previously applied in the case of *C. vulgaris*. However, limited analysis was accomplished due to the limited amount of biomass harvested at the end of each experiment.

	<i>H. pluvialis</i>							
	Low light intensity				High light intensity			
	DSC-T1	DSC-T1'	DSC-R	DSC-G	DSS-T1	DSC-T1'	DSC-R	DSC-G
Specific growth rate (d^{-1})	0.42 \pm 0.02	0.68 \pm 0.03	0.52 \pm 0.01	0.54 \pm 0.04	-0.09	0.25 \pm 0.02	0.55 \pm 0.05	0.46 \pm 0.02
Doubling time (d)	1.47	1.01	1.33	1.28	-	2.772	1.26	1.46
DW (g/L)	0.4 \pm 0.05	0.8 \pm 0.07	0.65 \pm 0.02	0.66 \pm 0.05	0.29 \pm 0.09	0.36 \pm 0.03	0.59 \pm 0.03	0.55 \pm 0.05

Growth rate (μ) was determined individually for each replicate using a linear regression of the log-transformed cell density over time. Doubling time (td) was established by dividing log2 over the growth rate.

Table 17: Only data collected during the exponential growth phase were used for growth kinetic analyses.

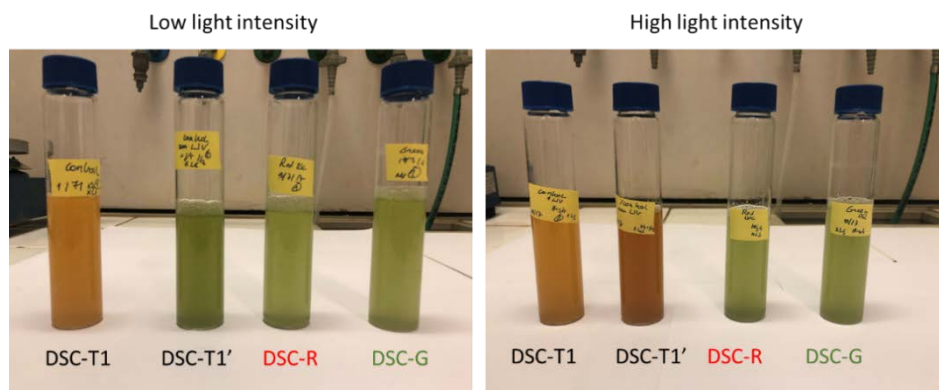


Figure 49: Picture of samples taken from *H. pluvialis* growth tests under high light intensity DSC-T1 (standard glass); DSC-T1' (all DSC compounds except the dye); DSC-G (green solar panel); DSC-R (red solar panel)

Under low light intensity, according to **Table 17**, higher growth rates were obtained in DSC-T1' and coloured DSC compared to *H. pluvialis* control culture DSC-T1, and only DSC-T1 culture was subject to colour changes. This switch to the red stage in *H. pluvialis* cell is an indication of a stressful environment. At this stage, DSC-T1' cultures preserved its green colour as the two-coloured DSC-cultures. In fact, *H. pluvialis* (Chlorophyta) is a unicellular alga with a rather complicated life cycle. Its ovoid vegetative cells are motile by way of two flagella, and during growth, non-motile cells (cysts) also occur. The cells are generally green, but under stress conditions (in this case, high irradiance) the green vegetative cells produce thicker walls and change to globular cysts with a significant increase in cell volume and pigmentation to orange-red, due to an increased carotenoid content. This excess excitation energy leads to an increase in the lifetime of singlet excited chlorophyll, increasing the chances of the formation of long-lived chlorophyll triplet states by inter-system crossing. Triplet chlorophyll is a potent photo-sensitiser of molecular oxygen forming singlet oxygen which can cause oxidative damage to the pigments, lipids and proteins of the photosynthetic thylakoid membrane.

To counter this problem, the photo-protective mechanism NPQ involves conformational changes within the light-harvesting proteins of photosystem (PSII) that bring about a change in pigment interactions causing the formation of energy traps. The conformational changes are stimulated by a combination of a transmembrane proton gradient, the PsbS subunit of PS II and the enzymatic conversion of a secondary pigment, the carotenoid violaxanthin to zeaxanthin (the xanthophyll cycle). Under higher light intensity, at day 3, both control cultures changed colour to orange, and both DSC-cultures preserved their green colour. However, a drastic decrease in growth rate was observed with DSC-T1 with $\mu = -0.09 \text{ d}^{-1}$ compared to $\mu = 0.42 \text{ d}^{-1}$ under low light intensities due probably to photoinhibition and cell bleaching.

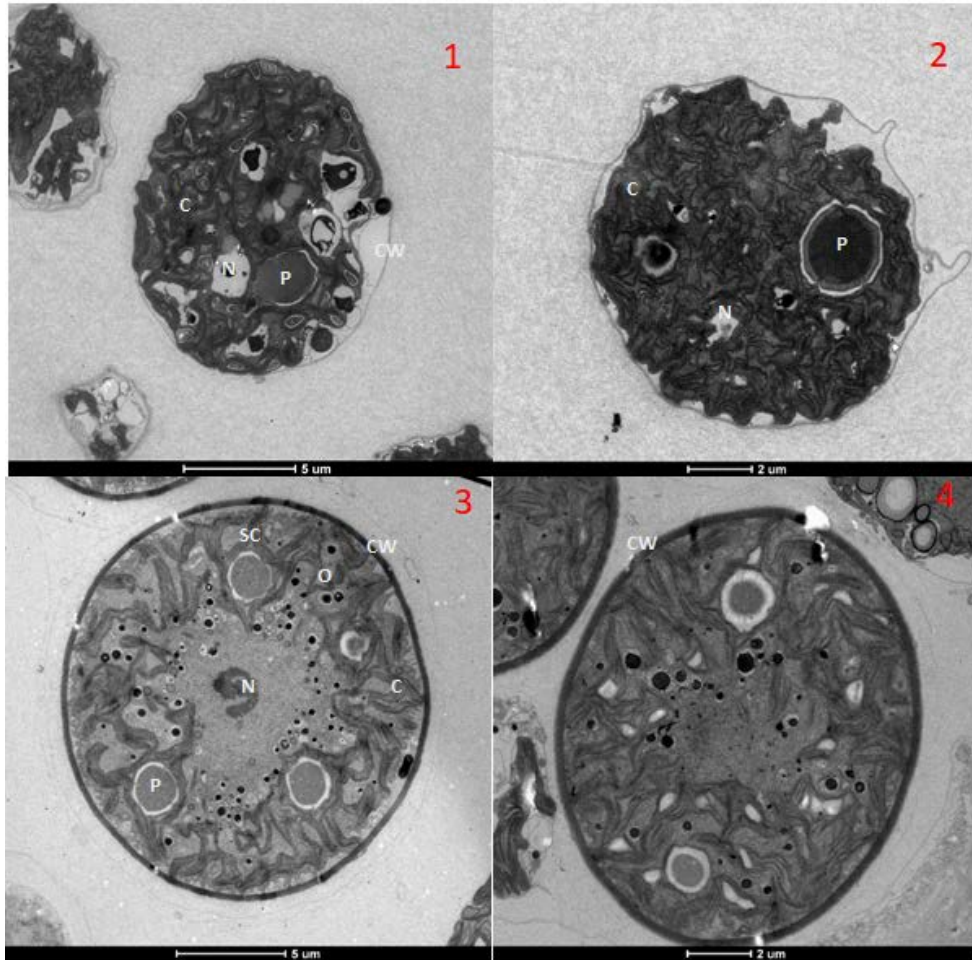


Figure 50: Transmissions electron micrographs TEM of *h. pluvialis* at day 3. 1) DSC-G, 2) DSC-R, 3) DSC T1'4) DSC-T1 Nucleus (N) Chloroplast (C), Pyrenoid (P), Oil droplet (O), cell wall (CW).

Figure 50 exposes transmission electron from *H. pluvialis* growth tests at high light intensity (day3). Standard components are presented such as the nucleus and chloroplasts. Several pyrenoids are involved in CO_2 uptake in the case of *H. pluvialis*. Under high light intensity accompanied with UV radiation, **Figure 50** (3 and 4) also shows the formation of a thick wall in the case of both control cultures with the appearance of oil droplets inside the cells. This result suggests that coloured DSC applied at the top of the PBR acted as a protection filter and slowed down the activation of the xanthophyll cycle. These results are very encouraging as the applying of DSC panel could prolongate the green phase of *H. pluvialis* for maximum productivity before the stress phase (red cells, lower productivity). Simple cell walls and flagellates (green stage) were preserved in both cases of red and green DSC-PBR.

5.4 Algal biomass and energy production under DSC-bioreactor

Materials (glass and aluminium) required for the construction of a bioreactor are reported in **Table 18**. **Table 18** also presents amounts of water, CO_2 , nutrients and bubbling energy required to operate the PV bioreactor. The bubbling energy is calculated for a blower by using the pressure at the bottom of culture (plus 20% extra) in the PV bioreactor [74]. Note that bubbling is required for 24h hours each day. Parisi et al. [127] calculated cradle-to-gate GHG emissions expressed as 530 g CO_2 -eq for producing 125 cm^2 of DSC PV panel. The GHG emissions were characterised by IPCC (Intergovernmental Panel on Climate Change, 2013 GWP 100a).

Bioreactor	
Size of the glass chamber*	10 cm × 10 cm × 8 cm
Glass used in glass chamber	411.6 g
Aluminum used in glass chamber	8.4 g
Lifetime of glass chamber*, +	20 years
DSC-panel	
Area of DSC panel	100 cm ²
GHG emissions in the manufacturing of 1 DSC panel	424 gCO ₂ -eq
Lifetime of DSC panel*, +	20 years
Input to DSC-Bioreactor operation	
<i>C. vulgaris</i> batch time*, +	8 days
Water (or culture) used in 1 batch	240 mL
CO ₂ concentration in airflow*	2 v/v
Airflow rate*	0.8 L/m
CO ₂ used in 1 batch (from nature)	0.09 m ³ (0.18 kg)
Urea used in 1 batch	0.044 g
Potassium carbonate used in 1 batch	0.019 g
Phosphoric acid used in 1 batch	0.026 g
Manganese sulphate used in 1 batch	0.0136 g
Calcium chloride used in 1 batch	0.007 g
Sodium hydroxide used in 1 batch	0.020 g
Iron sulphate used in 1 batch	0.006 g
EDTA-Na ₂ used in 1 batch	0.002 g
Bubbling energy (electricity) in 1 batch	2.11 kJ
Output of DSC-PBR operation	
Algae production rate*	1.19 g/L
Algae produced in 1 batch	0.286 g
CO ₂ present in microalgae produced*	0.106 g
Wastewater (25% loss: evaporation, harvesting) in 1 batch	180 mL
Electricity produced by DSC panel in 1 batch	41.47 kJ
*These are not direct input-output for DSC-PBR design/operation.	
+These are used to calculate the multiplication factor for bioreactor and DSC panel use.	

Table 18: Design and operation parameters of a DSC-PBR.

Alsema et al. calculated cradle-to-gate GHG emissions (35 g CO₂-eq/kWh) for producing electricity by silicon PV panels [128]. The GHG emissions for Swiss electricity mix are 128.9 g CO₂-eq/kWh (Ecoinvent dataset - v3.3, www.ecoinvent.org). For performing LCA of DSC-PBR, SimaPro software (v8.5; simapro.com) along with the Ecoinvent dataset have been used. In order to produce 1 kg of microalgae (8 days), 3501 units of DSC-PBR are required which covers a surface of 35.01 m². On this surface, DSC panels generate 40.332 kWh in 8 days, i.e. 36803 kWh over 20 years. As a result, the emitted CO₂ from the DSC production is equal to 0.040 kg CO₂/kWh (3501*0.424 kg CO₂). Furthermore, higher solar conversion efficiency could decrease the CO₂ footprint of DSC and compete with standard PV with 0.035 kgCO₂/kWh.

LCA results for the three cases are provided in **Table 19** in terms of total GHG emissions to produce 1 kg of microalgae. The operation of a DSC-PBR has a large share in GHG emissions, mainly due to nutrients supplied for microalgae growth. The production and end-of-life of the DSC-PBR (glass is considered being landfilled, whereas aluminum considered being recycled) contributes about 71.6% of the overall GHG emissions. However, this contribution can be easily reduced when bigger photobioreactor is considered. For

instance, by combining small DSC PBR of 100 cm² into big DSC-PBR of 1 m², 68.57% reduction of materials and related CO₂-eq emissions can be achieved (see supplementary information: LCA).

Bubbling of culture using air/CO₂ (air/2 % CO₂ mix) feed requires a small amount of electrical energy for blowers, and its contribution to the overall GHG emission remains below 2%. In Case I, 40.332 kWh electricity is generated by DSC PV panel (solar irradiation to electricity conversion efficiency = 3%). A fraction of the generated electricity, 2.05 kWh, is used by the bioreactor in bubbling of microalgae, and the difference, 38.281 kWh extra electricity is injected into the Swiss electricity grid, which generates 4.935 kg CO₂-eq credits. The net GHG emissions to produce 1 kg of microalgae is therefore -0.3481 kgCO₂-eq. However, even if the net GHG obtained here was negative, microalgae production system generally contains more GHG contributors such as harvesting, dewatering steps. This can significantly increase GHG.

To produce 1 kg of microalgae, Case II and Case III generate 3.033 and 3.225 kgCO₂-eq emissions over the entire life cycle, respectively. In Case II, electricity for bubbling is supplied by Silicon PV panel, which has 0.072 kg CO₂-eq emissions to produce 2.05 kWh electricity. In Case III, electricity for bubbling is provided by Swiss electricity mix, which contributes 0.264 kg CO₂-eq emissions.

	Case I (kg)	Case II (kg)	Case III (kg)
Bioreactor including end-of-life	1.658	1.658	1.658
DSC PV panel	1.627	-	-
Silicon PV panel	-	0.072 ⁺	-
Operation of PV bioreactor	1.302	1.302	1.567
Water	0.166	0.166	0.166
Urea	0.525	0.525	0.525
Potassium carbonate	0.192	0.192	0.192
Phosphoric acid	0.144	0.144	0.144
Manganese sulphate	0.044	0.044	0.044
Calcium chloride	0.020	0.020	0.020
Sodium hydroxide	0.096	0.096	0.096
Iron sulphate	0.006	0.006	0.006
EDTA-Na₂	0.030	0.030	0.030
Wastewater Treatment	0.080	0.080	0.080
Electricity for bubbling	-	-	0.264
Avoided electricity production*	- 4.935	-	-
Total CO₂ emissions	-0.348	3.033	3.225

Table 19: All contributors of GHG emissions (in CO₂-eq) of bioreactor producing 1 kg of microalgae (DW). (*) The negative number indicates the avoided electricity production. (+) This value indicates the CO₂ impact of electricity provided from an existing silicon PV platform (including CO₂ contribution from the construction of Si-panel)

Table 20 illustrates the surface coverage by DSC-PBR needed to produce 1 kg of *C. vulgaris* (8 days) using extrapolated data obtained from the previous experiments. At low irradiance, 50.8 m² area is required to produce 1 kg of microalgae with an electricity of 29.27 kWh. At 600 W/m², a reduction of 31% in space occupation can be obtained with the same DSC-R compared to the low-intensity case, with which only 35 m² area is needed to produce 1 kg of algae and two-times higher electricity production 60.50 kWh. These results are of interest as they show the potential of DSC-PBR technology in highly sunny regions. The benefits of DSC presence in PBR is even more relevant when DSC panel efficiency is close to their typical efficiency 8% [127]. Note that DSC panels do not use any extra space, as they are placed on the top of bioreactor.

Parameters		Units	Low light intensity	High light intensity
	Solar irradiation	W/m ²	200	600
		μmol photons/m ² s ⁻¹	540	1620
	Top surface area of 1 bioreactor	m ²	0.01	0.01
	Duration of an algae growth cycle	days	8	8
	Solar energy (per day, 12 h)	kJ	86.4	259.2
DSC-R	Solar energy (per day, 12 h)	kWh	0.024	0.072
	Algae production per batch (2 compartments)	g	0.196	0.285
	Solar energy efficiency of DSC unit	%	3	
	DSC unit needed for 1 kg algae / surface required	DSC-unit or m ²	5081 or 50.8	3501 or 35.0
	Electricity produced by all DSC unit in 8 days (1kg biomass)	kWh	29.27	60.50
DSC-G	Algae production per batch (2 compartments)	g	0.228	0.269
	Solar energy efficiency of DSC unit	%	2.8	
	DSC unit needed for 1 kg algae / surface required	DSC-unit or m ²	4385 or 44	3720 or 37
	Electricity produced by all DSC unit in 8 days (1kg biomass)	kWh	23.57	60.00

Table 20: Electricity production based on 10 cm*10 cm DSC-R and DSC-G for 8 days batch culture of *Chlorella vulgaris* at variable light intensities and DSC efficiency. Two different efficiencies were used for DSC-R and DSC-G: 2.8% and 3% respectively obtained from our study.

Chapter 6 Biomass valorisation: Extraction of carotenoids from *Chlorella vulgaris* using green solvents and syngas production from residual biomass

Abstract:

A combined process for carotenoids extraction and efficient bioenergy recovery from the wet microalgae biomass is proposed. High added-value products could thus be extracted prior hydrothermal gasification of the algal biomass into synthetic natural gas. The economic sustainability of biofuel production from algal biomass as well as the large energy demands of microalgae cultivation and harvesting is addressed in this chapter. Two green solvents, ethanol and 2-methyl tetrahydrofuran (MTHF) were used to achieve the maximum extractability of selected carotenoids. Pure MTHF was tested for the first time as an alternative renewable solvent for carotenoid extraction from wet biomass, and promising results were obtained (30 minutes at 110 °C), with 45% of total carotenoids being extracted. The energy content of the residual biomass corresponds to a high heating value (HHV) of 18.1 MJ kg⁻¹. With a 1:1 mixture of both MTHF and ethanol, more carotenoids were extracted from wet biomass (66%), and the remaining HHV of the residual biomass was 15.7 MJ kg⁻¹. The perspectives of combined carotenoid extraction and energy recovery for a better microalgae valorisation are discussed.

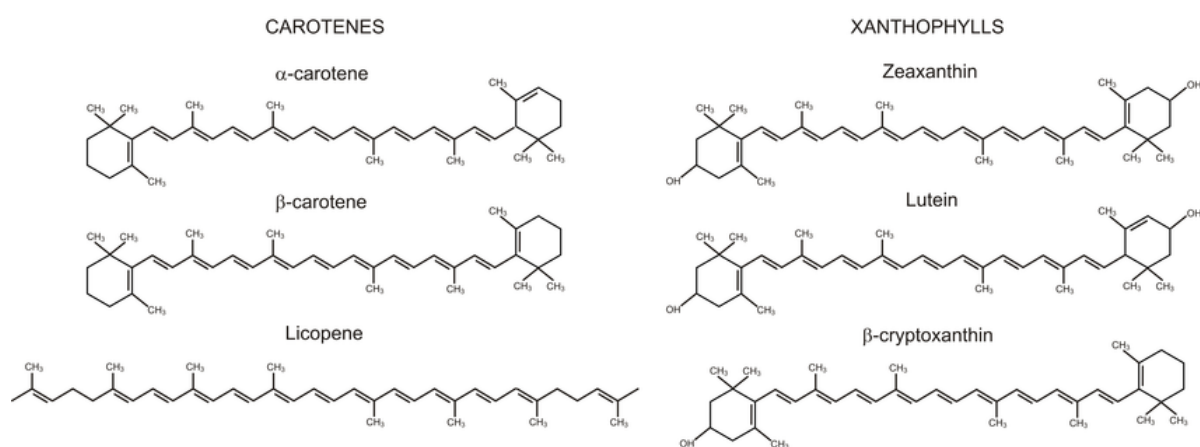


Figure 51: Structures of carotenoids and xanthophylls [129].

Materials from this chapter has been published in:

(I) [E. Damergi](#); J.-P. Schwitzgu  bel; D. Refardt; S. Sharma; C. Holliger et al.: Extraction of carotenoids from *Chlorella vulgaris* using green solvents and syngas production from residual biomass; Algal Research. 2017. DOI: 10.1016/j.algal.2017.05.003.

The author performed all experiments related to microalgae carotenoids extraction, as well as data treatment and interpretation.

The author took the lead in compiling the first draft of the manuscript, resulting in the publication listed above.

6.1 Hansen solubility parameters

The present research focused on using wet biomass and opted for more environmentally friendly extraction techniques that employ green solvents (MTHF alone or combined with ethanol) instead of petroleum-derived ones. The chemical profile of the extracts was determined by High-Performance Liquid Chromatography coupled with Diode Array Detector (HPLC-DAD). The effect of this pre-processing step on the residual microalgae biomass was evaluated for the potential energy recovery by calculating the high heating value. The perspective about integrating the carotenoids extraction step into an existing hydrothermal energy recovery process for better microalgae valorisation is also discussed.

To predict the compatibility of the tested solvent and solutes, Hansen solubility parameters (HSP) were studied (**Table 21**) to forecast miscibility and solvation and were compared with hexane, which is generally used for carotenoid extraction [130]. The Hansen method provides a convenient and efficient way to characterize solute/solvent interactions.

HSP is given by $\delta_{total}^2 = \delta_d^2 + \delta_p^2 + \delta_H^2$ which consists of its three partitioned HSP in terms of dispersion force δ_d , polar (permanent dipole forces) δ_p , and (hydrogen-bonding force) δ_H , respectively. In general, the more similar the two δ_{total} are, the greater the affinity between solutes and solvents. MTHF was chosen for carotenoid extraction since it has a δ_{total} which is very close to the one of carotenoids and since it is a green solvent.

Hansen solubility parameters (MPa ^{1/2})	Solvents				Solutes		
	MTHF	Ethanol	Water	Hexane	β -carotene	Lutein	Zeaxanthin
δ_{total}	17.69	26.5	47.8	15	17.5	18.4	18.5
Dispersion δ_d	16.4	15.8	15.6	15	17.4	17.8	17.8
Polar δ_p	4.8	8.8	16.0	0	0.8	1.3	1.4
Hydrogen Bonding δ_H	4.6	19.4	42.3	0	1.7	4.5	4.8

Table 21: Hansen solubility parameters: solvent/solute interactions. MPa^{1/2} (equivalent to joules/cubic centimeter; $2.0455 \times (\text{cal/cc})^{1/2}$) at 25  C. HSP is given by $\delta_{total}^2 = \delta_d^2 + \delta_p^2 + \delta_H^2$ which now consists of its three partitioned HSP in terms of dispersion force δ_d , polar (permanent dipole forces) δ_p , and hydrogen-bonding δ_H force, respectively [130].

6.2 Elemental composition before and after the extraction

The elemental composition of non-extracted *C. vulgaris* dry biomass was measured, and the proportions of the main elements relative to the weight of the biomass are given in **Table 22**. The high heating value (HHV) computed from the elemental composition

Biomass	Extraction conditions			Carbon %	Nitrogen %	Sulfur %	Hydrogen %	Oxygen %
Before extraction				49.2 ±0.45	6.30 ±0.27	0.89 ±0.04	7.45 ±0.15	33.9 ±0.5
After extraction	15 min	40°C	100%MTHF	45.0 ±0.25	5.76 ±0.48	0.82 ±0.03	6.86 ±0.21	31.3 ±1.4
	30 min	40°C	100%MTHF	42.8 ±0.37	5.57 ±0.47	0.81 ±0.04	6.49 ±0.19	31.6 ±0.7
Dry biomass (<5% moisture)	15 min	110°C	100%MTHF	40.3 ±0.74	5.12 ±0.12	0.74 ±0.04	6.25 ±0.13	29.4 ±1.6
	30 min	110°C	100%MTHF	38.6 ±0.66	5.07 ±0.04	0.71 ±0.01	6.07 ±0.24	28.5 ±1.4
	15 min	40°C	MTHF+ETOH	37.1 ±0.81	4.66 ±0.12	0.70 ±0.04	5.72 ±0.24	27.4 ±2.1
	30 min	40°C	MTHF+ETOH	36.3 ±0.17	4.53 ±0.13	0.69 ±0.09	5.61 ±0.12	25.9 ±2.2
	15 min	110°C	MTHF+ETOH	31.8 ±0.78	4.21 ±0.15	0.61 ±0.02	5.06 ±0.04	22.1 ±0.8
	30 min	110°C	MTHF+ETOH	29.9 ±1.30	4.19 ±0.09	0.65 ±0.04	4.79 ±0.05	23.8 ±1.2
After extraction	15 min	40°C	100%MTHF	41.9 ±0.09	5.40 ±0.06	0.74 ±0.03	6.36 ±0.16	31.8 ±0.04
	30 min	40°C	100%MTHF	41.4 ±0.35	5.21 ±0.16	0.81 ±0.04	6.27 ±0.09	31.1 ±0.23
Wet biomass (50% moisture)	15 min	110°C	100%MTHF	47.5 ±0.46	5.93 ±0.13	0.80 ±0.01	7.47 ±0.22	31.4 ±0.47
	30 min	110°C	100%MTHF	42.0 ±0.11	5.56 ±0.13	0.73 ±0.04	5.86 ±0.17	31.5 ±0.01
	15 min	40°C	MTHF+ETOH	45.9 ±0.57	6.10 ±0.15	0.74 ±0.01	7.04 ±0.08	30.0 ±0.17
	30 min	40°C	MTHF+ETOH	39.4 ±0.39	4.40 ±0.16	0.71 ±0.01	6.00 ±0.12	29.9 ±0.32
	15 min	110°C	MTHF+ETOH	37.7 ±0.38	4.67 ±0.12	0.68 ±0.02	4.79 ±0.04	27.2 ±1.90
	30 min	110°C	MTHF+ETOH	35.0 ±0.33	6.30 ±0.12	0.63 ±0.04	5.60 ±0.08	25.4 ±0.66

Table 22: Elemental composition of *C. vulgaris* before and after the extraction.

was 22.5 MJ/kg, and the total content of carotenoids was 417 µg/g DW (Table 23). Chlorophyll a, chlorophyll b and total chlorophyll concentrations were 2016 µg/g DW, 147 µg/g DW and 2173 µg/g DW, respectively.

As expected, HHV was lower in residual biomass after extraction, corresponding to set-up, which achieved a high extraction yield. Moreover, the correlation between remaining HHV and extraction yield was of -0.93, indicating that leftover HHV decreased almost linearly with increasing the extraction yield Table 23. Parameter changes in set-up inducing An increase in biomass and carotenoids extraction yields were the use of dry biomass (< 5% moisture content), a longer extraction time (30 min), a higher extraction temperature (110 °C), and the use of a mixture of MTHF and ethanol, instead of MTHF only

6.3 Carotenoids extraction yields

Although the proportion of total carotenoids extracted, reaching 311 µg/g DW, was higher for dry biomass with a mixture of solvents Table 23, a high yield of carotenoids (277 µg/g DW) was also obtained from wet biomass (50% moisture). In both cases, xanthophylls represented more than 75% of carotenoids, with 80-90 µg/g DW lutein, 60-70 µg/g DW astaxanthin, around 40 µg/g DW violaxanthin, and 28-35 µg/g DW canthaxanthin (Figure 52). The content of carotenes (22-24 % of total carotenoids) was around 45-50 µg/g DW for β-carotene and 18-22 µg/g DW for lycopene.

Biomass / Extrac- tion conditions	Remaining HHV (MJ kg ⁻¹)		Extracted biomass (% initial DW)		Carotenoids extracted (µg/g DW)	
Biomass before ex- traction	22.54 ±0.24				417 ±1.6	
Dry/Wet Biomass	Dry	Wet	Dry	Wet	Dry	Wet
15 min 40°C 100%MTHF	20.48 ±0.30	18.68 ±0.19	6.9	12.8	94 ±8.1	107 ±2.4
30 min 40°C 100% MTHF	19.19 ±0.38	18.45 ±0.16	9.0	14.8	102 ±5.2	127 ±2.1
15 min 110°C 100% MTHF	18.15 ±0.34	22.12 ±0.31	16.0	14.0	145 ±2.1	154 ±2.5
30 min 110°C 100% MTHF	17.37 ±0.39	18.14 ±0.20	16.4	13.9	159 ±1.0	186 ±1.2
15 min 40°C MTHF+ETOH	16.48 ±0.45	20.64 ±0.22	23.0	13.6	162 ±5.2	188 ±6.1
30 min 40°C MTHF+ETOH	16.17 ±0.27	17.52 ±0.20	21.9	18.7	183 ±6.7	216 ±8.9
15 min 110°C MTHF+ETOH	14.14 ±0.29	15.60 ±0.24	28.8	11.4	267 ±8.3	252 ±8.9
30 min 110°C MTHF+ETOH	12.98 ±0.48	15.71 ±0.16	29.3	19.4	311 ±6.1	277 ±3.9

Table 23: High Heating Value (HHV), extracted biomass (in % of the total dry weight of biomass before extraction) and the sum of carotenoids extracted. violaxanthin, astaxanthin, lycopene, β -carotene, lutein and canthaxanthin as a function of extraction conditions (time, temperature, solvents). Mean values are given with the Standard deviation.

Even if the total amount of extracted carotenoids was much lower when only 2-MTHF was used as a solvent, more xanthophyll was extracted from wet biomass than from dry biomass under such conditions **Figure 52**, which was not the case for carotenes. This was probably due to the polarity of water that improved the extraction of polar carotenoids not extracted with MTHF. After 30 minutes at 110 °C, the xanthophylls (more than 80% of extracted carotenoids) recovered in the highest amount from wet biomass were astaxanthin and lutein (48-50 µg/g DW), followed by canthaxanthin and violaxanthin (26-27 µg/g DW) **Figure 52**, whereas carotenes represented less than 20% of carotenoids extracted, with β -carotene (23 µg/g DW), and lycopene (11 µg/g DW). The proportion of compounds extracted varied between the different conditions used, also depending on the type of carotenoid **Figure 52** and **Figure 53**.

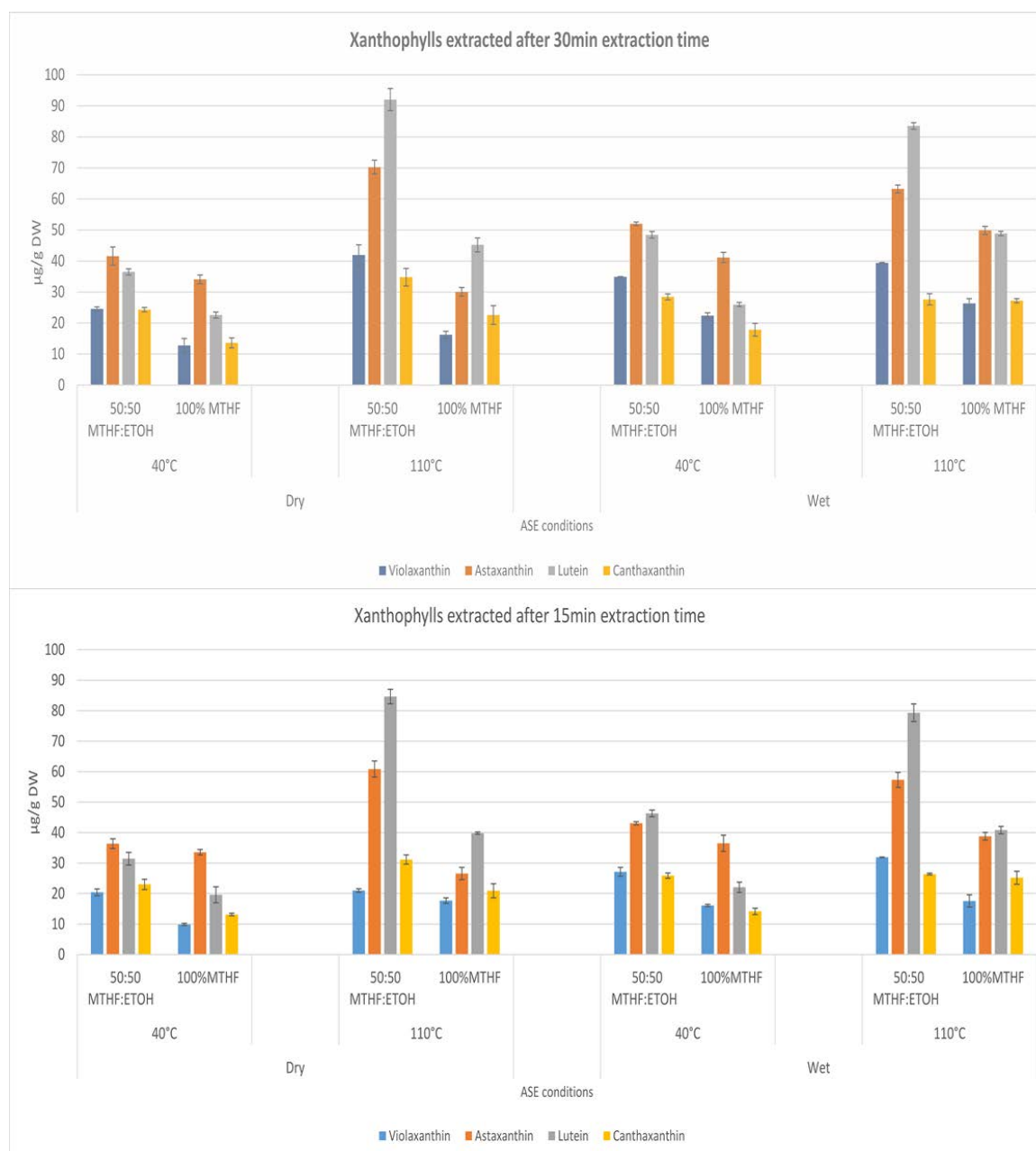


Figure 52: Effect of temperature (40 and 110 °C) and solvents (2-methyltetrahydrofuran, MTHF; ethanol, EtOH) on the extraction of xanthophylls from *C. vulgaris* dry (left) or wet (right) biomass, after 15 min (bottom) or 30 min (top) extraction time.

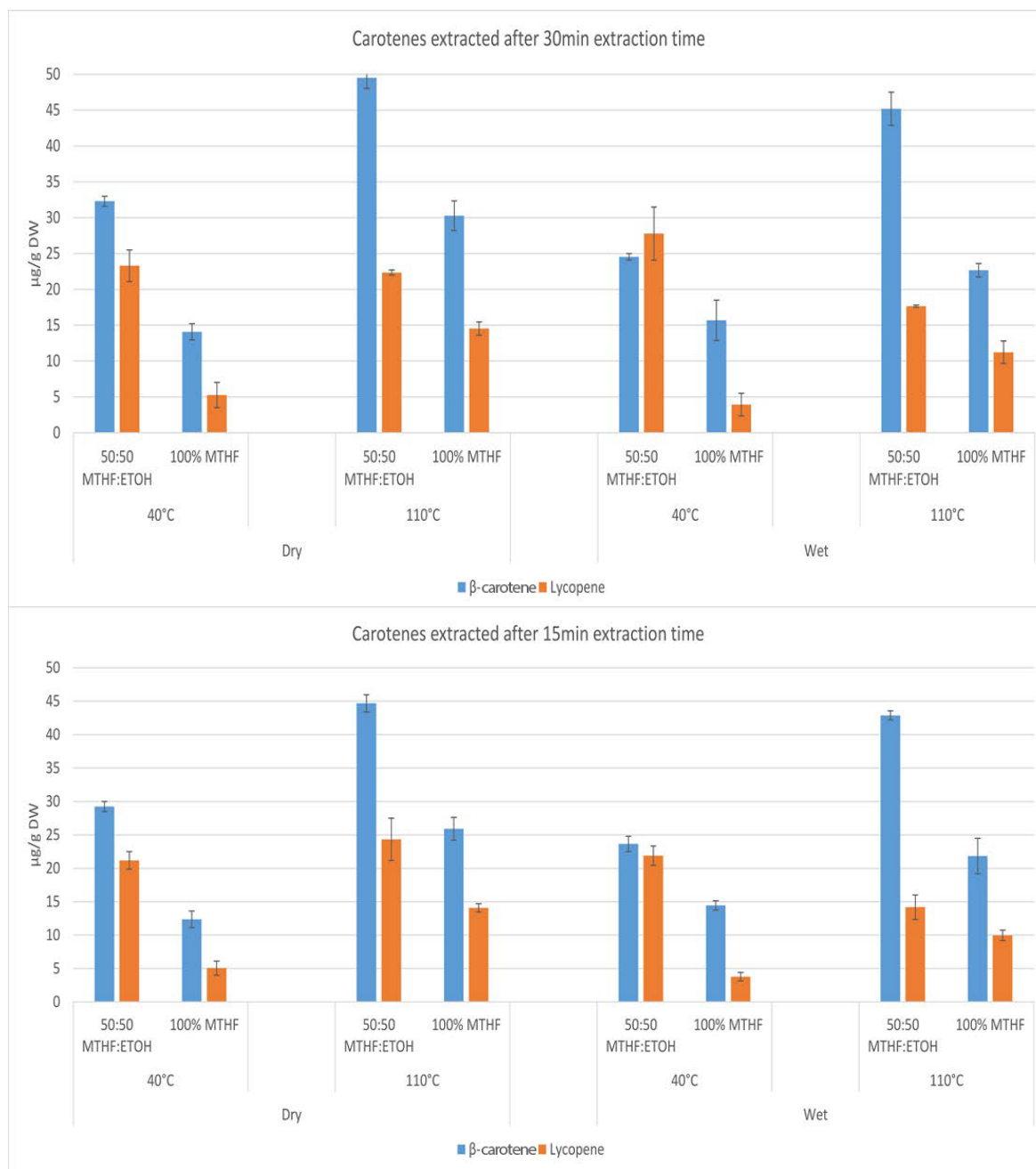


Figure 53: Effect of temperature (40 and 110 °C) and solvents (2-methyl tetrahydrofuran, MTHF; ethanol, EtOH) on the extraction of carotenoids from *C. vulgaris* dry (left) or wet (right) biomass, after 15 min (bottom) or 30 min (top) extraction time.

6.4 Effect of changes in extraction set-up on mean extraction yield and mean extracted carotenoids

The combined use of MTHF and ethanol instead of MTHF only was the parameter, which improved extraction the most (70% increase of extraction yield and 73% of total carotenoids being extracted). Drying the biomass favoured the extraction yield but negatively affected the extraction of most carotenoids.

Parameter changes	Mean extraction yield change	Mean carotenoids extracted change
Extraction time	+38%	+14%
Drying	+57%	-6%
Extraction temperature	+23%	+49%
Number of solvents	+70%	73%

Table 24: Effect of changes in extraction set-up on mean extraction yield and mean extracted carotenoids for different parameters.

The elemental composition of *C. vulgaris* was converted from dry weight proportions in molar proportions, as shown by Tuantet et al. [131]. It was expected to have HHV decreasing with increasing extraction yield because the solvents used have an affinity to other biomolecules such as lipids as well. This could explain the significant decrease of the calculated HHV in the remaining residues when more matter was removed during the extraction.

Studying the moisture effect on the extraction yield of pigment was investigated. Even if dry algal biomass is often used for pigment extraction [132–135], a slight increase in the carotenoids yield was reported in this study, **Table 23**. Drying is one of the most energy-consuming steps during the processing of microalgal biomass into various products. Therefore, if it can be avoided, the energy efficiency of the whole system would be improved, and the use of wet biomass is thus attractive, despite the need to process the biomass rapidly after harvesting [136]. The obtained results are in agreement with those of Papaioannou et al. [137] where carotenoids extraction yield from wet fungal biomass *Blakeslea trispora* was significantly higher than the dried ones.

The use of high temperature combined with the use of ethanol added to MTHF as solvent highly favours carotenoids extraction. For lycopene, β -carotene and lutein, the quantity extracted was significantly increased (**Figure 52**, **Figure 53**). In this case, the total biomass extraction yield was less pronounced than that of the carotenoids, resulting in a higher proportion of carotenoids in the extract. However, rising temperature could increase the energy demand of the system. Therefore, adding ethanol to MTHF allows decreasing the operating costs as ethanol enhance the penetration of solvent through the extracellular membrane of *C. vulgaris* to the cellular matrix, and like this reduce the need of deploying higher temperatures.

As all species have not the same amount of pigments and cell complexity as *C. vulgaris*, it is likely that the amount of carotenoids extracted will not be similar, if other species are chosen. As cell walls of *C. vulgaris* consist of a very strong matrix made of polysaccharide and glycoprotein providing the cells with a formidable defence, this makes it more challenging for carotenoids extraction. Other species such as *Dunaliella sp* and *Haemotococcus pluvialis* known for their high carotenoids content [138] have a less rigid cellular membrane. This could improve solvents penetration and thus improving the carotenoids extraction yield. However, the highest increase in quantity extracted was observed at the same extraction conditions for all carotenoids investigated (higher temperature and ethanol mixed with MTHF).

The production of biofuels from microalgae appears to be promising [133,139–141], but remains limited because of economic reasons [142]. In addition to the fluctuating price of fossil fuels, the development of low-cost cultivation systems, low-energy harvesting techniques and cost-effective downstream processing are still challenging to be addressed successfully [142,143]. In such a context, the co-culture of microalgae with other microorganisms such as fungi has been shown to facilitate the harvesting step and has the potential to reduce operational costs [143].

To improve the economic and ecological sustainability of large-scale production of microalgal biofuels, the extraction of high-value chemicals should be integrated with the use of residual biomass for energy production in a biorefinery [26,28,136,144]. This is the

purpose of the work presented here, which is part of the SunChem project that aims to develop an integrated process for the hydrothermal production of methane from microalgae, after extraction of added-value chemicals like carotenoids [38,88,143].

This additional extraction step may also serve to prevent deactivation of the Ru/C catalyst caused by the sulphur released from the biomass. According to the results obtained here, the sulphur content can be reduced by up to 30.6% (extraction from dry biomass for 15 min at 110 °C using a mixture of both solvents). With further optimisation of the extraction parameters, this may improve the lifetime of the catalyst prior to the hydrothermal treatment substantially.

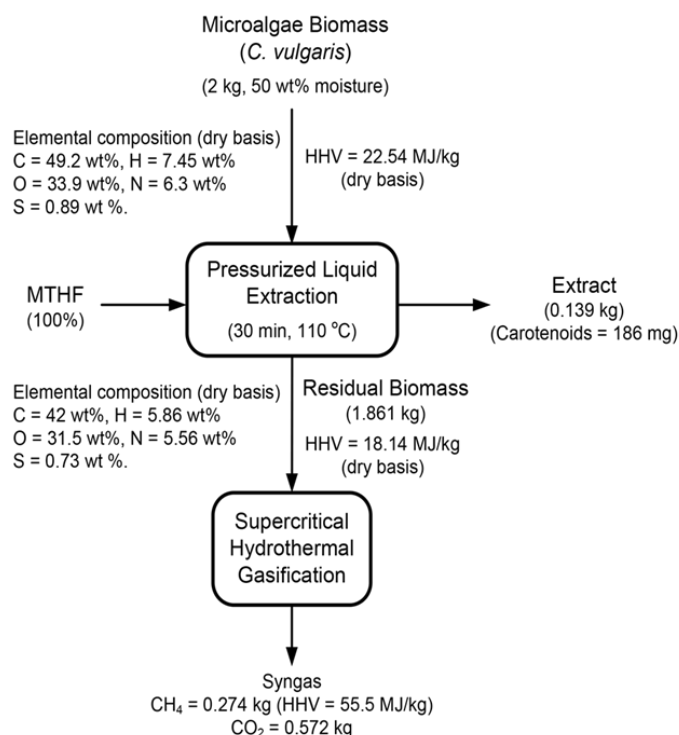


Figure 54: Microalgae processing using pressurised liquid extraction and supercritical hydrothermal gasification.

Figure 54 presents the complete processing of microalgae biomass using pressurised liquid extraction and supercritical hydrothermal gasification. It also reports the elemental compositions of microalgae and residual biomass: for illustration purpose, 2 kg of microalgae biomass (i.e. 1 kg dry microalgae) are used to extract carotenoids with 100% MTHF for 30 min at 110°C. In this particular case, 0.139 kg (13.9%) of the extract is obtained based on the total dry weight of biomass (**Figure 54, Table 23**).

The residual biomass has 42, 5.86, 31.5, 5.56 and 0.73 wt% of carbon, hydrogen, oxygen, nitrogen and sulphur, respectively, and that can be converted to 3.5, 5.86, 1.97, 0.4 and 0.023 atoms of carbon, hydrogen, oxygen, nitrogen and sulphur, respectively. Nitrogen, sulphur and ash have to be removed via salt separation before hydrothermal gasification (HTG). The residual biomass, entering the HTG, can be represented as $\text{CH}_{1.67}\text{O}_{0.56}$ without considering nitrogen, sulphur and ash. The conversion of biomass into CH_4 and CO_2 is based on the conceptual overall net reaction [145], which can be written for residual biomass as follows:



Equation 29: The conversion of algal biomass into CH_4 and CO_2 .

Based on Equation 1, 12 kg of carbon in the residual biomass can produce 9.104 and 18.964 kg of CH_4 and CO_2 , respectively. The residual biomass has 0.362 kg (42 wt% of 0.861 kg residual biomass on dry basis) of carbon, which can produce 0.274 and 0.572 kg

of CH₄ and CO₂, respectively. Finally, HHV value for syngas from the HTG is 15.22 MJ/kg, based on the amount of CH₄ present in the syngas. Note that CH₄ has HHV of 55.5 MJ/kg.

Carotenoids extraction is enhanced by the use of high temperature and with a mixture of MTHF and ethanol compared to low temperature and MTHF only. However, the optimal temperature, which would allow optimising the balance between the processing costs, the economic value of the chemicals extracted, and the energy content of the residual biomass remains to be determined. This optimisation should, in particular, investigate the effects on the extraction of intermediate temperatures along with different proportions between MTHF and ethanol since the optimal ratio could also depend on the temperature. Furthermore, microalgae can produce other added-value chemicals that could be extracted as well. Taking these fine chemicals into account in the process of optimization should increase the overall economic and ecological value of the system in a sustainable biorefinery concept. Moreover, according to our calculations, not negligible amount of energy is recyclable from the gasification of the residues after the extraction of carotenoids, which improve the overall system energy by reducing the energy consumption.

Chapter 7 Final remarks

7.1 Sustainable production of algal biomass and energy: OSS-SOFC-HTG combined system

This study illustrates a complex concept based on waste stream OSS and combined HTG and SOFC processes with potential algal biomass production. Nutrients, when recovered at source level, are more concentrated than in wastewater treatment plants. For instance, the phosphorus content of effluents from composted human excreta (leachate) was 50-fold higher than a typical wastewater effluent. This shows the potential of on-site sanitation over the current existent system, where nutrients present in a very diluted form, are difficult to recover. As phosphorus is a limited and vital resource, achieving high phosphorus recovery was one of the objectives of this study. The successful tests at KIT-Karlsruhe have shown that: (1) principally the hydrothermal gasification of the leachate is technically feasible even if the gasification efficiency was not high. (2) High recovery yields for phosphorus, and nitrogen were achieved through the HTG treatment. (3) Microalgae growth tests in AP were successful after an adaptation period. (4) Syngas produced during the gasification was successfully used as a fuel for the SOFC. The results of this work showed interesting new opportunities for further research towards OOS stream valorisation, contributing to closing the nutrient loop while producing carbon-neutral biofuels and valuable co-products from microalgae cultivation. A decentralised hydrothermal treatment of household effluents could provide a system that valorises nutrients and chemical energy which is very promising if the technological and economical challenge could be solved.

However, how efficient and affordable most of the on-site sanitation systems might be, they often need a certain open-mindedness from dwellers to change their "classical" Water-Closet comfort to an alternative system. This is indeed the case in Cressy: the whole building conception was discussed during numerous months between the future inhabitants that already were convinced of a changing paradigm necessity regarding wastewater management. How environmentally justifiable it can be, is it fair to ask people to change their daily life regarding their private hygiene? We have seen that even environmentally sensitive people might be disheartened by alternative systems. From this perspective, it is no more a matter of engineers but a real psychosocial limitation.

Answers to the scientific questions addressed earlier in the thesis:

RQ1-1: *Can we use on-site sanitation effluent as a feedstock for HTG process to recover nutrients and produce energy-rich gas?*

Yes, a successful 40h steady-state gasification was achieved using the leachate effluent. Nevertheless, the modest carbon conversion efficiency of 40% suggests that carbon content was not fully converted into energy-rich gas. Only part of the missing organic fraction was detected in the HTG aqueous effluent, which indicates that tar formation potentially occurred during the gasification. Moreover, an increase in nickel concentration was observed in the HTG effluent indicating the corrosion of the HTG reactor wall. The high salt content of the leachate can cause clogging issues. To increase the carbon conversion efficiency, a higher temperature can be applied. However, a trade-off between higher temperature and energy consumption of the gasification unit must be made. Another option will be the use of hydrothermal catalytic gasification. As leachate effluents have a substantial amount of sulphur content, a salt separator and sulphur removal units should be added before the hydrothermal gasification reactor.

RQ1-2: What is the potential to use this energy-rich gas to generate electricity using a SOFC?

The major gas obtained from HTG experiment in this work was mainly H_2 . For SOFC operations, H_2 is the ideal gas for high electrical conversion efficiency production. CH_4 can also be used in SOFC, but a steam reforming step is generally needed to avoid carbon deposition within the SOFC cell. The presence of higher amount of non-methane hydrocarbon (C_2H_4 , C_2H_6 and C_3H_8) increased the degradation rate of the SOFC cell significantly up to 11%/kh. Consistent and stable performance can be achieved if the amount of non-methane hydrocarbon is reduced. The addition of steam in the fuel gas also allows to shift the reaction from the carbon disposition region. Finally, an electrical conversion efficiency (ECE) of 74.7% was predicted using HTG fuel gas operating in a combined SOFC and inverted Brayton cycle mode gas turbine system.

7.2 Nitrogen-containing organics from the hydrothermal conversion of algal biomass.

During the gasification of algal biomass and/or leachate effluents, the build-up of some measured recalcitrant nitrogen organic substances (NOC's) in the salt brine effluent cannot be avoided owing to continuous operation. The most important N-containing compounds observed in the salt brine effluent studied were amines, alkyl-pyrrolidones, cyclic amides and traces of piperazinediones. These compounds showed high toxicity to microalgae when salt brine effluent was used as a growth medium. The assimilation of these compounds as carbon and nitrogen sources by three microalgae strains showed that the tested algae were not able to metabolise the NOC's compounds. Therefore, the salt brine effluent was further gasified to completely convert the organics to methane while releasing nitrogen from the complex NOC's molecules as a liquid ammonium fertiliser. However, the cost and energy demand of an additional gasification step should be studied. The advantages of such a process were presented in a detailed techno-economic assessment for the integration of algae production and hydrothermal gasification technology in earlier study [146].

Studying the effect of biochemical composition in the formation of these recalcitrant organics should be investigated. Microalgae are composed of carbohydrates, proteins, nucleic acids and lipids and contain substantial amounts of heteroatoms such as nitrogen (0.1 to > 10 wt. %), sulphur (0.1 to > 1 wt. %), chlorides (0.1 to > 16 wt. %) and phosphorus (0.1 to > 2 wt. %). This complex interaction between macromolecular structure and heterogeneous nature of algal biomass makes algal biomass decomposition very difficult to predict during HT process. Thus, an understanding of decomposition pathways of algal biomass as a function of HT parameters (temperature, residence time and pressure) is essential to predict the formation and decomposition of recalcitrant organics compounds.

RQ2-1: Is it feasible to use the HTG effluent as a microalgae growth medium (Leachate HTG effluent by-product)?

Leachate HTG effluent can be used as a growth medium for microalgae production after a few adaptations. Due to high salt content, and the presence of some recalcitrant organics, a dilution factor of 5 was applied. Moreover, the pH was adjusted to 7 as the HTG effluent was strongly alkaline (pH varied from 9-10). Nevertheless, microalgae were able to grow on the HTG effluents after a remarkable lag phase compared to control cultures. The presence of some organics such as phenols and recalcitrant organics could be the reason behind this lag phase. Less organics compound should be found in the HTG effluent if the carbon conversion efficiency is higher. Nevertheless, the removal of trace organics from HTG effluent can also be performed using a filter, such as activated carbon, prior to the use as a culture medium.

RQ2-2: Is it feasible to use the HTG effluent as a microalgae growth medium? (algal biomass HTG effluent by-product)?

Three microalgae species ranging from brackish to freshwater species were grown successfully in an algal biomass HTG effluent by-product. Despite the high carbon conversion efficiency obtained under catalytic conditions (75%), some recalcitrant organic compounds (NOC's) were detected in the aqueous phase mainly. High concentrations of NOCs were detected in HTG effluent, for example,

2-pyrrolidinone 193mg/L and piperidine 148mg/L. The HTG effluent by-product was subject to dilution and pH adjustment before using as a microalgae culture medium. At concentration of 100ppm of the tested NOC's, the growth rate of all microalgae species tested diminished significantly compared to the control. The IC50 for all cases is roughly 75 ppm. For a continuous algae production, a cleaning step or a dilution factor could be applied before the use of HTG effluent as a growth medium.

7.3 Dye sensitised solar cells for enhanced algae biomass production

Even with low solar light conversion efficiency of 3%, the presence of DSC panels allows a reduction of GHG emissions compared to the alternative of a PBR without DSC panel. Further potential for improving the environmental performance of the whole system relies on improving the efficiency of DSC panels. This can also lead to a reduction in space requirement of microalgae production systems. Even if some results are promising, the DSC-PBR system is still far from a real large-scale implementation, the construction of the bioreactor should also be optimised in terms of material weight and type and additional factors will need to be considered. For example, an important aspect which hasn't been considered yet is the variation of light intensity during the day and the weather change during seasons in real outdoor conditions. Techno-economic analyses of large-scale production in a hybrid cultivation mode will reveal whether this system is also economically more viable or not. Combining the positive effects of dye sensitised solar cells to scale-up research would be interesting by using a solar greenhouse, for instance, this technology could be applied to several (existing or not) installations without much effort and have a positive effect.

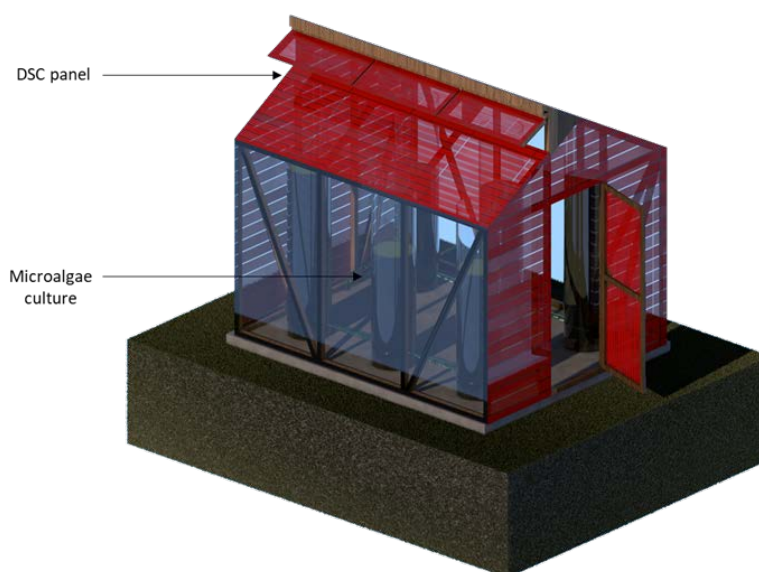


Figure 55: DSC-Greenhouse for microalgae production idea.

RQ3-1: What is the effect of DSC filter on the growth kinetics and the final microalgae biomass composition?

The results obtained for high light intensity with DSC-PBR for both tested algae are very promising. A significant increase in growth rate and final biomass was observed in the case of the green algae *C. vulgaris*. This increase was not accompanied by a change in the macromolecule composition. Moreover, in the case of *H. pluvialis*, a slowdown of the stress mechanism was demonstrated in the presence of both DSC-panels.

These results are very encouraging as applying of a DSC panel could prolongate the green phase of *H. pluvialis* for maximum productivity before the stress phase (red cells, lower productivity). The knowledge acquired from this work gave rise to new perspectives concerning the culture of *H. pluvialis* at large scale. For the future investigation, DSC panel absorbing the infrared wavelength should be tested to reduce the heating generated inside microalgae photobioreactor.

RQ3-2: *In term of CO₂ emissions, what is the impact of adding a DSC panel to the structure of a microalgae photobioreactor?*

Even with low solar light conversion efficiency of 3%, the amount of CO₂ equivalent is almost similar to the one of silicon PV with 40g CO₂-eq/KWh compared to 35g CO₂-eq/KWh. These values were calculated for the same operation period over 20 years and included the manufacturing process. Today, a new generation of a semi-transparent panel called perovskite reached up to 20% of solar conversion efficiency. Constructing new Perovskite-PBR system could be the next revolution in microalgae biotechnology.

7.4 Biomass valorisation: Extraction of carotenoids using green solvents and syngas production from residual biomass

For the economic viability of algae production, high-value products such as carotenoids were extracted from microalgae prior the HT step and using sustainable extraction methods. The philosophy behind was to extract carotenoids and to treat the residual biomass via HT treatment for energy recovery purposes. To avoid the use of conventional toxic solvents during the extraction step, 2-methyltetrahydrofuran (2-MTHF), a green solvent, was proposed as a replacement. High compatibility in terms of solvent-solute interactions was predicted using the theoretical value of the Hansen solubility parameter (HSP) confirmed by the obtained results. 2-MTHF has the advantages to be biodegradable and has a promising environmental footprint and can be easily recycled. This allows to optimise the balance between the processing costs, the economic value of the chemicals extracted, and the energy content of the residual biomass. The effects on the extraction of intermediate temperatures along with different proportions between 2-MTHF and ethanol should be investigated. Furthermore, microalgae can produce other added-value chemicals that could be extracted as well. Taking these fine chemicals into account in the process of optimisation should increase the overall economic and ecological value of the system in a sustainable biorefinery concept.

RQ4: *What is the efficiency of carotenoids extraction from wet algal biomass and the potential of energy recovery from residual biomass?*

45% of total carotenoids were extracted from wet algal biomass (50 wt% moisture) in the case of 100% 2-MTHF and a high heating value (HHV) of 18.1 MJ kg⁻¹ for residual biomass was calculated. To increase the solubility of some specific polar carotenoids, a 1:1 mixture of 2-MTHF and ethanol was used and the results showed an increase of carotenoids yields up to 66% of total carotenoids with remaining HHV of the residual biomass of about 15.7 MJ kg⁻¹.

7.5 Conclusion

The PAWaSto approach of an integrated facility in an urban area, to co-produce bioenergy and high-value chemicals from algae biomass, seems to be a promising solution to towards the implementation of microalgae production. On the one hand, this project has shown that an on-site sanitation system (OSS) could be a solution for nutrient and energy supply in microalgae production in combination with a hydrothermal gasification (HT) treatment system. However, further improvements should be considered to increase the gasification yield when using effluent with high inorganic content. Moreover, during the gasification of algal biomass and/or leachate effluents, the build-up of some measured recalcitrant nitrogen organic substances (NOC's) in the HT effluent cannot

be avoided owing to continuous operation. These compounds showed high toxicity to microalgae when HT aqueous phase (AP) was used as a growth medium. A cleaning step is required for continuous gasification if AP effluents are used as a microalgae growth medium. On the other hand, the addition of transparent dye-sensitised solar cells on top of the photobioreactor allowed (1) an addition production of electrical energy and (2) the reduction of ultraviolet radiation and light intensity reaching the algae culture. The results were different for *H. pluvialis* and *C. vulgaris*, but both algae showed that the use of these panels was beneficial for the growth of microalgae. This opens a lot of possibilities for combining different algae strains with different DSC-colours. Besides, the combination of DSC-PBR decreased the carbon footprint of the overall system, thanks to the CO₂ credit for electricity production avoiding. For the economic viability of algae production, high-value products can be extracted from microalgae using sustainable extraction methods. Moreover, after the extraction, a substantial amount of biomass residues can be used for energetic purposes. The overall combination of the different processes as proposed in the PAWaSto project was proven to have a high potential. However, weak points within the system were also identified. Yet, the ability to run all these processes over long times without interruption and scale-up effects need to be studied. Works on scale-up and optimisation of such systems are already under study for example at Karlsruher Institut für Technologie (KIT), Germany with the VERENA plant. Regardless of the huge potential portrayed by the microalgae biorefinery concept, there is an evident lack of experimental data for such complex systems. Many studies report on the importance of the biorefinery concept based on modelling and simulation studies. This thesis provides data which can be used to improve such models, which are needed to plan and implement such a highly complex system.

References

- [1] Food and Agriculture Organization of the United Nations, *The future of food and agriculture: trends and challenges* (2017), ISBN 978-92-5-109551-5.
- [2] An IPCC Special Report on the impacts of global warming of 1.5°C above pre-industrial levels and related global greenhouse gas emission pathways (2019), ISBN 978-92-9169-153-1.
- [3] Global Energy and carbon dioxide Status Report (2019), <https://www.iea.org/reports/global-energy-co2-status-report-2019>.
- [4] Renewable Energy Agency, *Global Energy Transformation: A Roadmap to 2050* (2019), ISBN : 978-92-9260-121-8.
- [5] What are the greenhouse gas changes since the Industrial Revolution? ACS Climate Science Toolkit, IPCC Fourth Assessment Report (2007), Chapter 2.
- [6] Chapter Climate Change 2014 Synthesis Report Summary for Policymakers Summary for Policymakers, (2014).
- [7] R.A. Feely, S.C. Doney, S.R. Cooley, Ocean acidification: Present conditions and future changes in a high carbon dioxide world, (2009) *Oceanography*, (22) 36–47. <https://doi.org/10.5670/oceanog.2009.95>.
- [8] A. Schilt, M. Baumgartner, T. Blunier, J. Schwander, R. Spahni, H. Fischer, T.F. Stocker, Glacial-interglacial and millennial-scale variations in the atmospheric nitrous oxide concentration during the last 800,000 years, (2010) *Quat. Sci. Rev.* (29) 182–192. doi:10.1016/j.quascirev.2009.03.011.
- [9] H.K. Solomone Fifita, Piers Forster, Veronika Ginzburg, Collins Handa, Mitigation pathways compatible with 1.5°C in the context of sustainable development, (2018), IPCC SR1.5.
- [10] Myhre, G., D. Shindell, F.-M. Bréon, W. Collins, J. Fuglestad, J. Huang, D. Koch, J.-F. Lamarque, D. Lee, B. Mendoza, T. Nakajima, A. Robock, G. Stephens, T. Takemura and H. Zhang, Anthropogenic and Natural Radiative Forcing. In: *Climate Change 2013*, (2013), The Physical Science Basis. Cambridge University Press, Cambridge, United Kingdom and New York, NY, USA.
- [11] Energy and climate policy for low-carbon growth in Europe -Energy Post (2013). <https://ec.europa.eu/clima/policies.com>
- [12] F. Von Hippel, *The Uncertain Future of Nuclear Energy*, (2010). ISBN 978-0-9819275-7-2.
- [13] I. Staffell, D. Scamman, A. Velazquez Abad, P. Balcombe, P.E. Dodds, P. Ekins, N. Shah, K.R. Ward, The role of hydrogen and fuel cells in the global energy system, *Energy Environ. Sci.* 12 (2019) 463–491, DOI: 10.1039/c8ee01157e.
- [14] Combating climate change, Fact Sheets on the European Union, European Parliament website (accessed January 12, 2020).
- [15] Federal Council aims for a climate-neutral Switzerland by 2050, website www.admin.ch (accessed January 12, 2020).
- [16] M. Bagnoud-Velásquez, D. Refardt, F. Vuille, C. Ludwig, Opportunities for Switzerland to contribute to the production of algal biofuels: The hydrothermal pathway to bio-methane, *Chimia (Aarau)*. 69 (2015) 614–621, DOI: 10.2533/chimia.2015.614.
- [17] M.A. Perea-Moreno, E. Samerón-Manzano, A.J. Perea-Moreno, Biomass as renewable energy: Worldwide research trends, *Sustain.* 11 (2019). doi:10.3390/su11030863.
- [18] R. Kumar, A.K. Ghosh, P. Pal, Synergy of biofuel production with waste remediation along with value-added co-products recovery through microalgae cultivation: A review of membrane-integrated green approach, *Sci. Total Environ.* 698 (2020), <https://doi.org/10.1016/j.scitotenv.2019.134169>.
- [19] E.M. Trentacoste, A.M. Martinez, T. Zenk, The place of algae in agriculture: Policies for algal biomass production, *Photosynth. Res.* 123 (2015) 305–315, DOI 10.1007/s11120-014-9985-8.
- [20] P.K. Usher, A.B. Ross, A. Camargo-Valero, A.S. Tomlin, W.F. Gale, An overview of the potential environmental impacts of large-scale microalgae cultivation, *Biofuels*, 5:3, (2014) 331-349, DOI: 10.1080/17597269.2014.913925.
- [21] M.I. Khan, J.H. Shin, J.D. Kim, The promising future of microalgae: Current status, challenges, and optimization of a sustainable and renewable industry for biofuels, feed, and other products, *Microb. Cell Fact.* 17 (2018), <https://doi.org/10.1186/s12934-018-0879-x>.

-
- [22] L. Delgadillo-Mirquez, F. Lopes, B. Taidi, D. Pareau, Nitrogen and phosphate removal from wastewater with a mixed microalgae and bacteria culture, *Biotechnol. Reports*. 11 (2016) 18–26. <https://doi.org/10.1016/j.btre.2016.04.003>.
- [23] K. Tuantet, H. Temmink, G. Zeeman, M. Janssen, R.H. Wijffels, C.J.N. Buisman, Nutrient removal and microalgal biomass production on urine in a short light-path photobioreactor, *Water Res.* 55 (2014) 162–174, <https://doi.org/10.1016/j.watres.2014.02.027>.
- [24] S. Gupta, S.B. Pawar, R.A. Pandey, Current practices and challenges in using microalgae for treatment of nutrient rich wastewater from agro-based industries, *Sci. Total Environ.* 687 (2019) 1107–1126, <https://doi.org/10.1016/j.scitotenv.2019.06.115>.
- [25] D. Parlevliet, N. Moheimani, Efficient conversion of solar energy to biomass and electricity, *Aquat. Biosyst.* 10 (2014) 4. <https://doi.org/10.1186/2046-9063-10-4>.
- [26] H.W. Yen, I.C. Hu, C.Y. Chen, S.H. Ho, D.J. Lee, J.S. Chang, Microalgae-based biorefinery - From biofuels to natural products, *Bioresour. Technol.* 135 (2013) 166–174. <https://doi.org/10.1016/j.biortech.2012.10.099>.
- [27] M. Naruka, M. Khadka, S. Upadhayay, S. Kumar, Potential Applications Of Microalgae In Bioproduct Production : A Review Potential Applications Of Microalgae In Bioproduct Production : A Review, *Octa J. Biosci.* Vol 7(2019), 01-05 ISSN 2321-3663.
- [28] I. Hariskos, C. Posten, Biorefinery of microalgae - opportunities and constraints for different production scenarios, *Biotechnol. J.* 9 (2014) 739–752. <https://doi.org/10.1002/biot.201300142>.
- [29] World bioenergy association, Bioenergy statistics 2018: Summary Report, <https://worldbioenergy.org/global-bioenergy-statistics>, (accessed January 12, 2020).
- [30] Paul L. Younger, Environmental impacts of coal mining and associated wastes: a geochemical perspective, *Geo Society*, 236 (2004) 169–209, <https://doi.org/10.1144/GSL.SP.2004.236.01.12>.
- [31] B. Steubing, R. Zah, P. Waeger, C. Ludwig, Bioenergy in Switzerland: Assessing the domestic sustainable biomass potential, *Renew. Sustain. Energy Rev.* 14 (2010) 2256–2265, doi:10.1016/j.rser.2010.03.036.
- [32] C. Bauer, S. Hirschberg, Y. Bauerle, S. Biollaz, A. Calbry-Muzyka, B. Cox, T. Heck, M. Lehnert, A. Meier, H.-M. Prasser, W. Schenler, K. Treyer, F. Vogel, H.C. Wieckert, X. Zhang, M. Zimmerman, V. Burg, G. Bowman, M. Erni, M. Saar, M.Q. Tran, Potentials, costs and environmental assessment of electricity generation technologies, Swiss Fed. Energy Off. (2017) PSI, WSL, ETHZ, EPFL. Paul Scherrer Institut, Villigen PSI, Switzerland.
- [33] D. Matschegg, S. Holzleitner, Monika Enigl, European Technology and Innovation Platform Bioenergy – Support of Advanced Bioenergy Stakeholders 2016 - 2017 Overview on general information for each of the 8 topics ETIP Bioenergy Overview on general information for each of the 9 topics, D.2.4 (2016).
- [34] R.A. Lee, J.-M. Lavoie, From first- to third-generation biofuels: Challenges of producing a commodity from a biomass of increasing complexity, *Anim. Front.* 3 (2013) 6–11, doi:10.2527/af.2013-0010.
- [35] M. Siedlecki, W. de Jong, A.H.M. Verkooyen, Fluidized bed gasification as a mature and reliable technology for the production of bio-syngas and applied in the production of liquid transportation fuels-a review, *Energies.* 4 (2011) 389–434. DOI: 10.3390/en4030389.
- [36] J. Reimer, G. Peng, S. Viereck, E. De Boni, J. Breinl, F. Vogel, A novel salt separator for the supercritical water gasification of biomass, *J. Supercrit. Fluids.* 117 (2016) 113–121, <https://doi.org/10.1016/j.supflu.2016.06.009>.
- [37] R. Toonssen, P. V. Aravind, G. Smit, N. Woudstra, A.H.M. Verkooyen, System study on hydrothermal gasification combined with a hybrid solid oxide fuel cell gas turbine, *Fuel Cells.* 10 (2010) 643–653. <https://doi.org/10.1002/fuce.200900188>.
- [38] A.G. Haiduc, M. Brandenberger, S. Suquet, F. Vogel, R. Bernier-Latmani, C. Ludwig, SunChem: an integrated process for the hydrothermal production of methane from microalgae and CO₂ mitigation, *J. Appl. Phycol.* 21 (2009) 529–541.
- [39] A.G. Chakinala, D.W.F. Brilman, W.P.M. Van Swaaij, S.R.A. Kersten, Catalytic and non-catalytic supercritical water gasification of microalgae and glycerol, in: *Ind. Eng. Chem. Res.* 49 (2010), 1113–1122. <https://doi.org/10.1021/ie9008293>.
- [40] M. Bagnoud-Velásquez, U. Schmid-Staiger, G. Peng, F. Vogel, C. Ludwig, First developments towards closing the nutrient cycle in a biofuel production process, *Algal Res.* 8 (2015). <https://doi.org/10.1016/j.algal.2014.12.012>.
- [41] S. Elsayed, N. Boukis, J. Sauer, Hydrothermal gasification of microalgae - prospects and challenges, *DGMK Tagungsbericht.* (2014) 221–228.

-
- [42] R.E. Blankenship, Early Evolution of Photosynthesis, *Plant Physiol.* 154 (2010) 434–438, DOI: <https://doi.org/10.1104/pp.110.161687>.
- [43] L. Barsanti, P. Gualtieri, Algae: Anatomy, Biochemistry, and Biotechnology, *J. Phycol.* 43 (2007) 412–414, DOI: [10.1111/j.1529-8817.2007.00335.x](https://doi.org/10.1111/j.1529-8817.2007.00335.x).
- [44] G. Saefurahman, Effects of different light spectra on the growth composition, and productivity of microalgae from 4 different taxa with different pigment profiles, (2015) Corpus ID: 88544612.
- [45] A.S. Petsas, M.C. Vagi, effects on the photosynthetic activity of algae after exposure to various organic and inorganic pollutants: Review, *InTech* (2017), doi:10.5772/67991.
- [46] J. V. Moroney, R.A. Ynalvez, Proposed carbon dioxide concentrating mechanism in *Chlamydomonas reinhardtii*, *Eukaryot. Cell.* 6 (2007) 1251–1259. doi: [10.1128/EC.00064-07](https://doi.org/10.1128/EC.00064-07).
- [47] B.R. Green, D.G. Durnford, The chlorophyll-carotenoid proteins of oxygenic photosynthesis, *Annu. Rev. Plant Physiol. Plant Mol. Biol.* 47 (1996) 685–714, <https://doi.org/10.1146/annurev.arplant.47.1.685>.
- [48] M.R. Tredici, Photobiology of microalgae mass cultures: understanding the tools for the next green revolution, *Biofuels.* 1 (2010) 143–162. <https://doi.org/10.4155/bfs.09.10>.
- [49] E.C.S.Chan, *Handbook of Water and Wastewater Microbiology*; Chapter: Microbial nutrition and basic metabolism, ISBN: 9780080478197.
- [50] N.S. Garcia, J. Sexton, T. Riggins, J. Brown, M.W. Lomas, A.C. Martiny, High variability in cellular stoichiometry of carbon, nitrogen, and phosphorus within classes of marine eukaryotic phytoplankton under sufficient nutrient conditions, *Front. Microbiol.* 9 (2018). <https://doi.org/10.3389/fmicb.2018.00543>.
- [51] S.C. Lachmann, T. Mettler-Altmann, A. Wacker, E. Spijkerman, Nitrate or ammonium: Influences of nitrogen source on the physiology of a green alga, *Ecol. Evol.* 9 (2019) 1070–1082, <https://doi.org/10.1002/ece3.4790>.
- [52] R.A.E. Hamouda, G.W. Abou-El-Souod, Influence of various concentrations of phosphorus on the antibacterial, antioxidant and bioactive components of green microalgae *Scenedesmus obliquus*, *Int. J. Pharmacol.* 14 (2018) 99–107, <https://doi.org/10.3923/ijp.2018.99.107>.
- [53] Bomans E, Fransen K, Gobin A, Mertens J, Michiels P, Vandendriessche H, Vogels N, Addressing phosphorus related problems in farm practice, Final report to the European Commission, 2015.
- [54] C.J. Rhodes, Peak phosphorus - Peak food? The need to close the phosphorus cycle, *Sci. Prog.* 96 (2013) 109–152, <https://doi.org/10.3184/003685013X13677472447741>.
- [55] M. Cuaresma, M. Janssen, C. Vílchez, R.H. Wijffels, Horizontal or vertical photobioreactors? How to improve microalgae photosynthetic efficiency, *Bioresour. Technol.* 102 (2011) 5129–5137, <https://doi.org/10.1016/j.biortech.2011.01.078>.
- [56] J. Beardall, A. Johnston, J. Raven, Environmental regulation of CO₂-concentrating mechanisms in microalgae, *Can. J. Bot.* 76 (1998) 1010–1017, <https://doi.org/10.1139/b98-079>.
- [57] H. Begum, F.M. Yusoff, S. Banerjee, H. Khatoon, M. Shariff, Availability and Utilization of Pigments from Microalgae, *Crit. Rev. Food Sci. Nutr.* 8398 (2015), <https://doi.org/10.1080/10408398.2013.764841>.
- [58] Z. Dubinsky, N. Stambler, Photoacclimation processes in phytoplankton: mechanisms, consequences, and applications, *Aquat. Microb. Ecol.* 56 (2009) 163–176, <https://doi.org/10.3354/ame01345>.
- [59] H. Oldenhof, V. Zachleder, H. Van Den Ende, Blue- and red-light regulation of the cell cycle in *Chlamydomonas reinhardtii* (Chlorophyta), *Eur. J. Phycol.* 41 (2006) 313–320, <https://doi.org/10.1080/09670260600699920>.
- [60] M. Janssen, Microalgal Photosynthesis and Growth in Mass Culture, *Adv. Chem. Eng., Academic Press Inc.* (2016) 185–256, <https://doi.org/10.1016/bs.ache.2015.11.001>.
- [61] M. Ras, J.P. Steyer, O. Bernard, Temperature effect on microalgae: A crucial factor for outdoor production, *Rev. Environ. Sci. Biotechnol.* 12 (2013) 153–164, <https://doi.org/10.1007/s11157-013-9310-6>.
- [62] S.P. Cuellar-Bermudez, J.S. Garcia-Perez, B.E. Rittmann, R. Parra-Saldivar, Photosynthetic bioenergy utilizing CO₂: An approach on flue gases utilization for third generation biofuels, *J. Clean. Prod.* 98 (2015) 53–65,

- <https://doi.org/10.1016/j.jclepro.2014.03.034>.
- [63] R. Slade, A. Bauen, Microalgae cultivation for biofuels: Cost, energy balance, environmental impacts and future prospects, *Biomass and Bioenergy*. 53 (2013) 29–38, <https://doi.org/10.1016/j.biombioe.2012.12.019>.
- [64] S. Mishra and S.K. Ojha, Potentials of Oilgae: The Prospects and Challenges, *Microbiology applications*, (2013) 84–112.
- [65] M. Kent, H.M. Welladsen, A. Mangott, Y. Li, Nutritional evaluation of Australian microalgae as potential human health supplements, *PLoS One*. 10 (2015) e0118985. <https://doi.org/10.1371/journal.pone.0118985>.
- [66] *Algae-based biofuels: applications and co-products*, (2010), ISBN 978-92-5-106623-2 .
- [67] J. Masojídek, G. Torzillo, M. Koblížek, Photosynthesis in Microalgae, *Handb. Microalgal Cult. Appl. Phycol. Biotechnol.* (2013) 21–36, <https://doi.org/10.1002/9781118567166.ch2>.
- [68] M.N. Merzlyak, O.B. Chivkunova, I.P. Maslova, K.R. Naqvi, A.E. Solovchenko, G.L. Klyachko-Gurvich, Light absorption and scattering by cell suspensions of some cyanobacteria and microalgae, *Russ. J. Plant Physiol.* 55 (2008) 420–425, <https://doi.org/10.1134/S1021443708030199>.
- [69] R. Hill, F. Bendall, Function of the two cytochrome components in chloroplasts: A working hypothesis, *Nature*. 186 (1960) 136–137, <https://doi.org/10.1038/186136a0>.
- [70] M.D. Ooms, C.T. Dinh, E.H. Sargent, D. Sinton, Photon management for augmented photosynthesis, *Nat. Commun.* 7 (2016) 1–13, <https://doi.org/10.1038/ncomms12699>.
- [71] R.H. Wijffels, M.J. Barbosa, An outlook on microalgal biofuels, *Science* (80). 329 (2010) 796–799. <https://doi.org/10.1126/science.1189003>.
- [72] C. Cho, K. Nam, G.Y. Kim, Y.H. Seo, T.G. Hwang, J.W. Seo, J.P. Kim, J.I. Han, J.Y. Lee, Multi-bandgap Solar Energy Conversion via Combination of Microalgal Photosynthesis and Spectrally Selective Photovoltaic Cell, *Sci. Rep.* 9 (2019) 18999, <https://doi.org/10.1038/s41598-019-55358-6>.
- [73] J.A.V. Costa, M.G. de Moraes, An Open Pond System for Microalgal Cultivation, in: *Biofuels from Algae*, Elsevier Inc, (2013) 1–22, <https://doi.org/10.1016/B978-0-444-59558-4.00001-2>.
- [74] M.R. Tredici, N. Bassi, M. Prussi, N. Biondi, L. Rodolfi, G. Chini Zittelli, G. Sampietro, Energy balance of algal biomass production in a 1-ha “Green Wall Panel” plant: How to produce algal biomass in a closed reactor achieving a high Net Energy Ratio, *Appl. Energy*. 154 (2015) 1103–1111, <https://doi.org/10.1016/j.apenergy.2015.01.086>.
- [75] E. Sforza, E. Barbera, A. Bertucco, Improving the photoconversion efficiency: An integrated photovoltaic-photobioreactor system for microalgal cultivation, *Algal Res.* 10 (2015) 202–209, <https://doi.org/10.1016/j.algal.2015.05.005>.
- [76] M. Morales, A. Hélias, O. Bernard, Optimal integration of microalgae production with photovoltaic panels: environmental impacts and energy balance, *Biotechnol Biofuels*. 12 (2019) 239, <https://doi.org/10.1186/s13068-019-1579-4>.
- [77] N.R. Moheimani, D. Parlevliet, M.P. McHenry, P.A. Bahri, K. de Boer, Past, Present and Future of Microalgae Cultivation Developments, Springer, Cham. (2015)1–18, https://doi.org/10.1007/978-3-319-16640-7_1.
- [78] A.M. Detweiler, C.E. Mioni, K.L. Hellier, J.J. Allen, S.A. Carter, B.M. Bebout, E.E. Fleming, C. Corrado, L.E. Prufert-Bebout, Evaluation of wavelength selective photovoltaic panels on microalgae growth and photosynthetic efficiency, *Algal Res.* 9 (2015) 170–177, <https://doi.org/10.1016/j.algal.2015.03.003>.
- [79] E.G. Nwoba, D.A. Parlevliet, D.W. Laird, K. Alameh, N.R. Moheimani, Pilot-scale self-cooling microalgal closed photobioreactor for biomass production and electricity generation, *Algal Res.* 45 (2020), <https://doi.org/10.1016/j.algal.2019.101731>.
- [80] A. Brodu, C. Seydoux, G. Finazzi, C. Dublanche-Tixier, C. Ducros, Optical optimization of semi-transparent a-Si:H solar cells for photobioreactor application, *Thin Solid Films*. 689 (2019), <https://doi.org/10.1016/j.tsf.2019.137492>.
- [81] A. Pandikumar, S.P. Lim, S. Jayabal, N.M. Huang, H.N. Lim, R. Ramaraj, Titania gold plasmonic nanoarchitectures: An ideal photoanode for dye-sensitized solar cells, *Renew. Sustain. Energy Rev.* 60 (2016) 408–420, <https://doi.org/10.1016/j.rser.2016.01.107>.
- [82] S. Dai, K. Wang, J. Weng, Y. Sui, Y. Huang, S. Xiao, S. Chen, L. Hu, F. Kong, X. Pan, C. Shi, L. Guo, Design of DSC panel with efficiency more than 6%, *Sol. Energy Mater. Sol. Cells*. 85 (2005) 447–455, <https://doi.org/10.1016/j.solmat.2004.10.001>.

- [83] D. Puyol, D.J. Batstone, T. Hülsen, S. Astals, M. Peces, J.O. Krömer, Resource recovery from wastewater by biological technologies: Opportunities, challenges, and prospects, *Front. Microbiol.* 7 (2017), <https://doi.org/10.3389/fmicb.2016.02106>.
- [84] P.J.T.M. van Puijenbroek, A.H.W. Beusen, A.F. Bouwman, Global nitrogen and phosphorus in urban waste water based on the Shared Socio-economic pathways, *J. Environ. Manage.* 231 (2019) 446–456, <https://doi.org/10.1016/j.jenvman.2018.10.048>.
- [85] A.M.K. Mbaya, J. Dai, G.H. Chen, Potential benefits and environmental life cycle assessment of equipping buildings in dense cities for struvite production from source-separated human urine, *J. Clean. Prod.* 143 (2017) 288–302, <https://doi.org/10.1016/j.jclepro.2016.12.111>.
- [86] J.R. McConville, E. Kvarnström, H. Jönsson, E. Kärrman, M. Johansson, Source separation: Challenges & opportunities for transition in the swedish wastewater sector, *Resour. Conserv. Recycl.* 120 (2017) 144–156, <https://doi.org/10.1016/j.resconrec.2016.12.004>.
- [87] M.E. Borsuk, M. Maurer, J. Lienert, T.A. Larsen, Charting a path for innovative toilet technology using multicriteria decision analysis, *Environ. Sci. Technol.* 42 (2008) 1855–1862, <https://doi.org/10.1021/es702184p>.
- [88] S. Stucki, F. Vogel, C. Ludwig, A.G. Haiduc, M. Brandenberger, Catalytic gasification of algae in supercritical water for biofuel production and carbon capture, *Energy Environ. Sci.* 2 (2009) 535–541, <https://doi.org/10.1039/b819874h>.
- [89] G. Peng, F. Vogel, D. Refardt, C. Ludwig, Catalytic Supercritical Water Gasification: Continuous Methanization of *Chlorella vulgaris*, *Ind. Eng. Chem. Res.* 56 (2017) 6256–6265, <https://doi.org/10.1021/acs.iecr.7b00042>.
- [90] M. Bagnoud-Velásquez, E. Damergi, G. Peng, F. Vogel, C. Ludwig, Fate and reuse of nitrogen-containing organics from the hydrothermal conversion of algal biomass, *Algal Res.* 32 (2018), <https://doi.org/10.1016/j.algal.2018.04.005>.
- [91] G. Peng, F. Vogel, D. Refardt, C. Ludwig, Catalytic Supercritical Water Gasification: Continuous Methanization of *Chlorella vulgaris*, *Ind. Eng. Chem. Res.* 56 (2017) 6256–6265, <https://doi.org/10.1021/acs.iecr.7b00042>.
- [92] I. Doušková, F. Kaštánek, Y. Maléterová, P. Kaštánek, J. Doucha, V. Zachleder, Utilization of distillery stillage for energy generation and concurrent production of valuable microalgal biomass in the sequence: Biogas-cogeneration-microalgae-products, *Energy Convers. Manag.* 51 (2010) 606–611, <https://doi.org/10.1016/j.enconman.2009.11.008>.
- [93] S. Monkonsit, S. Powtongsook, P. Pavasant, Comparison between airlift photobioreactor and bubble column for *Skeletonema costatum* cultivation, *Eng. J.* 15 (2011) 53–64, <https://doi.org/10.4186/ej.2011.15.4.53>.
- [94] Flow Cytometry Fundamental Principle, <https://www.bosterbio.com/protocol-and-troubleshooting/flow-cytometry-principle> (accessed February 20, 2020).
- [95] J. Cosgrove, M. Borowitzka, Applying Pulse Amplitude Modulation (PAM) fluorometry to microalgae suspensions: Stirring potentially impacts fluorescence, *Photosynth. Res.* 88 (2006) 343–350, <https://doi.org/10.1007/s11120-006-9063-y>.
- [96] J.R.F. Malapascua, C.G. Jerez, M. Sergejevojová, F.L. Figueroa, J. Masojídek, Photosynthesis monitoring to optimize growth of microalgal mass cultures: Application of chlorophyll fluorescence techniques, *Aquat. Biol.* 22 (2014) 123–140, <https://doi.org/10.3354/ab00597>.
- [97] J. Doucha, K. Lívanský, High density outdoor microalgal culture, *Algal Biorefineries Vol. 1 Cultiv. Cells Prod.* (2014) 147–173, https://doi.org/10.1007/978-94-007-7494-0_6.
- [98] S.W. Jeffrey, G.F. Humphrey, New spectrophotometric equations for determining chlorophylls a, b, c1 and c2 in higher plants, algae and natural phytoplankton, *Biochem. Und Physiol. Der Pflanz.* 167 (1975) 191–194, [https://doi.org/10.1016/s0015-3796\(17\)30778-3](https://doi.org/10.1016/s0015-3796(17)30778-3).
- [99] I. Strati, V. Sinanoglou, L. Kora, S. Miniadis-Meimaroglou, V. Oreopoulou, Carotenoids from Foods of Plant, Animal and Marine Origin: An Efficient HPLC-DAD Separation Method, *Foods.* 1 (2012) 52–65, <https://doi.org/10.3390/foods1010052>.
- [100] E. Damergi, J.-P. Schwitzguébel, D. Refardt, S. Sharma, C. Holliger, C. Ludwig, Extraction of carotenoids from *Chlorella vulgaris* using green solvents and syngas production from residual biomass, *Algal Res.* 25 (2017) 488–495, <https://doi.org/10.1016/j.algal.2017.05.003>.
- [101] T. Dittrich, Basic Characteristics and Characterization of Solar Cells, *Mater. Concepts Sol. Cells*, (2018) 3–43, https://doi.org/10.1142/9781786344496_0001.

- [102] T. Rausch, The estimation of micro-algal protein content and its meaning to the evaluation of algal biomass I. Comparison of methods for extracting protein, *Hydrobiologia*. 78 (1981) 237–251, <https://doi.org/10.1007/BF00008520>.
- [103] T. Masuko, A. Minami, N. Iwasaki, T. Majima, S.I. Nishimura, Y.C. Lee, Carbohydrate analysis by a phenol-sulfuric acid method in microplate format, *Anal. Biochem.* 339 (2005) 69–72, <https://doi.org/10.1016/j.ab.2004.12.001>.
- [104] M. Axelsson, F. Gentili, A single-step method for rapid extraction of total lipids from green microalgae, *PLoS One*. 9 (2014), <https://doi.org/10.1371/journal.pone.0089643>.
- [105] M. Osada, T. Sato, M. Watanabe, T. Adschiri, K. Arai, Low-temperature catalytic gasification of lignin and cellulose with a ruthenium catalyst in supercritical water, *Energy and Fuels*. 18 (2004) 327–333, <https://doi.org/10.1021/ef034026y>.
- [106] W. Duan, F. Meng, Y. Lin, G. Wang, Toxicological effects of phenol on four marine microalgae, *Environ. Toxicol. Pharmacol.* 52 (2017) 170–176, <https://doi.org/10.1016/j.etap.2017.04.006>.
- [107] H. Madi, S. Diethelm, J. Van herle, N. Petigny, Effect of Steam-to-Carbon Ratio on Degradation of Ni-YSZ Anode Supported Cells, *ECS Trans.* 57 (2013) 1517–1525, <https://doi.org/10.1149/05701.1517ecst>.
- [108] S. Sharma, A.D. Celebi, F. Maréchal, Robust multi-objective optimization of gasifier and solid oxide fuel cell plant for electricity production using wood, *Energy*. 137 (2017) 811–822, <https://doi.org/10.1016/j.energy.2017.04.146>.
- [109] P. Cialiandro, L. Tock, A. V. Ensinas, F. Marechal, Thermo-economic optimization of a Solid Oxide Fuel Cell – Gas turbine system fuelled with gasified lignocellulosic biomass, *Energy Convers. Manag.* 85 (2014) 764–773, <https://doi.org/10.1016/j.enconman.2014.02.009>.
- [110] F. Jin, Æ.H. Enomoto, Application of hydrothermal reaction to conversion of plant-origin biomasses into acetic and lactic acids, (2013) 2463–2471, <https://doi.org/10.1007/s10853-007-2013-z>.
- [111] S.V. Mohan, M.P. Devi, Bioresource Technology Fatty acid rich effluent from acidogenic biohydrogen reactor as substrate for lipid accumulation in heterotrophic microalgae with simultaneous treatment, *Bioresour. Technol.* 123 (2012) 627–635, <https://doi.org/10.1016/j.biortech.2012.07.004>.
- [112] S.S. Toor, H. Reddy, S. Deng, J. Hoffmann, D. Spangsmark, L.B. Madsen, J.B. Holm-nielsen, L.A. Rosendahl, Bioresource Technology Hydrothermal liquefaction of *Spirulina* and *Nannochloropsis salina* under subcritical and supercritical water conditions, *Bioresour. Technol.* 131 (2013) 413–419. <https://doi.org/10.1016/j.biortech.2012.12.144>.
- [113] J.B. Müller, F. Vogel, The Journal of Supercritical Fluids Tar and coke formation during hydrothermal processing of glycerol and glucose . Influence of temperature , residence time and feed concentration, *J. Supercrit. Fluids*. 70 (2012) 126–136, <https://doi.org/10.1016/j.supflu.2012.06.016>.
- [114] L.D.S. Pinto, L.M. Freitas, B. Al-duri, R.C.D. Santos, Supercritical water oxidation of quinoline in a continuous plug flow reactor–part 1 : effect of key operating parameters, 918 (2006) 912–918, <https://doi.org/10.1002/jctb.1420>.
- [115] K.C.C. Morais, R.L.L. Ribeiro, K.R. Santos, D.M. Taher, A.B. Mariano, J.V.C. Vargas, *Phaeodactylum tricornutum* microalgae growth rate in heterotrophic and mixotrophic conditions, 8 (2009) 84–89, DOI: 10.5380/reterm.v8i1.61887.
- [116] L.I. Aluwihare, D.J. Repeta, S. Pantoja, C.G. Johnson, Two Chemically Distinct Pools of Organic Nitrogen Accumulate in the Ocean, 308 (2005) 1007–1010.
- [117] A. Kruse, P. Bernolle, N. Dahmen, E. Dinjus, P. Maniam, Hydrothermal gasification of biomass : consecutive reactions to long-living intermediates, (2010) 136–143, <https://doi.org/10.1039/b915034j>.
- [118] P. Biller, A.B. Ross, Bioresource Technology Potential yields and properties of oil from the hydrothermal liquefaction of microalgae with different biochemical content, *Bioresour. Technol.* 102 (2011) 215–225, <https://doi.org/10.1016/j.biortech.2010.06.028>.
- [119] Y. Guo, S. Wang, C.M. Huelsman, P.E. Savage, Kinetic model for reactions of indole under supercritical water gasification conditions, *Chem. Eng. J.* 241 (2014) 327–335, <https://doi.org/10.1016/j.cej.2013.11.012>.
- [120] K.W. C.Brown, Catalytic pyrolysis of microalgae for production of aromatics and ammonia, *RSC Publ.* 15 (2013) 675, <https://doi.org/10.1039/c3gc00031a>.
- [121] OECD Environment, Health and Safety Publications, JT03232745 (2007).
- [122] A. Kruse, Supercritical water gasification, *Biofuels, Bioprod. Biorefining*. 2 (2008) 415–437, <https://doi.org/10.1002/bbb.93>.

- [123] G. Peng, C. Ludwig, F. Vogel, Catalytic supercritical water gasification: Interaction of sulfur with ZnO and the ruthenium catalyst, *Appl. Catal. B Environ.* 202 (2017) 262–268, <https://doi.org/10.1016/j.apcatb.2016.09.011>.
- [124] E. Eroglu, P.K. Eggers, M. Winslade, S.M. Smith, C.L. Raston, Enhanced accumulation of microalgal pigments using metal nanoparticle solutions as light filtering devices, *Green Chem.* 15 (2013) 3155–3159, <https://doi.org/10.1039/c3gc41291a>.
- [125] K. Mohammed, Z.S. Ahammad, P.J. Sallis, C.R. Mota, Optimisation of red light-emitting diodes irradiance for illuminating mixed microalgal culture to treat municipal wastewater, *WIT Trans. Ecol. Environ.* 178 (2013) 263–270, <https://doi.org/10.2495/WS130221>.
- [126] K.K. Gary Anderson, Caner KocCaner, Use of red and blue light-emitting diodes (LED) and fluorescent lamps to grow microalgae in a photobioreactor, *Isr. J. Aquac.* (2012), ISSN 0792-156X.
- [127] M.L. Parisi, A. Sinicropi, R. Basosi, Life Cycle Assessment of Gratzel-Type Cell Production for Non Conventional Photovoltaics From Novel Organic Dyes, *Int. J. Heat Technol.* 29 (2011) 161–169, <https://doi.org/10.1111/psyg.12057>.
- [128] E.A. Alsema, M.J. de Wild-Scholten, V.M. Fthenakis, Environmental impacts of PV electricity generation-A critical comparison of energy supply options 21st Eur. Photovolt. Sol. Energy Conf. Dresden, Ger. (2006) 7.
- [129] G.M. Borrelli, D. Trono, Molecular approaches to genetically improve the accumulation of health-promoting secondary metabolites in staple crops-a case study: The lipoxygenase-b1 genes and regulation of the carotenoid content in pasta products, *Int. J. Mol. Sci.* 17 (2016) 1177, doi: 10.3390/ijms17071177.
- [130] A.G. Sicaire, M. Vian, F. Fine, F. Joffre, P. Carré, S. Tostain, F. Chemat, Alternative bio-based solvents for extraction of fat and oils: Solubility prediction, global yield, extraction kinetics, chemical composition and cost of manufacturing, *Int. J. Mol. Sci.* 16 (2015) 8430–8453, <https://doi.org/10.3390/ijms16048430>.
- [131] K. Tuantet, H. Temmink, G. Zeeman, M. Janssen, R.H. Wijffels, C.J.N. Buisman, Nutrient removal and microalgal biomass production on urine in a short light-path photobioreactor, *Water Res.* 55 (2014) 162–174, <https://doi.org/10.1016/j.watres.2014.02.027>.
- [132] H.C. Kwang, H.J. Lee, S.Y. Koo, D.G. Song, D.U. Lee, C.H. Pan, Optimization of pressurized liquid extraction of carotenoids and chlorophylls from *Chlorella vulgaris*, *J. Agric. Food Chem.* 58 (2010) 793–797. <https://doi.org/10.1021/jf902628j>.
- [133] D.B. Rodrigues, É.M.M. Flores, J.S. Barin, A.Z. Mercadante, E. Jacob-Lopes, L.Q. Zepka, Production of carotenoids from microalgae cultivated using agroindustrial wastes, *Food Res. Int.* 65 (2014) 144–148, <https://doi.org/10.1016/j.foodres.2014.06.037>.
- [134] P. Přibyl, V. Cepák, P. Kaštánek, V. Zachleder, Elevated production of carotenoids by a new isolate of *Scenedesmus* sp., *Algal Res.* 11 (2015) 22–27. <https://doi.org/10.1016/j.algal.2015.05.020>.
- [135] D. Singh, C.J. Barrow, A.S. Mathur, D.K. Tuli, M. Puri, Optimization of zeaxanthin and β -carotene extraction from *Chlorella saccharophila* isolated from New Zealand marine waters, *Biocatal. Agric. Biotechnol.* 4 (2015) 166–173, <https://doi.org/10.1016/j.bcab.2015.02.001>.
- [136] L. Brennan, P. Owende, Biofuels from microalgae-A review of technologies for production, processing, and extractions of biofuels and co-products, *Renew. Sustain. Energy Rev.* 14 (2010) 557–577, <https://doi.org/10.1016/j.rser.2009.10.009>.
- [137] E. Papaioannou, T. Roukas, M. Liakopoulou-Kyriakides, Effect of biomass pre-treatment and solvent extraction on β -carotene and lycopene recovery from *Blakeslea trispora* cells, *Prep. Biochem. Biotechnol.* 38 (2008) 246–256, <https://doi.org/10.1080/10826060802164942>.
- [138] FAO, Algae based biofuels: Applications and co-products, (2010, ISBN 978-92-5-106623-2).
- [139] A.Z.A. Saifullah, A. Karim, A. Ahmad-yazid, Microalgae : An Alternative Source of Renewable Energy, *Am. J. Eng. Res.* 03 (2014) 330–338, ISSN : 2320-0936.
- [140] J.A. Del Campo, M. García-González, M.G. Guerrero, Outdoor cultivation of microalgae for carotenoid production: Current state and perspectives, *Appl. Microbiol. Biotechnol.* 74 (2007) 1163–1174. <https://doi.org/10.1007/s00253-007-0844-9>.
- [141] L. Gouveia, A.C. Oliveira, Microalgae as a raw material for biofuels production, *J. Ind. Microbiol. Biotechnol.* 36 (2009) 269–274, <https://doi.org/10.1007/s10295-008-0495-6>.
- [142] G.B. Leite, A.E.M. Abdelaziz, P.C. Hallenbeck, Algal biofuels: Challenges and opportunities, *Bioresour. Technol.* 145 (2013) 134–141, <https://doi.org/10.1016/j.biortech.2013.02.007>.

References

- [143] S. Mackay, E. Gomes, C. Holliger, R. Bauer, J.P. Schwitzguébel, Harvesting of *Chlorella sorokiniana* by co-culture with the filamentous fungus *Isaria fumosorosea*: A potential sustainable feedstock for hydrothermal gasification, *Bioresour. Technol.* 185 (2015) 353–361, <https://doi.org/10.1016/j.biortech.2015.03.026>.
- [144] G. Markou, E. Nerantzis, Microalgae for high-value compounds and biofuels production: A review with focus on cultivation under stress conditions, *Biotechnol. Adv.* 31 (2013) 1532–1542, <https://doi.org/10.1016/j.biotechadv.2013.07.011>.
- [145] M. Gassner, F. Vogel, G. Heyen, F. Maréchal, Optimal process design for the polygeneration of SNG, power and heat by hydrothermal gasification of waste biomass: Thermo-economic process modelling and integration, *Energy Environ. Sci.* 4 (2011) 1726–1741, <https://doi.org/10.1039/c0ee00629g>.
- [146] M. Brandenberger, J. Matzenberger, F. Vogel, C. Ludwig, Producing synthetic natural gas from microalgae via supercritical water gasification: A techno-economic sensitivity analysis, *Biomass and Bioenergy*. 51 (2013) 26–34, <https://doi.org/10.1016/j.biombioe.2012.12.038>.
- [147] T.A. Larsen, K.M. Udert, J. Lienert, Source Separation and Decentralization for Wastewater Management, (2015) 45-58. <https://doi.org/10.2166/9781780401072>.

List of Tables

Table 1: Basic reactions involved in the hydrothermal gasification of biomass.* (x): H/C molar ratio, (y): O/C molar ratio * ΔH° : Reaction enthalpy at reference temperature (25 °C). Adapted from [41].	22
Table 2: Comparison between microalgae production in open and closed bioreactors [61].	27
Table 3: Chemical composition of algae expressed on a dry matter basis [63].	28
Table 4: Parameters used during the non-catalytic hydrothermal gasification of Leachate effluent.	44
Table 5: Gas composition obtained after the hydrothermal gasification; the given results are mean values \pm Standard deviation ($n = 10$), all the results were measured during the steady-state of the HTG experiment. * Gas composition used in the solid oxide fuel cell experiment; steam was added to avoid carbon deposition according to thermodynamic prediction.	60
Table 6: Elemental analysis of Leachate feedstock and the aqueous phase produced via hydrothermal gasification without a catalyst; AP(1) is the aqueous phase obtained from test M1 (200g/h feedstock) and AP(2) is the aqueous phase obtained from test M2 ((350 g/h feedstock). M1 and M2 feedstock were obtained both from the same homogenised leachate collector tank.); all values are given as value \pm standard deviation (\pm SD) except wt%, were expressed as value \pm relative standard deviation (%RSD).	61
Table 7: Theoretical vs. experimental value of OCV for the gas compositions.	64
Table 8: Process parameters of hydrothermal catalytic gasification of <i>P. Tricornutum</i> and <i>C. vulgaris</i> .	70
Table 9: Main nitrogen-containing organics NOC'S used in this study: chemical structure and physical properties.	71
Table 10: Organics compounds in the salt brine of <i>P.tricornutum</i> before the treatment (1) and salt brine after the treatment via hydrothermal catalytic gasification (2); NQ= not quantified, DL= below detection limit; mean values are given \pm SD ($n=3$).	72
Table 11: Results for the hydrothermal catalytic gasification experiments of the salt brine and model brine effluents.	75
Table 12: Irradiance PAR ($\mu\text{mol photon m}^{-2} \text{ s}^{-1}$) at the reactor front surface and at the back measured in all photo-bioreactor. DSC-T1 (normal glass); DSCT-1' (DSC without the dye); DSC-G (DSC-Green); DSC-R (DSC-Red).	78
Table 13: Dye absorption wavelength max (nm).	79
Table 14: Photovoltaic performance of the DSC panels: I_{sc} (short circuit current), V_{oc} (open circuit voltage), ff (fill factor), η efficiency, P (output power). The measurements were done at a light intensity of 100 mW/cm^2 . * Energy production per year was calculated using the solar panel efficiency (%) without including the potential losses that can occur (Equation 23) **Energy production per year was calculated in this case using Performance Ratio (Equation 24).	80

Table 15: Only data collected during the exponential growth phase were used for growth kinetic analyses. Growth rate (μ) was determined individually for each replicate using a linear regression of the log-transformed cell density over time. Doubling time (td) was determined by dividing log 2 over the growth rate.....	81
Table 16: Total Chlorophyll, carotenoid and macromolecule content.	85
Table 17: Only data collected during the exponential growth phase were used for growth kinetic analyses. Growth rate (μ) was determined individually for each replicate using a linear regression of the log-transformed cell density over time. Doubling time (td) was determined by dividing log 2 over the growth rate.....	86
Table 18: Design and operation parameters of a PV bioreactor.....	89
Table 19: All contributors of GHG emissions (in CO ₂ -eq) of bioreactor producing 1 kg of microalgae (DW). The negative number indicates the avoided electricity production (*).	90
Table 20: Electricity production based on 10cm*10cm DSC-R and DSC-G for 8 days batch culture of <i>Chlorella vulgaris</i> at variable light intensities and DSC efficiency. Two different efficiencies were used: 2.8% and 3% obtained from our study.	91
Table 21: Hansen solubility parameters: solvent/solute interactions. MPa ^{1/2} (equivalent to joules/cubic centimeter; 2.0455 x (cal/cc) ^{1/2}) at 25°C. HSP is given by $\delta_{\text{total}}^2 = \delta_d^2 + \delta_p^2 + \delta_H^2$ which now consists of its three partitioned HSP in terms of dispersion force δ_d , polar (permanent dipole forces) δ_p , and hydrogen-bonding δ_H force, respectively [129].	94
Table 22: Elemental composition of <i>C. vulgaris</i> before and after the extraction	95
Table 23: High Heating Value (HHV), extracted biomass (in % of the total dry weight of biomass before extraction) and sum of carotenoids extracted. violaxanthin, astaxanthin, lycopene, β -carotene, lutein and canthaxanthin as a function of extraction conditions (time, temperature, solvents). Mean values are given with the Standard deviation.	96
Table 24: Effect of changes in extraction set-up on mean extraction yield and mean extracted carotenoids for different parameters.	99
Table 25: Nominal and proportional nutrient and pollutant loads in greywater and blackwater (urine faeces, toilet paper). g.p ⁻¹ .d ⁻¹ : gram per person per day.	124

List of Figures

Figure 1: CO ₂ levels in the past and the estimated increase scenarios of atmospheric CO ₂ concentration at year 2100 (left). Present-day atmospheric levels of CO ₂ , methane (CH ₄), and nitrous oxide (N ₂ O) are notably higher than their pre-industrial averages (Right). The historical composite CO ₂ record based on measurements from the EPICA (European Project for Ice Coring in Antarctica) Dome C and Dronning Maud Land sites and the Vostok station, adapted from [8].	15
Figure 2: (Left) Total energy supply globally in 2016 adapted from [29]. (Right) Total Primary Energy Supply (TPES) or energy supply defined as production of energy sources including import and export of the source as well as storage in bunkers.	18
Figure 3: (Left) Total primary energy supply of all renewables in 2016. (Right) Total primary energy supply of all renewables per continent. Adapted from [29].	18
Figure 4: Schematic illustration of the Swiss technical biomass potential and constraints to the sustainable biomass potentials as well as the currently used and remaining biomass potentials modified from [31][32].	19
Figure 5: Main biomass conversion routes adapted from [35].	21
Figure 6: Influence of different catalysts on gas efficiency (GE) of hydrothermal gasification of microalgae biomass obtained at 400 °C, 500 °C and 600 °C [39].	22
Figure 7: The Z-scheme of electron transfer processes involved in the light-dependent reactions of photosynthesis [45].	23
Figure 8: Inorganic carbon is fixed in the cells through the Calvin cycle [49].	23
Figure 9: Spectral distribution of artificial lamps employed in microalgae research adapted from [60].	25
Figure 10: Net energy ratio (NER) for micro-algae biomass production: comparison of published values with normalised values. (The NER is defined as the sum of the energy used for cultivation, harvesting and drying, divided by the energy content of the dry biomass). Taken from [62].	28
Figure 11: From sunlight-to-algal biomass: Solar conversion efficiency and strategies adapted from [69].	30
Figure 12: Splitting the solar spectrum for the coproduction of biomass and electricity. The shaded regions illustrate the portions of the solar spectrum that can be delivered to electrical generation and microalgae cultivation without reducing the productivity of the microalgae. Figure taken from [76].	31
Figure 13: Schematic representation of a dye-sensitised solar cell constructed with a photo anode consisting of a dye-sensitised semiconducting oxide film, a counter electrode made of Pt coated glass substrate, and an electrolyte filled between the dye adsorbed photo anode and counter electrode [80].	32
Figure 14: Simplified scheme of the Photovoltaic assisted Algae production, and Wastewater treatment combined heat and power generation and Storage project, so-called (PAWaSto).	35
Figure 15: Production of <i>C. Vulgaris</i> and its valorisation within the scope of PAWaSto project.	39

Figure 16: On-site sanitation (OSS) systems developed by atba architects office, cooperative equilibre, Geneva: a 50-users building were constructed with an objective of treating 100% of effluents and valorise the dejections (black water and urine) via composting and phyto-purification.	40
Figure 17: Composter chamber, a) fresh compost (2-month-old), b) Leachate effluent recovered at the bottom of the composter.	41
Figure 18: The Elena hydrothermal gasification unit, KIT Germany.....	43
Figure 19: Gas separated from aqueous phase AP.	44
Figure 20: F01 filter cleaning and recovery of precipitated salts.....	44
Figure 21: Detailed flow-scheme of the hydrothermal unit [92].	46
Figure 22: Flow Cytometry Fundamental Principle, adapted from [93].	47
Figure 23: Open thin layer photobioreactor situated in a greenhouse on the Grüental campus of the Zurich University of Applied Sciences in Wädenswil.....	50
Figure 24: Dye sensitised solar cell principle and structure.....	54
Figure 25: A schematic view of the experimental set-up inside the XLS+ solar simulator: DSC-G: Green DSC; DSC-R: Red DSC; DSC-T1': Blank DSC, DSC-T1: normal glass	54
Figure 26: Simplified chart of the HTG-SOFC and microalgae production systems	57
Figure 27: Simplified flow-scheme of the human faeces-composting chamber combined with HTG-SOFC and algae production unit. Biomass with low sulfur content was processed in the presence of a Ru/C catalyst, e.g. Residual algal biomass (**) (data reported from Damergi et al. (2017)). Biomass with high sulfur content was processed without the presence of a catalyst (this study), e.g. in the case of leachate (*).	58
Figure 28: Leachate cation and anion concentration measured during 1-month period.	59
Figure 29: Left) Visual aspect of the aqueous phase effluent samples taken during the gasification of leachate from M1 and M2 tests. Right) lyophilised feedstock and aqueous phase samples.	61
Figure 30: Left) Autofluorescence intensity signal comparison between Control culture, M1 and M2 testes using BL3 filter. Right): Average cell size comparison between Control culture, M1 and M2 testes using the forward scatter signal.	62
Figure 31: a) Growth rate curve of <i>C. vulgaris</i> using dilute aqueous phase from hydrothermal gasification of leachate. Control medium using standard control medium, M1 medium using aqueous medium obtained from test 1); M2 medium using aqueous medium obtained from test 2. b): Flow cytometry analysis of M1, M2 and control culture at day 4. The autofluorescence signal was acquired using BL3 filter (670 nm) where strong autofluorescence signal was detected in the control culture. This signal was used as a reference for M1 and M2 experiments. R1 and R2 gates were applied to differentiate respectively, normal microalgae cells from damaged ones.....	63
Figure 32: Carbon deposition region in a C–H–O phase diagram at 1 atm. It is calculated based on the anode feed balance.	64

Figure 33: IV curves for the M1, M2 and AL gas composition. b) Polarisation with time under a constant bias (0.3 A/cm ²) for the different gas composition at 750 °C.	65
Figure 34: Pressure increase with time for the three experiments, indicative of carbon deposits formation during SOFC operation. The AL experiment showed the largest increase in pressure build-up at the fuel inlet. b) Solid carbon formation at the fuel inlet (right) and on the evaporator tube which was inserted to the fuel inlet tube (left) – Test M1 – Test 1.	66
Figure 35: Valorisation chain of effluents from composted human excreta; processes and streams with greenish, reddish and yellowish backgrounds respectively represent experimental, modelling and Damergi et al. (2017) parts of the valorisation chain.	67
Figure 36: Simplified flow-scheme of the continuous-flow system, SB: Concentrated salt brine effluent (high salt and organic content), RW: Reactor water (low salt and organic content) used to dilute the SB, AL: <i>P. tricornutum</i> biomass, (1): Direct use of SB in the preparation of algae culture medium, (2) Treatment of SB via hydrothermal catalytic gasification when recalcitrant nitrogen organics NOC'S reaches toxic concentrations upon continuous recycling.	69
Figure 37: GC-MS chromatogram showing the different nitrogen-containing organics detected in the salt brine	71
Figure 38: Microalgae toxicity assay with 2-pyrrolidinone (left) and β -phenylethylamine (right) with three microalgae species <i>P. tricornutum</i> , <i>C. sorokiniana</i> and <i>S. vacuolatus</i> . All experiments were performed in triplicate; mean values are given \pm SD (n=3).....	73
Figure 39: <i>P. tricornutum</i> toxicity assay using 20-fold diluted salt brine effluent. All experiments were performed in triplicate; mean values are given \pm SD (n=3), <i>P. tricornutum</i> control cultures were prepared with modified F2 medium.....	74
Figure 40: Trend of chemical oxygen demand (left) and total nitrogen (right) during the toxicity assay with <i>P. Tricornutum</i> using untreated salt brine effluent. All measurements were performed in triplicate (n=3).....	74
Figure 41: A schematic view of the experimental set-up inside the XLS+ solar simulator: DSC-G: DSC-Green; DSC-R: DSC-Red; DSC-T1: normal glass; DSCT-T1': DSC without the dye.	77
Figure 42: Absorbance spectra of DSC-T1 (normal glass); DSC-T1' (all DSC compounds except the dye); DSC-G (green solar panel); DSC-R (red solar panel).	79
Figure 43: <i>C. vulgaris</i> absorbance spectrum and major pigment peaks (inset adapted from [123]).	79
Figure 44: Current-voltage curves for DSC-R and DSC-G panels.	80
Figure 45: shows the logarithmic growth and stationary phases of <i>C. vulgaris</i> . Growth curves (Cells/ml) and biomass concentration (g/l): (left) growth under low light intensity (Right) and high light intensity using DSC-T1; DSC-T1; DSC-G and DSC-R.	81
Figure 46: The analysis by means of flow cytometry of <i>C. vulgaris</i> cells at the end of the experiment under high light intensity using a) DSC-T1 (normal glass); a) DSC-T1' ((all DSC compounds except the dye) DSC-G (green solar panel); d) DSC-R (red solar panel). R1 represent the gating for autofluorescent cells due to the presence of Chlorophyll a.....	83

Figure 47) Fv/Fm fluorescence ratio of <i>C. vulgaris</i> and <i>H. pluvialis</i> at low and high light intensity; FV is the difference between the maximum fluorescence FM (all QA reduced) and minimum fluorescence F0 (all QA oxidised).....	84
Figure 48: $\phi(II)$, photochemical conversion, $\phi(NPQ)$, regulated thermal energy dissipation related to NPQ, $\phi(NO)$, "primarily constitutive losses", corresponding to the sum of non-regulated heat dissipation and fluorescence emission.	85
Figure 49: Picture of samples taken from <i>H. pluvialis</i> growth tests under high light intensity DSC-T1 (standard glass); DSC-T1'(all DSC compounds except the dye); DSC-G (green solar panel); DSC-R (red solar panel)	87
Figure 50: Transmissions electron micrographs TEM of <i>h. pluvialis</i> at day 3. 1) DSC-G, 2) DSC-R, 3) DSC T1'4) DSC-T1 Nucleus (N) Chloroplast (C), Pyrenoid (P), Oil droplet (O), cell wall (CW).	88
Figure 51: Structures of carotenes and xanthophylls [128].	93
Figure 52: Effect of temperature (40 and 110 °C) and solvents (2-methyltetrahydrofuran, MTHF; ethanol, EtOH) on the extraction of xanthophylls from <i>C. vulgaris</i> dry (left) or wet (right) biomass, after 15 min (top) or 30 min (bottom) extraction time.	97
Figure 53: Effect of temperature (40 and 110 °C) and solvents (2-methyl tetrahydrofuran, MTHF; ethanol, EtOH) on the extraction of carotenes from <i>C. vulgaris</i> dry (left) or wet (right) biomass, after 15 min (top) or 30 min (bottom) extraction time.	98
Figure 54: Microalgae processing using pressurised liquid extraction and supercritical hydrothermal gasification.....	100
Figure 55: DSC-Greenhouse for microalgae production idea	104
Figure 56: Four pathways have been selected for climate modelling and research. They describe different climate futures, all of which are considered possible depending on the volume of greenhouse gases (GHG) emitted in the years to come. The four RCPs, namely RCP2.6, RCP4.5, RCP6, and RCP8.5, are labelled after a possible range of radiative forcing values in the year 2100 (2.6, 4.5, 6.0, and 8.5 W/m ² , respectively).....	123
Figure 57: Dye used in the sensitized solar cells.....	123
Figure 58: Main nutrient in source separated wastewater [146].	124
Figure 59: Water volume and energy content [146].....	125

List of Equations

Equation 1: Nitrate as nitrogen source for microalgae.....	25
Equation 2: Ammonium as nitrogen source for microalgae.....	26
Equation 3: Urea as nitrogen source for microalgae.....	26
Equation 4: Chemical equation of the Calvin cycle.....	26
Equation 5: Total organic carbon conversion (Xc).....	45
Equation 6: Carbon gasification efficiency GEC (%).....	45
Equation 7: Nitrogen recovery N (%).....	45
Equation 8: Phosphorus recovery P (%).....	45
Equation 9: Sulphur recovery S (%).....	45
Equation 10: Specific growth rates (μ).....	47
Equation 11: Doubling time.....	48
Equation 12: The maximum quantum efficiency related to PS II.....	48
Equation 13: ϕ (PSII), the quantum yield of photochemical energy conversion PS II.....	48
Equation 14: ϕ (NPQ), quantum yield of regulated non-photochemical energy loss in PS II.....	49
Equation 15: ϕ (NO), the quantum yield of non-regulated non-photochemical energy loss in PS II.....	49
Equation 16: The sum of the three quantum yields.....	49
Equation 17: Chlorophyll a content ($\mu\text{g/mL}$).....	50
Equation 18: Chlorophyll b content ($\mu\text{g/mL}$).....	50
Equation 19: Chlorophyll a+b content ($\mu\text{g/mL}$).....	50
Equation 20: Carotenoids content ($\mu\text{g/mL}$).....	50
Equation 21: Carotenoids content in ($\mu\text{g/g}$) of dry biomass.....	51
Equation 22: High Heating Value (HHV) calculation.....	52
Equation 23: Ash mass fraction calculation.....	52
Equation 24: Fill factor of a solar cell.....	53
Equation 25: Efficiency of a solar cell.....	53
Equation 26: Electrical energy generated in the output of a photovoltaic system (losses not included).....	53
Equation 27: Electric energy generated in the output of a photovoltaic system (losses are included).....	53
Equation 28: The theoretical open-circuit voltage (OCV).....	64

Equation 29: The conversion of algal biomass into CH₄ and CO₂.....	100
---	------------

Appendix A : Supplementary information

1. Supplementary information: introduction

Representative Concentration Pathway (RCP) is a greenhouse gas concentration (not emissions) trajectory adopted by the Intergovernmental Panel on Climate Change (IPCC) for its fifth Assessment Report (AR5) in 2014. It supersedes the Special Report on Emissions Scenarios (SRES) projections published in 2000.

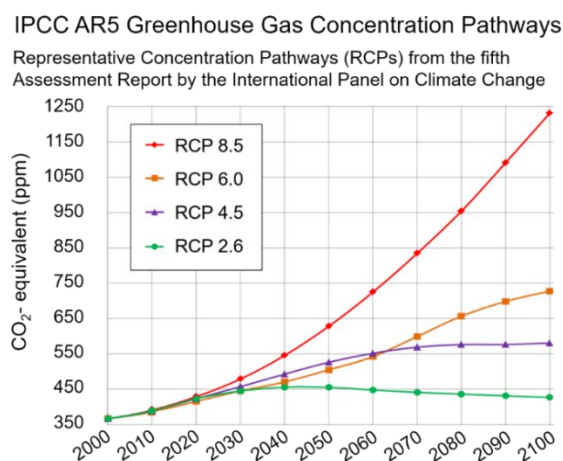


Figure 56: Four pathways have been selected for climate modelling and research. They describe different climate futures, all of which are considered possible depending on the volume of greenhouse gases (GHG) emitted in the years to come. The four RCPs, namely RCP2.6, RCP4.5, RCP6, and RCP8.5, are labelled after a possible range of radiative forcing values in the year 2100 (2.6, 4.5, 6.0, and 8.5 W/m², respectively).

2. Supplementary information: Material and methods

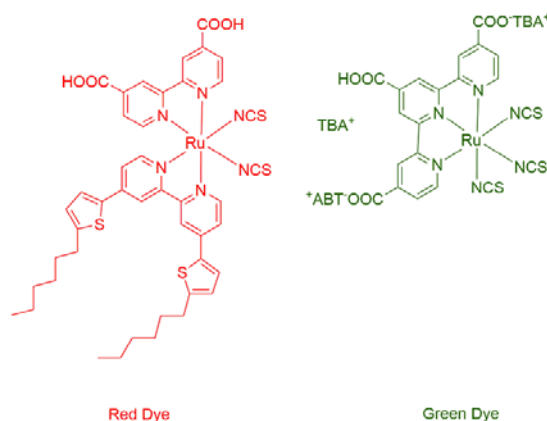
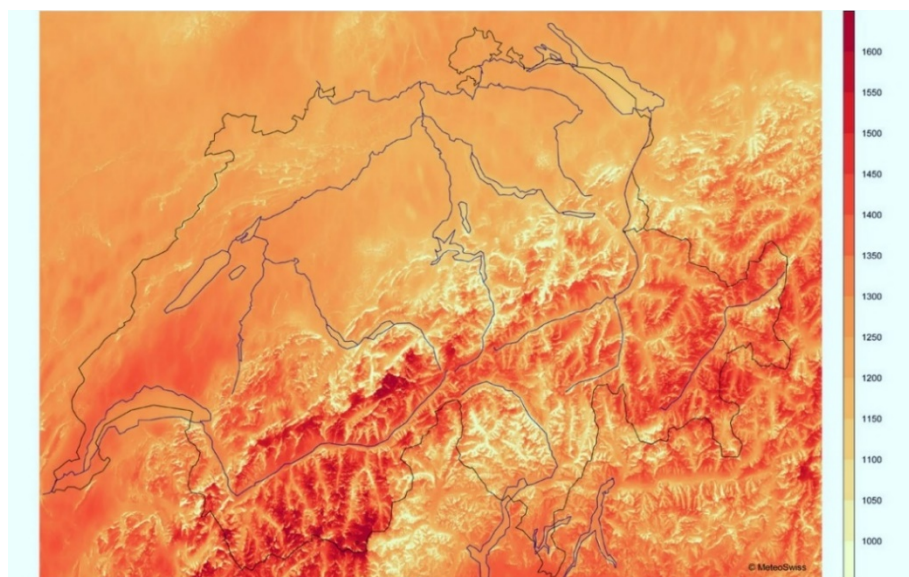


Figure 57: Dye used in the sensitised solar cells.



Global radiation in Switzerland in kWh per m² and year for 2012, derived from satellite data. The spatial resolution is 25 m.

<http://photovoltaic-software.com/PV-solar-energy-calculation.php>.

3. Supplementary information: Water volume, nutrient content and energy content in on-site sanitation system

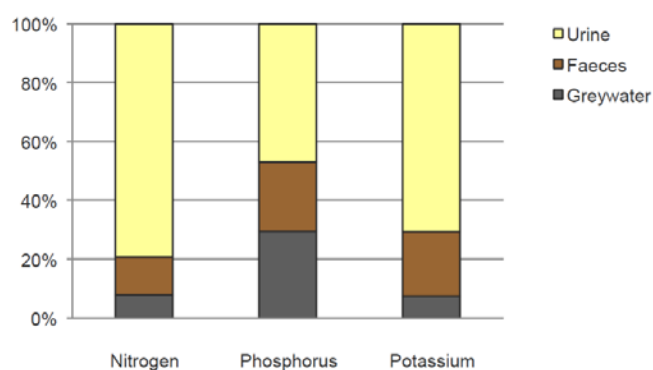


Figure 58: Main nutrient in source separated wastewater [147].

	Load [g·p ⁻¹ ·d ⁻¹]					Contribution [%]			
	GW	Urine	Faeces	Toilet paper	Total	GW	Urine	Faeces	Toilet paper
TSS	19	12	23	6.8	61	32	19	38	11
BOD _{5t}	19	5.8	12	n.a.	37	52	15	33	n.a.
COD _t	51	13	31	8.8	104	50	11	31	8
N _t	0.9	9.2	1.5	0.0	11.6	8	79	13	0
P _t	0.5	0.8	0.4	0.0	1.8	28	47	25	0
K	0.3	2.9	0.9	n.a.	4.1	7	71	22	n.a.

Table 25: Nominal and proportional nutrient and pollutant loads in greywater and blackwater (urine faeces, toilet paper). g·p⁻¹·d⁻¹: gram per person per day [147].

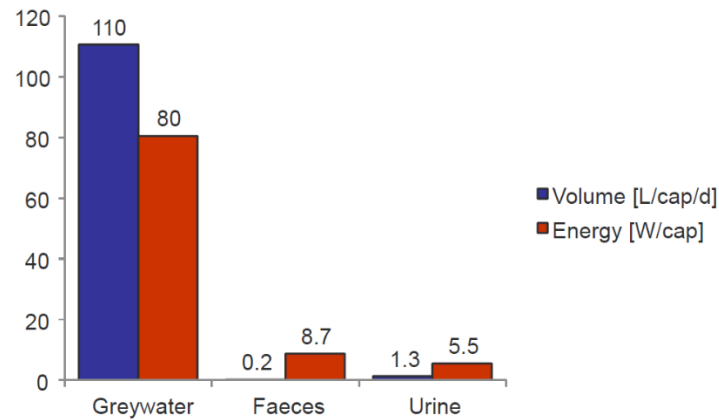


Figure 59: Water volume and energy content [147].

4. Supplementary information: Life cycle assessment

a. Calculate Weight Reduction Factor by combining 100 small DSC PBR (0.01 m² each) into 1 big DSC PBR (1 m²):

Dimension of small DSC PBR = 10 cm*10 cm*8 cm

Total area (base + walls) of 1 small DSC PBR = $10*10 + 4*(10*8) = 420 \text{ cm}^2$

Total area of 100 small DSC PBR = $420*100 = 42,000 \text{ cm}^2$

Total area of 1 big DSC PBR = $100*1000 + 4*(100*8) = 13200$

Weight Reduction Factor = $13200/42000 = 0.3143$

b. Glass and aluminium weights of 3501 small DSC PBR and 35 big DSC PBR:

Glass weight in 1 small DSC PBR = 0.4116 kg

Aluminium weight in 1 small DSC PBR = 0.0084 kg

Glass weight in 3501 small DSC PBR = $3501*0.4116 = 1441.01 \text{ kg}$ aluminium weight in 3501

Small DSC PBR = $3501*0.0084 = 29.41 \text{ kg}$

Glass weight in 35 big DSC PBR = $1441.01*0.3143 = 452.91 \text{ kg}$

Aluminium weight in 35 big DSC PBR = $29.41*0.3143 = 9.23 \text{ kg}$

c. CO₂-eq emissions:

CO₂-eq emissions of 3501 small DSC PBR and 35 big DSC-PBR: 3501 small DSC PBR (including end of life) = 1.658 kg CO₂-eq

35 big DSC PBR (including end of life) = $1.658*0.3143 = 0.5211 \text{ kg CO}_2\text{-eq}$.

Appendix B: Additional contributions

1. Isolation of new thermophilic microalgae from Tunisian hot spring: CODEV project.

N. Mrabet; E. Damergi; and C. Ludwig, *Leptolyngbya* sp. INSTML01 16S ribosomal RNA gene, partial sequence, 04.02.2018

GenBank: MG753795.1

LOCUS MG753795 1453 bp DNA linear BCT 04-FEB-2018

DEFINITION *Leptolyngbya* sp. INSTML01 16S ribosomal RNA gene, partial sequence.

ACCESSION MG753795

VERSION MG753795.1

ORGANISM [Leptolyngbya sp. INSTML01](#)

Bacteria; Cyanobacteria; Synechococcales; Leptolyngbyaceae;

Leptolyngbya.

REFERENCE 1 (bases 1 to 1453)

TITLE Thermophilic cyanobacteria *Leptolyngbya* sp with high potential of

Sequencing Technology :: Sanger dideoxy sequencing

/organism="Leptolyngbya sp. INSTML01"

/mol_type="genomic DNA"

/strain="INSTML01"

/isolation_source="Ain El Atrous geothermal spring"

/db_xref="taxon:[2068665](#)"

/country="Tunisia: Korbous"

/lat_lon="[36.8342 N 10.5692 E](#)"

[rRNA](#) <1..>1453

/product="16S ribosomal RNA"

ORIGIN

1 gagtttgatc ttggctcagg atgaacgctg gcggtctgct taacacatgc aagtccaacg

61 gagtgcttcg gcacttagtg gcggacgggt gagtaacgcg tgagaatctg cccttaggag
121 ggggataacg actggaaacg gtcgctaaga ccccatatgc cgagaggtga aacagtttc
181 tgcctgagga tgagctcgcg tctgattagc tagttggtgg ggtaagagcc taccaaggcg
241 acgatcagta gctggtctga gaggatgacc agccacactg ggactgagac acggcccaga
301 ctctacggg aggcagcagt ggggaatttt ccgcaatggg cgaaagcctg acggagcaag
361 accgcgtggg ggaagaaggt ctgtggattg taaacctctt ttgaccggga agaagcctga
421 cggtagcggg cgaatcagcc tcggctaact ccgtgccagc agccgcggta atacggagga
481 ggcaagcgtt atccggaatt attgggcgta aagcgtccgc aggtggttta tcaagtcagc
541 tgttaaaggg tggggcttaa ctccataaag gcagttgaaa ctgataggct agagtgcgat
601 aggggcaagg ggaattccca gtgtagcggg gaaatgcgta gatattggga agaacaccgg
661 tggcgaaagc gccttgctgg gtctgcactg aactgaggg acgaaagcta ggggagcgaa
721 agggattaga taccctgta gtcctagctg taaacgatgg gtactaggcg ttgtccgtat
781 cgaccgggc agtgccgtag ctaacgcgtt aagtacccc cctggggagt acgctcgaa
841 gagtgaaact caaaggaatt gacgggggcc cgacaagcg gtggagtatg tggtttaatt
901 cgatgcaacg cgaagaacct taccagggtt tgacatgtcc ggaatcttct tgaaagggaa
961 gagtgcctac gggaaccgga acacaggtgg tgcatggctg tcgtcagctc gtgtcgtgag
1021 atgttgggtt aagtccgca acgagcgcaa cccacgtcct tagttgccag cattgagttg
1081 ggcaactctg ggagactgcc ggtgacaaac cggaggaagg tgtggatgac gtcaagtcag
1141 catgcccctt acgctctggg ctacacagt actacaatgc ttcggacaaa gggttgccaa
1201 ctgcgagag tgcgctaata ccataaacg aggctcagtt cagattgcag gctgcaactc
1261 gcctgcatga aggcggaatc gctagtaatc gcaggtcagc atactgcggt gaatacgttc
1321 ccgggccttg tacacaccgc ccgtcacacc atgggagttg gccacggcg aagtcgttac
1381 tccaaccgat tctgtcggag gaggatgccg aaggcagggc tgatgactgg ggtgaagtcg
1441 taaccaggta acc

//

2. Assistance hours during the thesis

Years	Topic	Type	Hours
2015-2016	Projet SIE/ENAC	Projet	56
2015-2016	Analyse des polluants dans l'environnement	Projet	30
2015-2016	Projet de master en sciences et ingénierie de l'environnement	Projet	136
2015-2016	Autre contribution à l'enseignement	Contribution	14
2016-2017	Projet de master en sciences et ingénierie de l'environnement	Projet	136
2016-2017	Projet SIE	Pendant le semestre	56
2016-2017	Autre contribution à l'enseignement	Contribution	14
2016-2017	Analyse des polluants dans l'environnement	Projet	30
2016-2017	Air pollution and climate change	Ecrit	6
2016-2017	Autre contribution à l'enseignement	Contribution	14
2016-2017	Air pollution and climate change	Ecrit	6
2016-2017	Air pollution and climate change	Ecrit	6
2016-2017	Air pollution and climate change	Ecrit	6
2016-2017	Air pollution and climate change	Ecrit	6
2017-2018	Analyse des polluants dans l'environnement	TP	30
2017-2018	Diagnostic en ENAC, démarche et outils de mesure	Projet	14
2017-2018	Projet de master en sciences et ingénierie de l'environnement	Projet	136
2018-2019	Analyse des polluants dans l'environnement	TP	30
Total heures:			726

3. Credits obtained during the thesis

Courses	Code	Credits
Advanced Microscopy for Life Science	<u>BIO-659</u>	3
Biotechnology lab (for CGC)	<u>BIOENG-433</u>	4 (ongoing)
Innosuisse Business Concept	<u>MGT-642</u>	4
Open Science in Practice (2017)	<u>ENG-801</u>	2
Optimisation and simulation	<u>MATH-600</u>	4
Waterborne Pathogens (2018)	<u>ENV-721</u>	3



Eya Damergi Nicodeme

📍 Route cantonale, 39b, 1025 St-Sulpice (VD)

☎ 078 681 04 52

✉ eya.damergi@epfl.ch ; e.damergi@enoilbioenergies.ch

🌐 <https://www.linkedin.com/in/damergi-eya-846b685b/>

Born 20 June 1988

B permis, married

WORK EXPERIENCE

January 2019 – present

Laboratory manager at Enoil bioenergies SA, Switzerland

Enoil bioenergies SA (EBREL), Geneva, Switzerland

- Initiate and actuate improved methods of services and direct their implementation within the algal production line in Geneva.
- Identifying and funding the programs for sustaining the lab, including investments in infrastructure upgrades.
- Recruits and coordinates research subjects, as appropriate, and serves as principle administrative liaison for the project.
- Accountable for planning, coordinating and overseeing all operational activities required to manage the life-cycle of algal products (including collection, processing, analysis, labeling).

January 2015 – February 2020

PhD assistant at EPFL

Ecole Polytechnique Fédérale de Lausanne (EPFL), Switzerland

- Thermo chemical conversion of biomass (microalgae and/or sludge) for energy and nutrients recycling purposes.
- Safety coordinator COSEC-EPFL: assignment of functions relating to health and safety in the workplace, chemical storage conditions, chemical waste management.
- Teaching assistant for the bachelor and master program at EPFL "Analysis of pollutants in the environment, advanced waste treatment technologies".
- Raising funds by submitting project proposals: " **Seedmoney project (2017)**", "**BioPack-Nestle (2019)**".

May 2018– present

Head of Communication at Swiss Algae Consortium Association (SWALG)

Villigen, Switzerland

- promote the research, development and commercialization of algal technology by knowledge transfer, collaborations, events and advisory services through its network of subject matter experts.

September 2014 – December 2014

Research assistant

EPFL, Switzerland

- Scientific collaborator at EPFL-PSI (Paul Scherrer Institute) in the field of solid and waste treatment.
- Teaching assistant for the bachelor and master program at EPFL: Course Analysis of pollutants in the environment. Course: advanced waste treatment technologies".

EDUCATION

2015 – 2020

Doctor of Philosophy in Civil and Environmental Engineering

EPFL, Switzerland

- Doctor degree in civil and Environmental Engineering.

- 2012 – 2014 **Master's degree in Analytical Chemistry**
 EPFL-FSM (Faculty of Sciences of Monastir, Tunisia)
- Analytic chemist degree.
 - One year internship at the laboratory of Environmental Biotechnology, EPFL. Thesis title: Effluents Recycling and the Production of High Value Co-products from Microalgae.
 - Annual project with honors.
- 2008 – 2011 **Bachelors's degree in Fine Chemistry**
 Faculty of Sciences of Monastir (FSM), Tunisia
- Senior technician diploma in chemistry, Ranked first.
 - Performed 3 Months internship at the laboratory of Material Science, FSM. Thesis title: Extraction and Identification of Active Bio-polymers from Red Macroalgae: Anti-Cancer Properties.
 - Annual project with honors.

PERSONAL SKILLS AND COMPETENCES

Languages

French – Fluent C2 level
 English – Fluent C1 level
 Arabic – Native language
 Italian– B1 level
 German– Beginner level A1 (Taking intensive courses)

- Skills**
- Analytic and thermo-chemical processes**
- Regular user of the following techniques: Ion Chromatography (IC), Liquid Chromatography(LC-MS), Gas Chromatography (GC-MS), Inductively Coupled Plasma Spectrometry (ICP-MS), Fourier transform Infrared Spectroscopy (FTIR), Rheology (Viscosity).
 - Thermochemical conversion techniques: hydrothermal gasification and hydrothermal liquefaction.
 - Regular user of different imaging techniques: fluorescence and optic microscope imaging, electron microscopic imaging (TEM / SEM)

Biology

.Flow cytometry for the analysis of microorganisms in water and the effect of micropollutants on their metabolism, cell culture, toxicity assay, macromolecules quantifications, purification and characterization of recombinant proteins (ELISA, gel electrophoresis).

IT Skills

- Competent handling of MS office applications, software for scientific visualizations (Origin, Overleaf, Latex), software for chemistry (HSP chemistry, Flowjo and Chemdraw).

Safety coordinator COSEC-EPFL

- Assignment of functions relating to health and safety of the workplace, Chemical storage conditions, Chemical waste management.
- First aid team member, Lausanne.

Entrepreneurial skills

- Innosuisse Start-up Training: 14-week intensive training program with the development of a business project that has been positively evaluated by the jury.

Others competences

- Hot air balloon crew member at Ballons du Leman, Switzerland.
- PADI diving certificate.

Peer reviewed journal publications

- Extraction of carotenoids from *Chlorella vulgaris* using green solvents and syngas production from residual biomass. **Eya Damergi**, Jean-Paul Schwitzguébel, Dominik Refardt, Shivom Sharma, Christof Holliger, Christian Ludwig (Accepted 2/05/2017, Algal research).
- Fate and reuse of nitrogen-containing organics from the hydrothermal conversion of algal biomass. Mariluz Bagnoud-Velásquez, **Eya Damergi**, Gaël Peng, Frédéric Vogel, Christian Ludwig (Accepted 21/04/2018, Algal research).
- Solid oxide fuel cell operation on syngas from hydrothermal gasification of human Excreta with integrated nutrient recycling cycle for algal biomass production. **Eya Damergi**, Hossein Madi, Shivom Sharma, Nikolaos Boukis, Francois Marechal, Jan Van Herle, Christian Ludwig (Accepted 15/05/2019, Algal research).
- Leptolyngbya sp. INSTML01 16S ribosomal RNA gene, partial sequence, N.Mrabet, **Eya Damergi**, and Christian Ludwig, (accepted 04/02/2018, Genbank NCBI).
- Enhancing algae biomass production by using dye-sensitized solar cells as filters; **Eya Damergi**, Peng Qin, Mohammed.K. Nazeeruddin, Christian Ludwig.

Conference talks and posters

- Sustainable solar energy conversion to biomass: dye sensitized solar cell for enhancing algae biomass production, **E. Damergi**, Q. Peng, L.F. De Alencastro, N. Mo-hammad Khaja, C. Ludwig. 11-13/06/2018, **Seattle, USA**, Algal Biomass, Biofuels and Bioproducts conference.
- Quand la photosynthèse naturelle et artificielle se réunissent ! 30/04/2017, **Scientastic Valais, Sion**.
- 2 Posters and a demonstration session titled : Quand la photosynthèse naturelle et artificielle se réunissent ! 30/04/2017, **Scientastic Valais, Sion**.

Events organisation

- Participated at the preparation of SunChem workshop at the World Resources Forum, 6-9/10/2013, **Davos, Switzerland**.
- Recycling of rare earth elements in Tunisia, Event organizer as intermediate between Swiss-Finland delegation (PSI and Outotec) and the Tunisian Chemical group (GCT), 20/2/2014, **Monastir, Tunisia**.
- Participated at the preparation of workshop at the World Resources Forum 24-25/10/2017, **Geneva, Switzerland**.
- Co-organisation of exposition stand at Scientastic Valais, Sion 30/04/2017 **Geneva, Switzerland**.

Master student supervision

- **Jordan Prieto**: *H. pluvialis* grown under autotrophic or mixotrophic conditions: Effects on astaxanthin accumulation.
- **Dorian Tosi Robinso**: Supercritical water gasification of effluents from composted human excreta and recycling of the aqueous phases for microalgae cultivation.
- **Vincent Carel**: Hydrothermal treatment of household wastewater: opportunity as on-site system combined with microalgae culture.
- **François Pontvianne**: Cultivation of microalgae *Chlorella vulgaris* in human urine using photovoltaic bioreactor technology.
- **Johanna Fernandez**: Biomolecules characterisation of algal biomass cultivated using photovoltaic-Bioreactor technology.
- **Oscar Urio**: Photovoltaic Assisted Algae Production: A Synergistic Combination of Urine Treatment and the Production of Valuable Compounds.